
# NUMERICAL AND EXPERIMENTAL PROCEDURES FOR DETERMINING CHARACTERISTICS OF STOCKBRIDGE DAMPERS

Zakhele Mathews_ Zondi_ 216249805

Submitted in fulfilment of the academic requirements for the degree of MEng: Mechanical Engineering qualification in the Department of Mechanical Engineering, Faculty of Engineering and the Built Environment

Department of Mechanical Engineering
Cape Peninsula University of Technology
Supervisor: Prof Modify Andrew Elton Kaunda
Cape town, South Africa
February 2021

# DECLARATION

I hereby declare that this dissertation has not been copied and it is my own work. I submit this thesis to the Cape Peninsula University as my own independent work. The experimental graphs presented in this thesis were not taken from other person's work and it has not been submitted to any other institution before for attainment of any qualification.

# ACKNOWLEDGEMENT

I would like to thank God for being with me with all my efforts that I have contributed to this thesis. Things were not going to be possible for me to finish my work without him throughout this study.

My great thanks goes to Professor M.A.E Kaunda for his dedicated supervision when I started this thesis I had no idea about research but his knowledge, time and guidance was helpful to me. I would not forget to thank Dr. Tiyamike Ngonda for his guidance in doing experiments and advising me to do modelling using Matlab.

Great thanks goes to Mangosuthu University of Technology for supporting my study with the financial support and to the research office for contributing with finance for travelling to Cape Peninsula University of Technology to visit my supervisor. I would also thank them for their support to buy some items which were needed for my project.

My sincere thank you goes to Professor D. Dorrell for allowing me to do my experiments at VRTC and Dr. Richard C. Loubser with some information regarding mathematics at UKZN University. I will not forget Pravesh Moodley (technician) for his contribution with assistance during the time when I was conducting experiments, he was always with me during the time of experiments to help me with the setup of experiments. My appreciation also goes to Dr. Ntumba Marc-Alain Mutombo for his contribution to my thesis.

I dedicate this dissertation to my late mother, late father and my family. I would like to take this opportunity to thank my wife for the support she contributed to my study because I used to come late and spent considerable time in my office and at VRTC doing my project.

Lastly I would like to thank all those who have contributed, either directly or indirectly to the preparation, research and compilation of this project report.

# ABSTRACT

The Stockbridge damper is a tuned mass absorber used to suppress wind-induced vibrations on slender structures such as overhead transmission power lines. The lines vibrate due to wind motion and this causes fatigue failure to transmission lines usually at the suspension clamp where the maximum stress occurs. The fatigue failure in transmission lines can lead to outage of electricity. There are three types of vibration motions, that is, Aeolian vibrations, conductor galloping and wake-induced oscillation. This is a preliminary study of the characteristics of an asymmetric Stockbridge damper in order to establish the efficiency and reliability of the current dampers. Experiments were conducted on dampers according to IEEE 664 standards at the Vibration Research and Testing Centre (VRTC) at the University of KwaZulu Natal (UKZN). Experiments were also conducted on a modified vibrating damper.

The mathematical model of a vibrating damper is also presented in this thesis and theoretical or computational results are validated by experimental results.

# TABLE OF CONTENTS

# LIST OF FIGURES

# LIST OF TABLES

# LIST OF SYMBOLS

| | |
|---|---|
| $f$ | Frequency |
| $m$ | Mass |
| S | Strouhal number |
| $V$ | Velocity |
| $D$ | Diameter |
| F | force |
| $D_c$ | Conductor diameter |
| $\omega$ | Angular frequency |
| $t$ | Time |
| $\rho$ | Density |
| $\mu$ | Dynamic viscosity of fluid |
| $L$ | Length |
| $\omega_n$ | Natural angular frequency |
| $c$ | Damping coefficient |
| $k$ | Spring constant |
| $P$ | Amplitude |
| $C_c$ | Critical damping factor |
| $c$ | Damping coefficient |
| G | Gravitational acceleration |
| g | Gravitational acceleration |
| g | grams |
| W | Weight |
| $\theta$ | Phase angle |
| $\zeta$ | Damping ratio |

# CHAPTER 1

# INTRODUCTION

## 1.1 Statement of the problem

Transmission lines vibrate because of wind motion and this causes a fatigue failure usually at the suspension clamp where the maximum stress occurs; the fatigue failure can lead to the shutdown of electricity. In order to protect them from induced forces there is a need to use a device called a Stockbridge damper to minimize vibration in the transmission lines. The Stockbridge dampers need to be improved by increasing their life span so that the transmission lines last longer. Stockbridge damper consists of a messenger cable with two masses or weights attached to the messenger cables. During its operation the two masses attached to the end of each cable vibrate, if the Stockbridge fails there is the probability of not protecting the transmission lines. The study of this research focuses more on asymmetrical Stockbridge damper's life which is the key piece in the system.

## 1.2 Aim and objectives

The purpose of the research is to propose improvements to the structural arrangement of Stockbridge dampers used on transmission lines, in order to increase the life of these dampers. Failure of a damper leads to failure of the transmission line, which then leads to power outage. An increase in the lifespan of Stockbridge dampers will reduce the life-cycle costs of transmission lines.

The objectives of the research project were to study the characteristics of an asymmetric Stockbridge damper, in order to determine its efficiency and reliability as a damping device for overhead transmission lines, and to develop a mathematical model of a vibrating damper. Experiments were to be conducted on samples of a Stockbridge damper and the results used to aid the design of an improved Stockbridge damper. The experimental results were to be used to validate the theoretical or computational mathematical model. Experiments were to be conducted also on a modified Stockbridge damper.

## 1.3 Brief chapter overviews

This section offers an overview and explanation of what each chapter consists of.

Chapter 1 presents the statement of the problem, aim and the objectives of the project

Chapter 2 offers different types of wind motion that affect transmission lines and Stockbridge dampers. It also presents different type of dampers.

Chapter 3 provides a literature review based on vibration from first principles and also includes the previous study done by other researchers.

Chapter 4 describes the standard tests and methodologies used to achieve the results of this research, it also presents the equipment and the material used for this project.

Chapter 5 provides the results in terms of graphs and the discussion of those results.

Chapter 6 presents an improved vibration damper using an analytical model.

Chapter 7 presents conclusions and recommendations for the project.

# CHAPTER 2

# WIND MOTION AND STOCKBRIDGE DAMPERS

## 2.1 Introduction

This chapter is an overview of the motions of conductors when subjected to wind motion and of the different types of damper used on transmission lines, including those variants designed to work on the Stockbridge principle.

## 2.2 Three different categories of cyclic conductor motion.

- Aeolian vibration
- Conductor galloping
- Wake-induced oscillation

### 2.2.1 Aeolian vibration

Aeolian vibration causes problems to transmission lines which lead to fatigue failure of the conductor strands or of the items associated with the support, use, and protection of the conductor. Aeolian vibration is characterized by having a low amplitude (conductor diameter) and high frequency (5 to 150 Hz) (Lilien et al., 2013). It is approximately in the range of 3 – 200 Hz and frequency depends on the size and tensile load of the conductor (Chan, 2006). Large conductors in low wind correspond to lower frequencies and small ground wires in moderate winds produce upper frequencies. Aeolian vibration in terms of the wind speed is caused by the wind velocity that ranges between 1 m/s – 7 m/s.

Vibration frequency is determined using the Strouhal formula: $f = S/D$, where $S$ is the Strouhal number (S = 0.18 – 0.22), $V$ is the wind velocity in m/s, and $D$ is the conductor diameter. The conductor vibration at any point is shown in the form of a beat pattern shown in Figure 2.1. This type of vibration is dangerous to transmission lines when conductor tensions are very high, the terrain is smooth, with frequent, low moderate, steady winds and the spans are long. The safest way to successfully control this vibration in most cases is by installing dampers and or spacer-dampers. Conductor vibration may lead to the bending or

fatigue failure of the conductor strands at the suspension clamps or at the clamps of spacers, spacer dampers and other devices installed on the conductors.

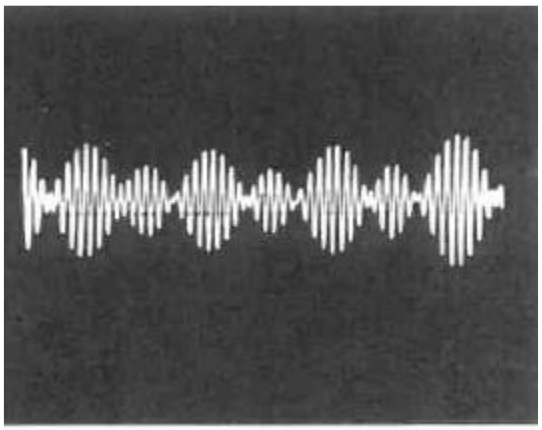

Figure 2. 1: Records of vibration at any chosen point on a conductor (Chan, 2006)

### 2.2.2 Conductor galloping

Conductor galloping is characterized by a low frequency, high amplitude, primarily vertical conductor motion. It is nearly always produced by moderately strong, steady crosswinds acting upon an asymmetrically iced conductor surface. Normally ice is deposited on the windward surface of the conductor; if ice or snow builds up on the conductor it creates an aerodynamically unstable shape and this can produce large forces and moments on the conductor. The motion of the conductor due to wind can lead to oscillations in a vertical direction.

### 2.2.3 Wake – induced oscillation

The shielding effect of windward subconductors on their leeward counterparts produces forces; wake induced vibrations only appear in bundle conductors for which some subconductors are in the wake induced by windward subconductors. One can distinguish four types of wake induced motions see Figure 2.2:

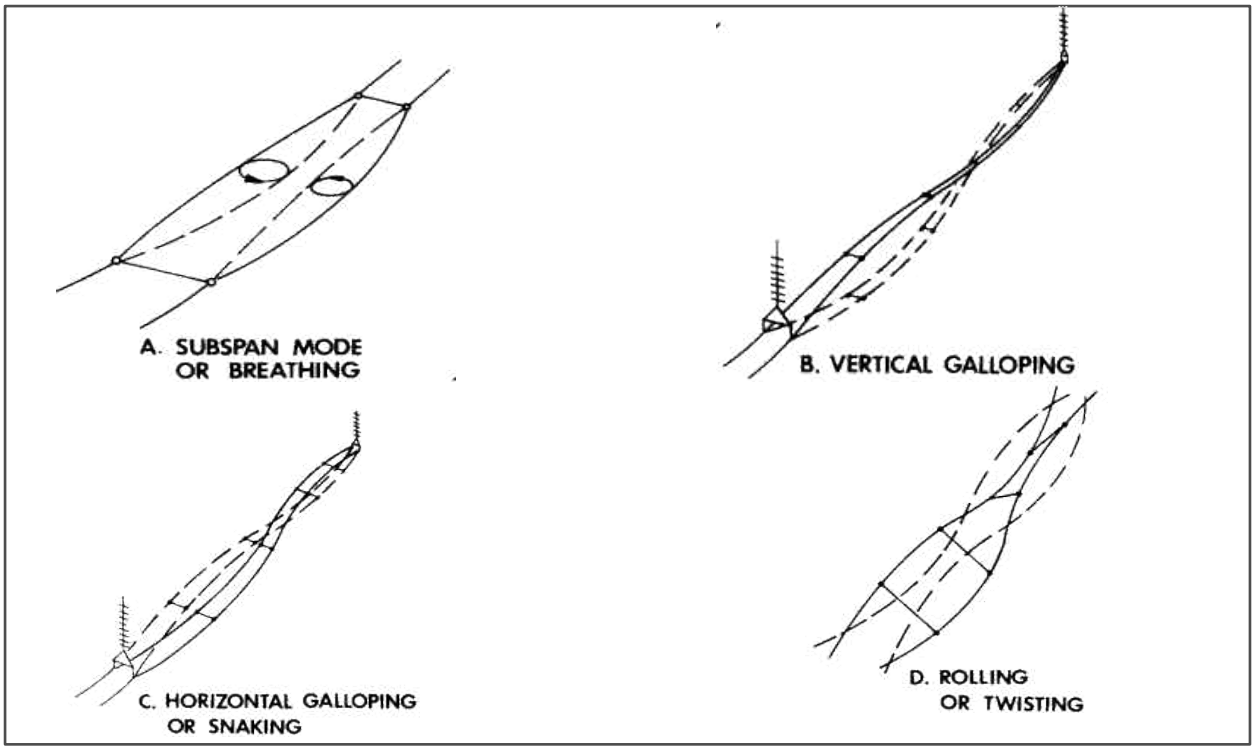


Figure 2. 2: Four types of wake – induced vibrations

## 2.3 Comparison of types of wind motion

Table 2.1 shown presents a comparison of the characteristics of the three types of wind motion namely Aeolian vibration, conductor galloping and wake-induced vibration

Table 2. 1: Comparison of types of cyclic conductor motion

| | **Aeolian vibration** | **Conductor galloping** | **Wake – induced** |
|---|---|---|---|
| Types of overhead lined affected | All | all | Limited to lines with bundled conductors |
| Frequency range | 3 Hz - 150 Hz | 0.08 Hz – 3 Hz | 0.015 Hz – 10 Hz |
| Range of vibration amplitudes (peak-peak) | 0.01 – 1 $D_c$ $D_c$ is the conductor diameter | 5 – 300 $D_c$ $D_c$ is the conductor diameter | 0.5 – 80 $D_c$ $D_c$ is the conductor diameter |
| Wind character | Steady | Steady | Steady |
| Wind velocity | 1 m/s – 7 m/s | 7 m/s – 18 m/s | 4 m/s – 18 m/s |
| Conductor surface | Bare or uniformly iced | Asymmetrical ice deposit on conductor | Bare , dry |
| Design Condition Affecting Conductor motion | Line tension, conductor self - damping, use of dampers, armor rods | Ratio of vertical natural frequency to torsional frequency; sag ratio and support conditions | Subconductor separation, tilt of bundle, subconductor arrangement, sub span staggering. |
| Damage | | | |
| Approx., time required to severe damage to develop | 3 months to 20 + years | 1 to 48 hours | 1 month to 8 + years |
| Direct causes of damage | Metal fatigue due to cyclic bending | High dynamic loads | Conductor clashing, accelerated wear in hardware |
| Line components most affected by damage | Conductor and shield wire strands | Conductor, all hardware, insulators, structures | Suspension hardware, spacers, dampers, conductor strand |

## 2.4 Vortex shedding from a circular cylinder

When a circular cylinder is positioned in a steady uniform air stream at an adequate velocity, flow separation occurs on the cylinder's surface, as shown in Figure 2.3. As the separation is formed it leads to vortex shedding from the cylinder and the formation of a wake behind the cylinder. Vortices are shed alternatively from the upper and lower surfaces of the cylinder at a constant frequency (Kelly, 1993).

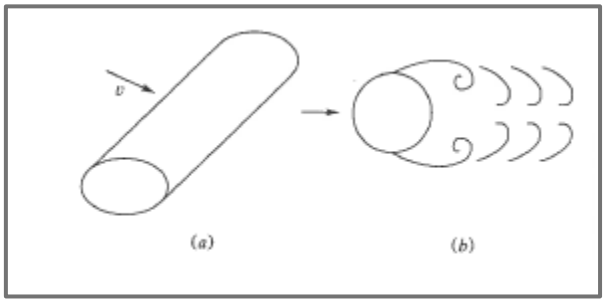


Figure 2. 3: (a) circular cylinder in the steady flow; (b) cross section of the cylinder, showing vortices shed alternatively from each surface of the cylinder resulting in a wake behind the cylinder and harmonic force acting on the cylinder (Kelly, 1993).

The shedding caused by the vortices produces oscillating streamlines in the wake which, in turn, leads to an oscillating pressure distribution; an oscillating force acting perpendicularly or normal to the cylinder is formed due to the oscillating pressure distribution (Kelly, 1993). This is the same as what happens to transmission lines when they vibrate due to wind speed. The force is given by

$$F(t) = F_0 \sin \omega t \qquad 2.1$$

Where $F_0$ is the magnitude of the force and $\omega$ is the frequency of vortex shedding. These parameters are dependent upon the fluid properties and the geometry of the cylinder (Kelly, 1993). That is,

$$F_0 = F_0(V, \rho, \mu, D, L) \qquad 2.2$$

$$\omega = \omega(V, \rho, \mu, D, L) \qquad 2.3$$

Where $V$ = magnitude of the fluid velocity, $[L]/[T]$

$\rho$ = the fluid density, $[M]/[L]^3$

$\mu$ = the dynamic viscosity of fluid, $[M]/[L][T]$

$D$ = the diameter of the cylinder, $[L]$

$L$ = the length of the cylinder

The dependent parameters $F_0$ and $\omega$ are both functions of five independent.

## 2.5 Types of dampers used to absorb vibration from transmission lines.

To absorb some vibration energy from transmission lines various types of damper are used; the main function of dampers is to protect power lines from being damaged by vibration caused by wind motion. The wind speed during the test is set in the range of 1 – 7 m/s, which is the speed of Aeolian vibration. Different types of damper are presented below in this section.

### 2.5.1 Stockbridge damper

The problem of conductor strand failures due to Aeolian vibration was first recognized in 1923 and Stockbridge damper were established by George. H Stockbridge in 1924; after this modifications were made to improve its operation. The damper consists of two shaped masses, rigidly attached at the ends of a stranded steel cable, which in turn is rigidly clamped to the conductor. The first design of the damper is shown in Figure 2.4.

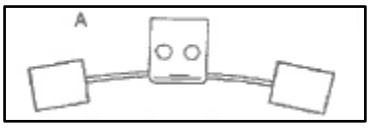


Figure 2. 4: The original type of Stockbridge damper (Chan, 2006)

After the Stockbridge damper was established, Monroe and Templin upgraded it with the two degrees of freedom damper shown in Figure 2.5 in which both the shape and the moment

of inertia of the masses were designed to take advantage of the second vibration mode of a cantilever beam, within the frequency range of operation of the damper.

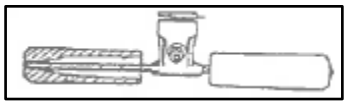

Figure 2. 5: Monroe and Templin damper

The Stockbridge damper after its invention was manufactured worldwide, with equal masses supported by equal lengths of steel stranded cable. In 1968 modification was made to the basic damper by Claren and Diana. The two halves were made asymmetrical, providing two different masses with different moments of inertia and different lengths of the messenger cable as shown in Figure 2.6.

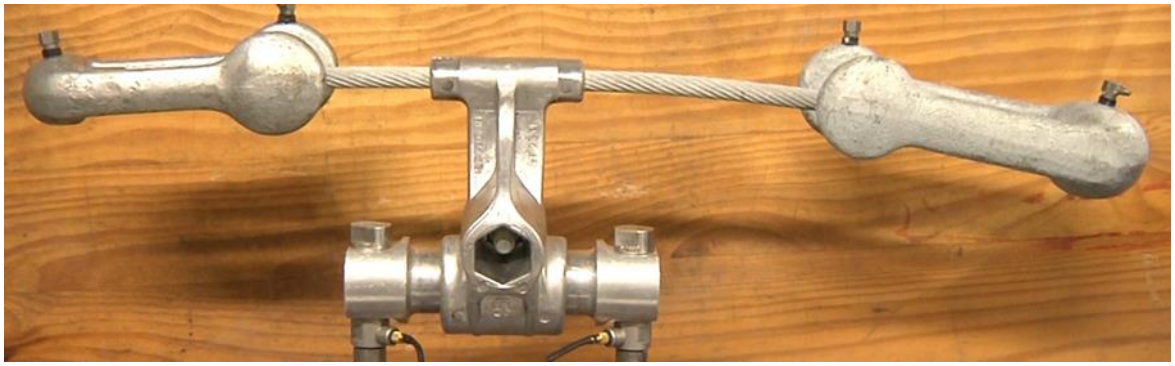

Figure 2. 6: Claren and Diana damper with four accelerometers (4-R Stockbridge-type Damper)

### 2.5.2 Haro damper

In 1970, Lauri Haro and Tapan Seppa established a vibration damper based on the Stockbridge principle, known as the Haro damper shown in Figure 2.7. It consists of three weights and two clamps for the connection to the conductor; the weights are of varying dimensions and are at different moment arms on the messenger cable. Each of the two external weights has two

degree of freedom and the central mass has only one degree of freedom; giving the device five resonances. It is over a meter in length and not easy to transport and install. Many became bent and damaged during transportation

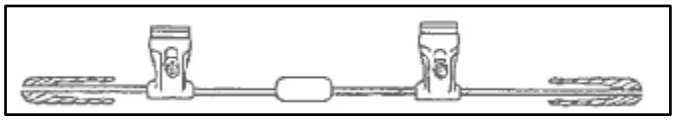

Figure 2. 7: Haro damper.

### 2.5.3 Torsional Stockbridge-type damper

Some expansions of the Stockbridge-type vibration damper include a symmetrical damper that, in addition to the flexural resonances, establishes a torsional resistance. This is achieved by using weights whose center of gravity is offset with respect to the axis of messenger cable. The most popular are the Australian “Dogbone” damper as shown in figure 2.8 and the Japanese Aahi torsional damper.

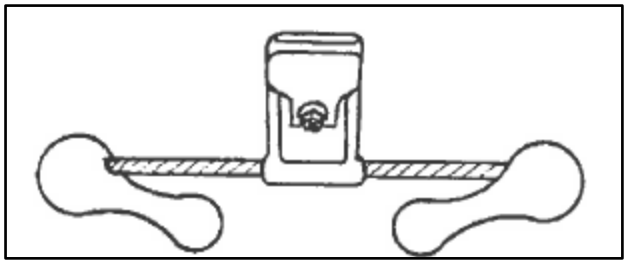

Figure 2. 8: “Dogbone” damper

### 2.5.4 Bretelle dampers

This is widely used in France and its discovery as a damper device was largely accidental. Normally it is made from pieces of scrap conductor that are the same size as the line on which it is used. The Bretelle concept seems to be economically attractive but there are numerous factors that need to be considered. It is difficult to conduct a definitive investigation of the design variables because its configuration does not lend itself to indoor laboratory

investigation. It has a jumper loop connecting two adjacent spans at the suspension points as shown below in Figure 2.9

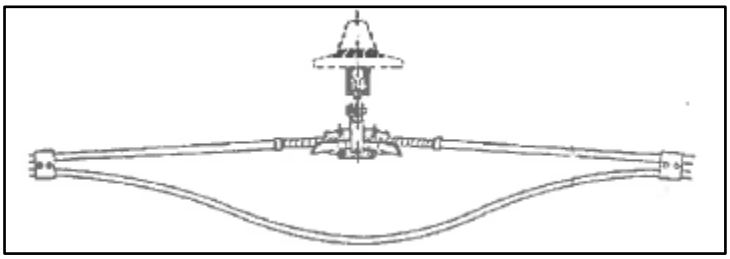

Figure 2. 9: Bretelle damper profile (Chan, 2006)

### 2.5.5 Elgra

Elgra is a Swedish damper consisting of a vertical stem having three cast masses loosely fitted to a vertical shaft. Each mass is separated by an elastomeric washer. This damper seems to be an interesting study in extrapolation; before a mass can be lifted from its pad, the acceleration of the damper must not exceed one gram. Tests have revealed that this type of damper performs well for acceleration of about two grams. When the damper was first established, transmission lines were smaller in diameter and, vibrated at higher frequencies. The size of the damper was adjusted accordingly as the conductor diameter was increased. Figure 2.10 shows Elgra damper

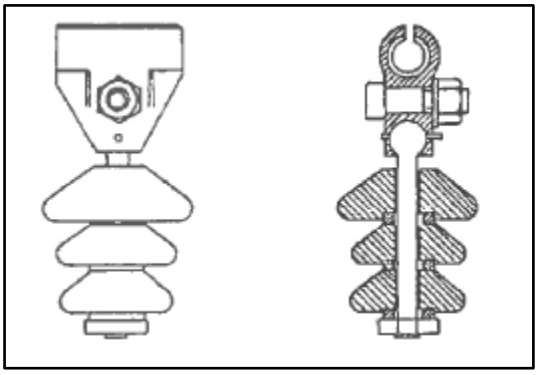

Figure 2. 10: Elgra damper

### 2.5.6 Festoon dampers

Festoon dampers have been used on numerous long spans and they consist of a scrap conductor like the Bretelle and are relatively inexpensive. Figure 2.11 shows festoon dampers at suspension points and tension points. The main problems that have been reported with the use of festoon dampers have occurred at their clamps. In places like Norway and other cold countries, festoon dampers are preferred to Stockbridge-type dampers on long fjords because the latter can be damaged by both conductor galloping and Aeolian vibration of increased severity, during periods of icing

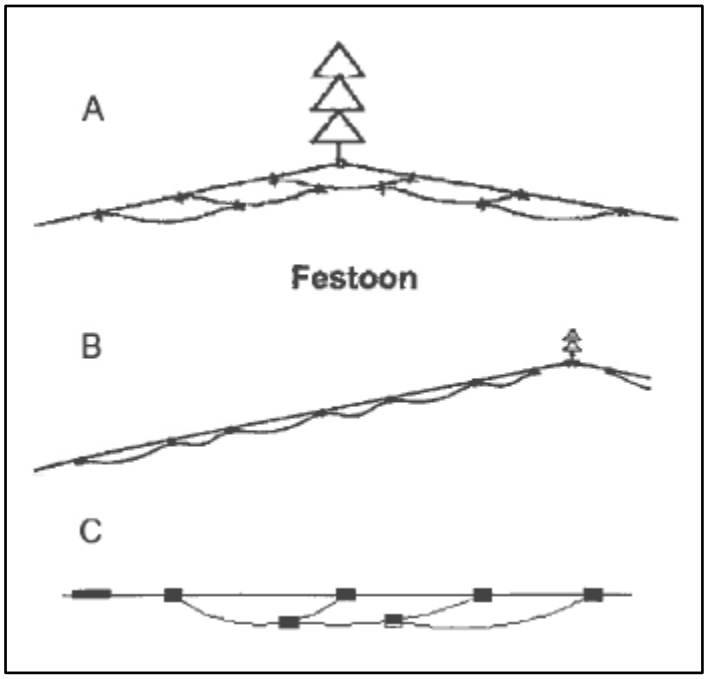


Figure 2. 11: Festoon dampers. (A) and (B) are festoon dampers for suspension; (C) is a festoon damper for tension points

# CHAPTER 3

# THEORY OF VIBRATION OF MECHANICAL SYSTEMS

## 3.1 Introduction

This chapter presents the theory of vibration of mechanical systems. Free and forced vibrations with varying degrees of damping and multi degrees of freedom were considered. The theory is based on standard text books for example Inman

The spring-mass system was used to derive the equations governing the vibration of a free structure, undamped and damped; the dashpot was introduced to represent damping. For forced vibration, both steady and transient states were considered for undamped vibration; damping was considered also. Thereafter, work carried out on Stockbridge dampers by others was reviewed.

## 3.2 Mechanical vibration

Mechanical vibration is taken as the measurement of periodic motion with respect to an equilibrium point. Vibration is also considered as a repetitive motion of mechanical systems from machine parts to large structures. Vibrations produced during the earthquake as in the case of vibrating ground motion are unwanted. Typical examples of vibration familiar to most are the motion of a guitar string, the quality of ride of an automobile or motorcycle, the motion of an airplane's wings and the swaying of a large building due to wind or an earthquake.

## 3.3 Analysis of mechanical vibrations

This section introduces the basic terminology used in the study of mechanical vibration, as well as two important elements found in vibration models. These are the spring element, which produces a restoring force or moment as a function of the displacement of the mass element, and the damping element, which produces a restoring force or moment as a function of the velocity of the mass element (Palm III, 2007).

There are many types of vibration but all of them start from analysing the free vibration of a spring mass system. In terms of vibration we have a vibration known as free vibration.

The phase angle $\theta$ describes the relative shift in the sinusoidal vibration of the spring-mass system.

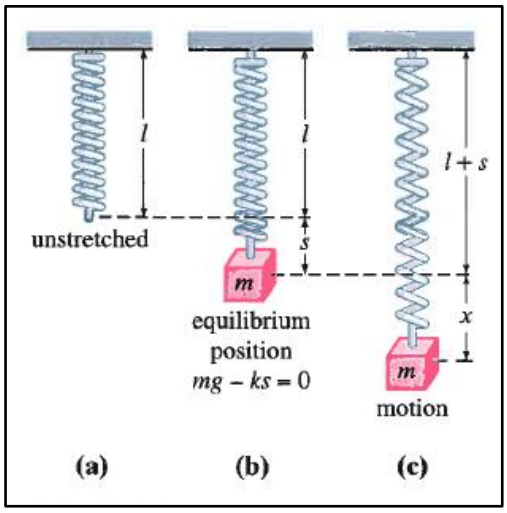


Figure 3. 1: Spring mass system (Zill and Cullen, 2005)

## Free undamped vibration (spring mass system)

From Figure 3.1 the spring **(a)** with no mass attached to it is a free spring, spring **(b)** has the mass attached to it and will stretch to a point where the mass/weight is in equilibrium to a force applied by the spring in the opposite direction of motion. By Hooke's Law, the spring itself exerts a restoring force *F* opposite to the direction of elongation and proportional to the amount of elongation (Zill and Cullen, 2005). Simply stated, *F= ks,* where *k* is a constant of proportionality called the **spring constant.** After the mass is attached to the spring, it stretches the spring with an amount *s* and attains a position of equilibrium at which the weight W is balanced by the restoring force *ks*. As shown in the above Figure 3.1 (b) it means the condition of equilibrium is *mg = ks or mg – ks = 0.* When the mass is displaced by an amount of *x* from its equilibrium position, the restoring force of the spring is then $k(x+s)$. It is assumed that there are no retarding forces acting on the system and the mass is assumed to vibrate free of other external forces (Zill and Cullen, 2005). By using Newton's second law for linear motion the sum of all the forces is equal to the product of an acceleration and the mass being accelerated

$$\ddot{x}m = -k(s+x) + mg \qquad 3.1$$

$$\ddot{x}m = -ks - kx + mg \quad 3.2$$

But $mg = ks$ it means they cancel each other in the equation

$$\ddot{x}m = -kx \quad 3.3$$

$$\ddot{x}m + kx = 0 \quad 3.4$$

$$\ddot{x} + \frac{k}{m}x = 0 \quad 3.5$$

Most of the equations of motion of many oscillatory systems have a solution of the form

$$\mathrm{x(t)} = \mathrm{A}\sin(\omega_n t + \theta) \quad 3.6$$

Equation 3.6 is a sine function in its most general form, where the constant A is the amplitude, or maximum value of the function; $\omega_n$, the angular frequency, determines the interval in time during which the function repeats itself, and $\theta$, called the phase, determines the initial value of the sine function. The frequency is measured in rad/sec and the phase angle is measured in radians. The related frequency is cycles per unit time and is often denoted by $\omega$ . The two frequencies are related by $\omega = 2\pi f$ (Palm III, 2007). The first derivative of equation 3.6 gives the velocity and the second derivative gives an acceleration

$$\dot{x}(t) = \omega_n A\cos(\omega_n t + \theta) \quad 3.7$$

$$\ddot{x}(\mathrm{t}) = -\omega_n^2 \mathrm{A}\sin(\omega_n t + \theta) \quad 3.8$$

Substitution of equations 3.6 and 3.8 into 3.4 yields

$$-\mathrm{m}\omega_n^2 \mathrm{A}\sin(\omega_n t + \theta) + \mathrm{kA}\sin(\omega_n t + \theta) = 0 \quad 3.9$$

From equation 3.9 $\omega_n^2 = \frac{k}{m} or\ \omega_n = \sqrt{\frac{k}{m}}$ therefore equation 3.5 becomes

$$\ddot{x} + \omega_n^2 x = 0 \quad 3.10$$

Alternative form of $\mathrm{x(t)} = \mathrm{A}\sin(\omega_n t + \theta)$ is

$$x(t) = C_1 \cos \omega_n t + \mathrm{C}_2 \sin\omega_n t \qquad 3.11$$

where x(t) is the displacement of a mass (Palm III, 2007). The radian frequency is $\omega_n$ and the period $T = 2\pi/\omega_n$. Equation 3.11 can be proved by using 3.6 the trigonometry identity as follows

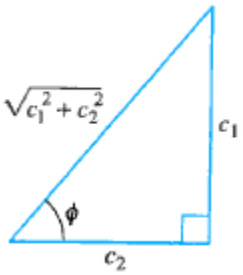


Figure 3. 2: A relationship between $C_1 > 0, \mathrm{C}_2 > 0$ and phase angle $\theta = \phi$ (Zill and Cullen, 2005).

$$\mathrm{x(t)} = \mathrm{A}\sin(\omega t + \theta) = \mathrm{A}\sin\theta\ \cos\omega t + \mathrm{A}\cos\theta\ \sin\omega t \qquad 3.12$$

$$\sin\theta = \frac{C_1}{A}, \cos\theta = \frac{C_2}{A} \text{ and } \tan\theta = \frac{C_1}{C_2}. \qquad 3.13$$

$A = \sqrt{{C_1}^2 + {C_2}^2}$ and $\theta$ is defined as the phase angle. It follows from Figure 3.2 that $\theta$ is defined by

$$\sin\theta = \frac{C_1}{\sqrt{{C_1}^2+{C_2}^2}} = \frac{C_1}{A}, \qquad \cos\theta = \frac{C_2}{\sqrt{{C_1}^2+{C_2}^2}} = \frac{C_2}{A}$$

Then 3.12 becomes

$$\mathbf{x(t)} = \mathrm{A}\,\frac{C_1}{A}\cos\omega_n t + \mathrm{A}\,\frac{C_2}{A}\sin\omega t = \boldsymbol{C_1 \cos \omega_n t + \mathrm{C}_2 \sin \omega_n t} \qquad 3.14$$

The *x (t)* is the displacement of the mass.

There is an alternative way to find the constant A and $\theta$. If the mass in the spring shown in Figure 3.1 is displaced to a position of $x_o$ at time $t = 0$, the potential energy in the spring will result in motion (Inman, 2001). Also if the mass is given initial velocity of $V_0$ at $t = 0$, motion will result. These are called initial conditions and when substituted into the solution 3.6 yield

$$x_o = x(0) = A\sin(\omega_n\, 0 + \theta) = A\sin\theta \quad 3.15$$

$$v_0 = \dot{x}(0) = \omega_n A\cos(\omega_n\, 0 + \theta) = \omega_n A\cos\theta \quad 3.16$$

Combining the square of each equation,

$$x_o{}^2 = (A\sin\theta)^2 \quad 3.17$$

$$(\sin\theta)^2 = \frac{x_o{}^2}{A^2} \quad 3.18$$

$$v_0{}^2 = \omega_n^2 A^2\,(\cos\theta)^2 \quad 3.19$$

$$(\cos\theta)^2 = \frac{v_0{}^2}{(\omega_n A)^2} \quad 3.20$$

Solving equations 3.18 and 3.20 simultaneously yields

$$(\cos\theta)^2 + (\sin\theta)^2 = \frac{x_o{}^2}{A^2} + \frac{v_0{}^2}{\omega_n(A)^2} \quad \text{but} \quad (\cos\theta)^2 + (\sin\theta)^2 = 1 \quad 3.21$$

$1 = \frac{\omega_n^2 x_o{}^2 + v_0{}^2}{\omega^2 A^2}$ Make A the subject of the formula

$$\boldsymbol{A = \frac{\sqrt{\omega_n^2 x_o{}^2 + v_0{}^2}}{\omega}} \quad 3.22$$

$$\boldsymbol{\theta = \tan^{-1}(\frac{\omega_n x_0}{v_0})} \quad 3.23$$

The solution of the equation of motion for the spring-mass system is called a free response of the system, because no external force to the system is applied at $t = 0$ (Inman, 2001) and is given by

$$\mathbf{x(t) = \frac{\sqrt{\omega_n^2 x_o{}^2 + v_0{}^2}}{\omega_n}\sin\left[\omega_n t + \tan^{-1}(\frac{\omega_n x_0}{v_0})\right]} \quad 3.24$$

With regard to the derived equations 3.24, Figure 3.3 shows harmonic motion and how the initial conditions determine the response of such a system.

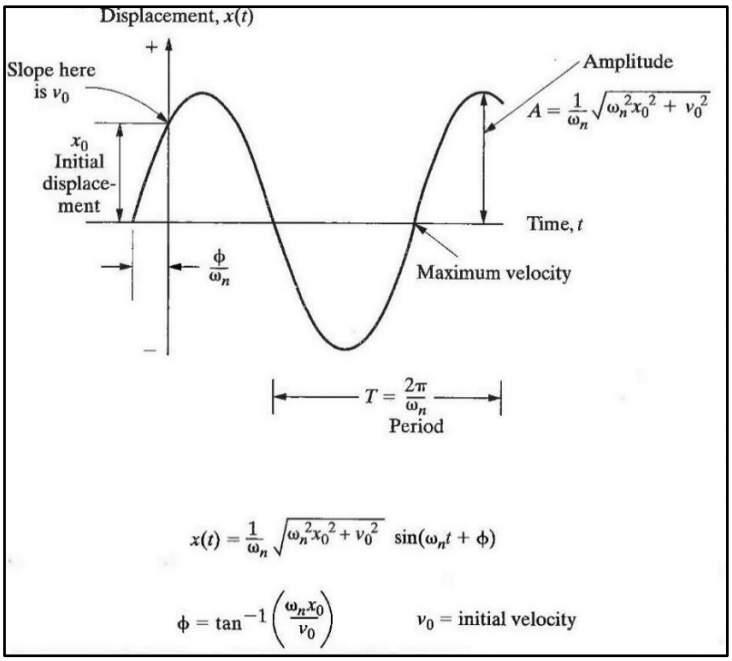


Figure 3. 3: Summary of the description of Simple Harmonic Motion (Inman, 2001)

### 3.3.1 Free damped motion (spring mass system)

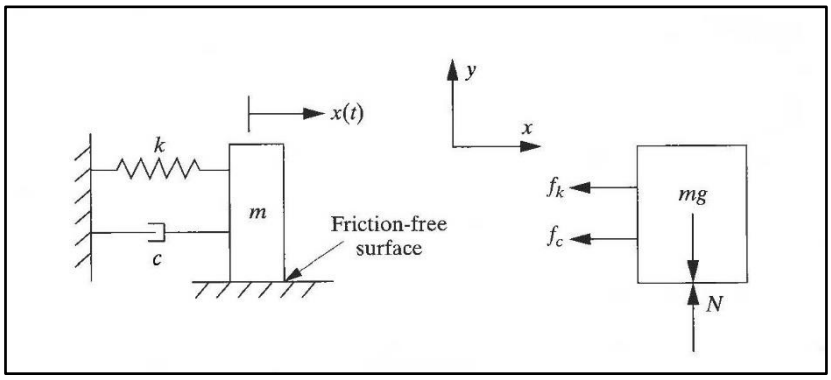


Figure 3. 4: Schematic of a single degree of freedom system with viscous damping indicated as dashpot (Inman, 2001).

From the free body diagram shown in Figure 3.4, the damping force, denoted by $f_c$ has the form

$$f_c = c\dot{x}(t) \qquad 3.25$$

where $c$ is a constant of proportionality related to the oil viscosity. The constant $c$, called the damping coefficient, has units of N s/m, or kg/s. The damping force is proportional to the velocity but it acts in the opposite direction of mass motion (Brownjohn, 2005, Inman, 2001). By using Hook's law, the spring itself exerts a force, denoted by $f_k$ which is opposite to the direction of displacement or elongation and proportional to the elongation (Zill and Cullen, 2005, Inman, 2001).

$$f_k = kx \qquad 3.26$$

The theory of simple harmonic motion is unrealistic, since the motion described by equation 3.1 assumes that there are no retarding forces acting on the moving mass unless the object is in a perfect vacuum but in real life there are retarding forces. By using Newton's law, taking all the forces acting horizontally on the free body diagram shown on figure 2.4

$$m\ddot{x} = -c\dot{x} - kx \qquad 3.27$$

Assume the solution

$$x(t) = Ae^{st} \qquad 3.28$$

$$\dot{x}(t) = ASe^{st} \qquad 3.29$$

$$\ddot{x}(t) = AS^2e^{st} \qquad 3.30$$

Substituting 3.28, 3.29 and 3.30 into 3.27

$$mAS^2e^{st} + cASe^{st} + kAe^{st} = 0 \qquad 3.31$$

Equation 3.31 forms the characteristic equation:

$$mS^2 + cS + k = 0 \qquad 3.32$$

Roots are $S_{1,2} = \frac{-b \pm \sqrt{b^2-4ac}}{2a}$ 3.33

$$S_{1,2} = \frac{-c \pm \sqrt{C^2-4mk}}{2m} \qquad 3.34$$

To examine the three cases in detail, we begin with critical damping $C_c$. In this case the discriminant equals to zero

$$C_c^2 - 4mk = 0 \qquad 3.35$$

$$C_c^2 = 4mk \qquad 3.36$$

$$\frac{C_c^2}{4m} = k \qquad 3.37$$

$$\left(\frac{C_c}{2m}\right)^2 = \frac{k}{m} = \omega_n \qquad 3.38$$

It is convenient to express damping in non – dimensional ratio, called damping ratio as

$$\zeta = \frac{C}{C_c} \qquad 3.39$$

$$\frac{C}{2m} = \frac{\zeta C_c}{2m} = \zeta\omega_n \qquad 3.40$$

Equation 3.34 becomes $S_{1,2} - \frac{-C \pm}{2m}\sqrt{\left(\frac{C}{2m}\right)^2 - \frac{4mk}{4m^2}} = -\frac{-C \pm}{2m}\sqrt{\left(\frac{C}{2m}\right)^2 - \frac{k}{m}}$ 3.41

Therefore equation 3.41 becomes

$$\boldsymbol{S_{1,2} = -\zeta\omega_n \pm \sqrt{\zeta^2\omega_n^2 - \omega_n^2}} \qquad 3.42$$

$$\boldsymbol{S_{1,2} = \omega_n\left(-\zeta \pm \sqrt{\zeta^2 - 1}\right)} \qquad 3.43$$

The general solution is given by:

$$\boldsymbol{x(t) = Ae^{s_1 t} + Bte^{s_1 t}} \qquad 3.44$$

Or

$$\boldsymbol{x(t) = e^{s_1 t}(A + Bt)} \qquad 3.45$$

Case 1: $c^2 > 4mk$. In this case the system is said to be overdamped, see figure 3.5

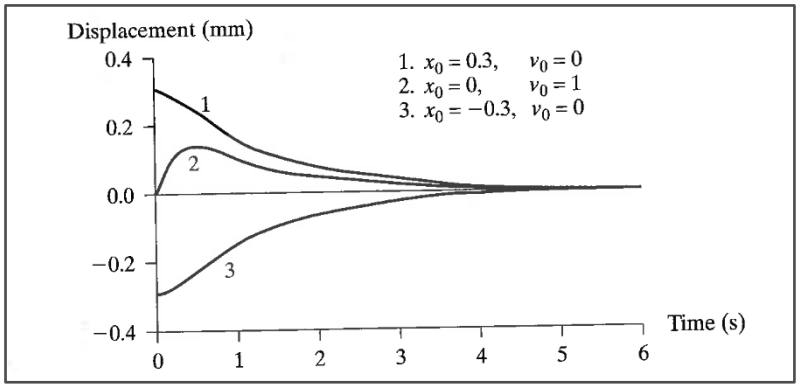


Figure 3.5: Response of an overdamped system $\zeta > 1$, for two values of the initial displacement and zero initial velocity and one case with $x_0 = 0$ and $v_0 = 1$ (Inman, 2001)

Case 2: $c^2 = 4mk$. In this case the system is said to be critically damped, see figure 3.6

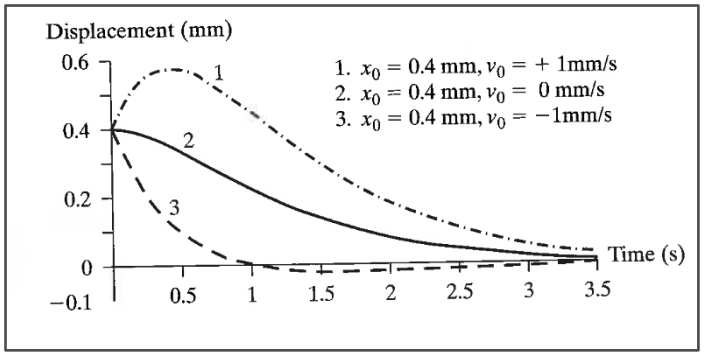


Figure 3. 6: Response of a critically damped system for three different initial velocities. The response properties are $k = 225$ N/m, $m = 100\ kg$ and $\zeta = 1$ (Inman, 2001).

Case 3: $c^2 < 4mk$. In this case the system is said to be underdamped, see figure 3.7

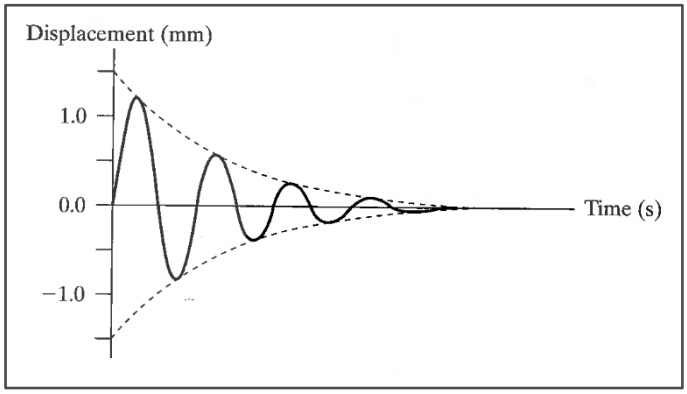


Figure 3. 7: Response of an underdamped system $0 < \zeta < 1$ (Inman, 2001).

### 3.3.2 Forced vibrations (steady state and transient state)

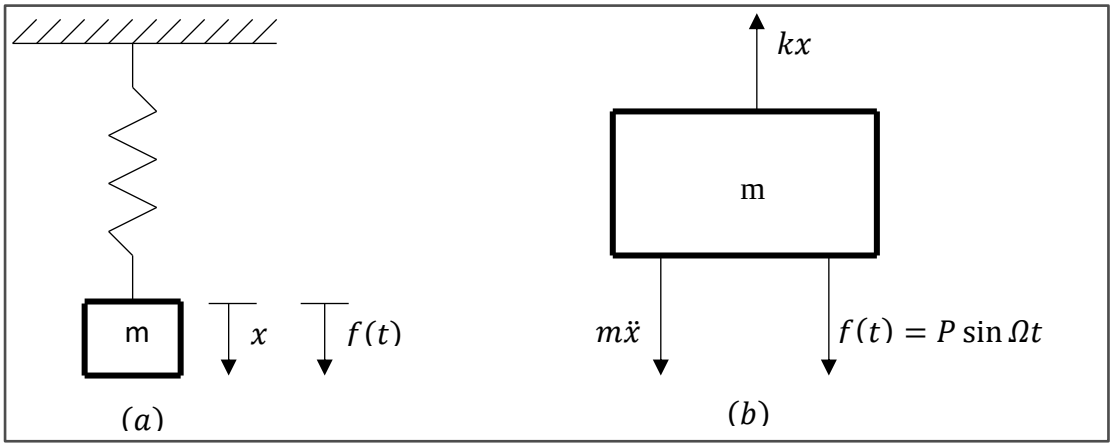


Figure 3. 8 Forced vibration steady state

Suppose we include an external force $f(t)$ acting on a vibrating mass on a spring in figure 3.8. For example $f(t)$ represents a driving force causing an oscillatory vertical motion of the spring. Sketch **(a)** is a free body diagram representing all the forces acting on the mass. The driving force $f(t)$ is chosen to be of the form $\boldsymbol{P \sin \Omega t}$ where $\boldsymbol{P}$ represents the magnitude, or maximum amplitude, of the applied force and $\boldsymbol{\Omega}$ denotes the frequency of the applied force (Inman, 2001). The frequency $\boldsymbol{\Omega}$ is also called the input frequency, or driving frequency, or forcing frequency and has units of $rad/s$. Using Newton's second law gives the differential equation of driven or forced motion:

$$m\ddot{x} = -kx + f(t) \quad 3.46$$

$$m\ddot{x} + kx = P \sin \Omega t \quad 3.47$$

$$\ddot{x} + \frac{k}{m}x = \frac{P}{m}\sin \Omega t \quad 3.48$$

But $\frac{P}{m} = q$ 3.49

$$\ddot{x} + \frac{k}{m}x = q \sin \Omega t \quad 3.50$$

$$\ddot{x} + \omega_n^2 x = q \sin \Omega t \quad 3.51$$

Let us assume solution to be

$$x = C_3 \sin \Omega t \quad 3.52$$

$$\dot{x} = C_3 \cos \Omega t \quad 3.53$$

$$\ddot{x} = -C_3 \Omega^2 \sin \Omega t \quad 3.54$$

Substitute 3.52 and 3.54 into 3.51

$$-C_3 \Omega^2 \sin \Omega t + \omega_n^2 C_3 \sin \Omega t = q \sin \Omega t \quad 3.55$$

$$-C_3 \Omega^2 + \omega_n^2 C_3 = q \quad 3.56$$

$$-C_3(\Omega^2 - \omega_n^2) = q \quad 3.57$$

$$C_3(\omega_n^2 - \Omega^2) = q \quad 3.58$$

$$C_3 = \frac{q}{(\omega_n^2 - \Omega^2)} \quad 3.59$$

Substitute 3.59 into 3.52 $\quad \boldsymbol{x(t) = \frac{q}{(\omega_n^2 - \Omega^2)} \sin \Omega t}$ 3.60

**Forced vibration transient state** is now shown, consider the equation 3.51

$$\ddot{x} + \omega_n^2 x = q \sin \Omega t$$

The general solution is given by

$$\boldsymbol{x(t) = C_1 \cos \omega_n t + C_2 \sin \omega_n t + \frac{q}{(\omega_n^2 - \Omega^2)} \sin \Omega t} \quad 3.61$$

Using the initial conditions

$$\dot{x}(t) = -C_1 \omega_n \sin \omega_n t + C_2 \omega_n \cos \omega_n t + \frac{q\Omega}{(\omega_n^2 - \Omega^2)} \cos \Omega t \quad 3.62$$

$$x(0) = C_1 + (0) + (0) \quad 3.63$$

$$x(0) = C_1 = x_0 \quad 3.64$$

$$\dot{x}(0) = (0) + C_2 \omega_n + \frac{q\Omega}{(\omega_n^2 - \Omega^2)} \quad 3.65$$

$$\dot{x}(0) = v_0 \quad 3.66$$

$$C_2 \omega_n = v_0 - \frac{q\Omega}{(\omega_n^2 - \Omega^2)} \quad 3.67$$

$$C_2 = \frac{v_0}{\omega_n} - \frac{q\Omega}{\omega_n(\omega_n^2 - \Omega^2)} \quad 3.68$$

$$C_2 = \frac{v_0(\omega_n^2 - \Omega^2) - q\Omega}{\omega_n(\omega_n^2 - \Omega^2)} \quad 3.69$$

Therefore the general equation 3.62 becomes

$$\boldsymbol{x(t) = x_0 \cos \omega t + \left(\frac{v_0(\omega_n^2 - \Omega^2) - q\Omega}{\omega_n(\omega_n^2 - \Omega^2)}\right) \sin \omega t + \frac{q}{(\omega_n^2 - \Omega^2)} \sin \Omega t} \quad 3.70$$

### 3.3.3 Forced damped vibration

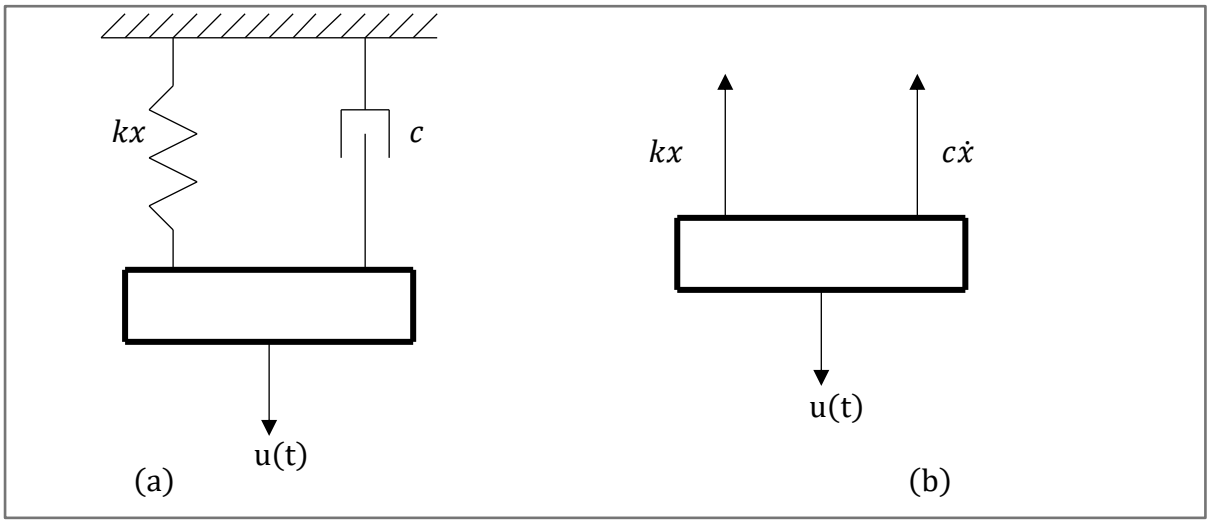


Figure 3. 9: Forced vibration viscous damped

Figure 3.9 (b) shows the free body diagram with an additional force called the damping force denoted by $\boldsymbol{f_c = c\dot{x}}$ and $\boldsymbol{u(t) = Psin\Omega t}$ represents the driving force causing an oscillatory vertical motion of the spring. Using Newton's second law gives the differential equation of driven or forced motion:

$$m\ddot{x} = -kx - c\dot{x} + f(t) \qquad 3.71$$

But $c = 2\zeta\omega_n m$

$$m\ddot{x} + kx + c\dot{x} = Psin\Omega t \qquad 3.72$$

$$m\ddot{x} + 2\zeta\omega_n m\dot{x} + kx = Psin\Omega t \qquad 3.73$$

$$\ddot{x} + 2\zeta\omega_n\dot{x} + \omega_n^2 x = q\sin\Omega t \qquad 3.74$$

Assume the solution to be

$$x(t) = Asin\Omega t \qquad 3.75$$

$$\dot{x}(t) = A\Omega\cos\Omega t \qquad 3.76$$

$$\ddot{x}(t) = -A\Omega^2\sin\Omega t \qquad 3.77$$

Substitute 3.75, 3.76 and 3.77 into equation 3.74

$$-A\Omega^2\sin\Omega t + 2\zeta\omega_n A\Omega\cos\Omega t + \omega_n^2 Asin\Omega t = q\sin\Omega t \qquad 3.78$$

$$-A\Omega^2\sin\Omega t + 2\zeta\omega_n A\cos\Omega t + \omega_n^2 Asin\Omega t - q\sin\Omega t = 0 \qquad 3.79$$

But $-A\Omega^2\sin\Omega t + \omega_n^2 Asin\Omega t - q\sin\Omega t = 0$ 3.80

$$-A\Omega^2 + \omega_n^2 A - q = 0 \qquad 3.81$$

From 3.78 $2\zeta\omega_n A\Omega\cos\Omega t = 0$ 3.82

$$2\zeta\omega_n\Omega A = 0 \qquad 3.83$$

Therefore 3.78 becomes

$$-A\Omega^2 + \omega_n^2 A - q + 2\zeta\omega_n A = 0 \qquad 3.84$$

$$\boldsymbol{A = \frac{q}{(\omega_n^2+\Omega^2)+2\zeta\omega_n\Omega}} \qquad 3.85$$

Therefore $$\boldsymbol{x(t) = \frac{q}{(\omega_n^2+\Omega^2)+2\zeta\omega_n\Omega} sin\Omega t} \qquad 3.86$$

### 3.3.4 Two degrees of freedom

This is a very important aspect of this study that deals with transmission line represented by $m_1$ and the Stockbridge Damper represented by $m_2$ .The mass $m_2$ is called mass vibration absorber because it absorbs energy of vibration from mass $m_1$, having forced vibration (Seto, 1964). In other words it cuts down as much as possible the amplitude of the driving force causing an oscillatory vertical motion of transmission line. The response of a multi-degree of freedom system due to harmonic excitation is the sum of the homogeneous solution and the particular solution (Kelly, 1993). The support of the mass-spring system is given a forced sinusoidal displacement $x(t) = F_0 \cos \omega t$. Find the steady state vibration of the masses (Seto, 1964).

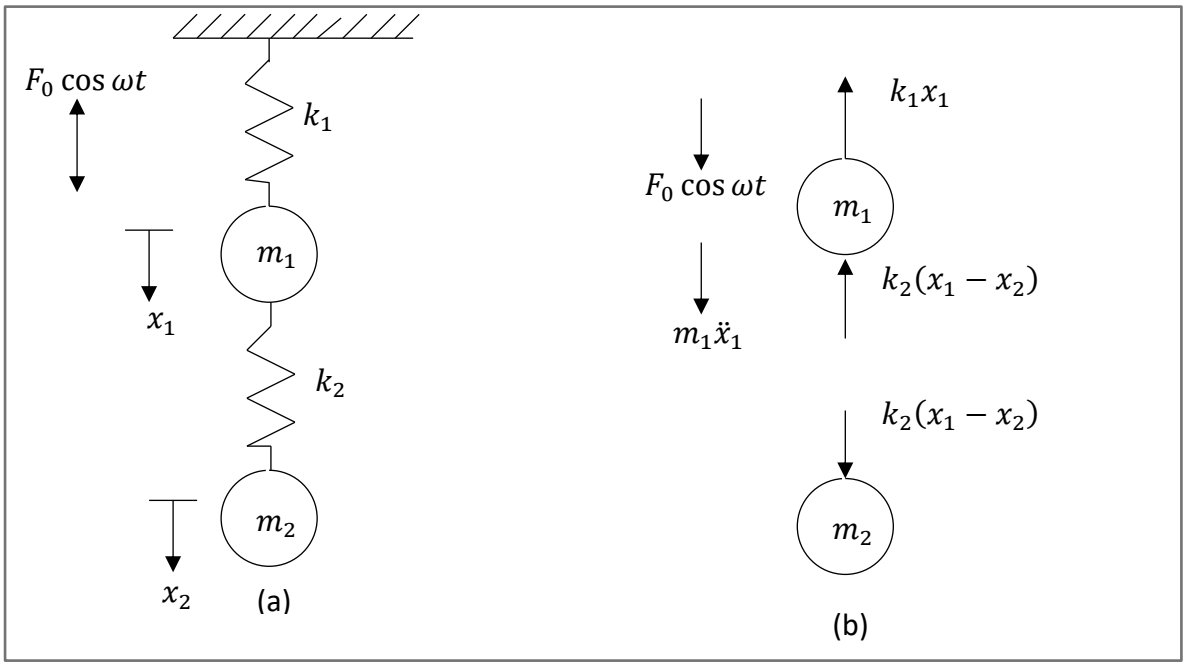


Figure 3. 10: (a) Simple two-degree of freedom model consisting of two masses connected in series by two springs. (b) Free body diagram of each mass in the system.

$$m_1\ddot{x}_1 = -k_1x_1 - k_2(x_1 - x_2) + F_0\cos\omega t \quad 3.87$$

$$m_1\ddot{x}_1 + k_1x_1 + k_2(x_1 - x_2) = F_0\cos\omega t \quad 3.88$$

$$\boldsymbol{m_1\ddot{x}_1 + (k_1 + k_2)x_1 - k_1x_2 = F_0\cos\omega t} \quad 3.89$$

$$m_2\ddot{x}_2 = k_2(x_1 - x_2) \quad 3.90$$

$$\boldsymbol{m_2\ddot{x}_2 - k_2x_1 + k_2x_2 = 0} \quad 3.91$$

Assume the solution

$$x_1(t) = A_1\cos\omega t \quad 3.92$$

$$\dot{x}_1(t) = -A_1\omega\sin\omega t \quad 3.93$$

$$\ddot{x}_1(t) = -A_1\omega^2\cos\omega t \quad 3.94$$

$$x_2(t) = A_2\cos\omega t \quad 3.95$$

$$\dot{x}_2(t) = -A_2\omega\sin\omega t \quad 3.96$$

$$\ddot{x}_2(t) = -A_2\omega^2\cos\omega t \quad 3.97$$

Using books by (Ayres, 1962, Seto, 1964, Stroud and Booth, 2001)

$$\begin{bmatrix} m_1 & 0 \\ 0 & m_2 \end{bmatrix}\begin{bmatrix} \ddot{x}_1 \\ \ddot{x}_2 \end{bmatrix} + \begin{bmatrix} (k_1 + k_2) & -k_2 \\ -k_2 & k_2 \end{bmatrix}\begin{bmatrix} x_1 \\ x_2 \end{bmatrix} = \begin{bmatrix} F_0\cos\omega t \\ 0 \end{bmatrix} \quad 3.98$$

$$\begin{bmatrix} m_1 & 0 \\ 0 & m_2 \end{bmatrix}\begin{bmatrix} -A_1\omega^2 \\ -A_2\omega^2 \end{bmatrix} + \begin{bmatrix} (k_1 + k_2) & -k_2 \\ -k_2 & k_2 \end{bmatrix}\begin{bmatrix} x_1 \\ x_2 \end{bmatrix} = \begin{bmatrix} F_0 \\ 0 \end{bmatrix} \quad 3.99$$

$$\begin{bmatrix} -m_1\omega^2 + (k_1 + k_2) & -k_2 \\ -k_2 & -m_2\omega^2 + k_2 \end{bmatrix}\begin{bmatrix} A_1 \\ A_2 \end{bmatrix} = \begin{bmatrix} F_0 \\ 0 \end{bmatrix} \quad 3.100$$

$$\text{Adjoint} = \begin{bmatrix} -m_2\omega^2 + k_2 & k_2 \\ k_2 & -m_1\omega^2 + (k_1 + k_2) \end{bmatrix} \quad 3.101$$

$$\text{Determinant} = [-m_1\omega^2 + (k_1 + k_2)]\,[-m_2\omega^2 + k_2] - [-k_2][-k_2] \quad 3.102$$

$$\begin{bmatrix} A_1 \\ A_2 \end{bmatrix} = \frac{adjoint\begin{bmatrix} F_0 \\ 0 \end{bmatrix}}{deteminant} \quad 3.103$$

$$\begin{bmatrix} A_1 \\ A_2 \end{bmatrix} = \frac{\begin{bmatrix} -m_2\omega^2 + k_2 & k_2 \\ k_2 & -m_1\omega^2 + (k_1 + k_2) \end{bmatrix}\begin{bmatrix} F_0 \\ 0 \end{bmatrix}}{[-m_1\omega^2 + (k_1 + k_2)]\,[-m_2\omega^2 + k_2] - [-k_2][-k_2]}$$

Therefore

$$\boldsymbol{A_1 = \frac{(-m_2\omega^2 + k_2)F_0}{[-m_1\omega^2 + (k_1 + k_2)]\,[-m_2\omega^2 + k_2] - [-k_2][-k_2]}} \quad 3.104$$

$$\boldsymbol{A_2 = \frac{k_2F_0}{[-m_1\omega^2 + (k_1 + k_2)]\,[-m_2\omega^2 + k_2] - [-k_2][-k_2]}} \quad 3.105$$

Therefore the displacement for $x_1$and $x_2$ are

$$x_1(t) = \frac{(-m_2\omega^2+k_2)F_0}{[-m_1\omega^2+(k_1+k_2)]\,[-m_2\omega^2+k_2]-[-k_2][-k_2]}\cos\omega t \qquad 3.106$$

$$x_2(t) = \frac{k_2F_0}{[-m_1\omega^2+(k_1+k_2)]\,[-m_2\omega^2+k_2]-[-k_2][-k_2]}\cos\omega t \qquad 3.107$$

### 3.3.5 Previous work done by other researchers on the Stockbridge Dampers

Barry et al. (2015) presented a nonlinear model dealing with the nonlinearity of the dynamics of the Stockbridge damper. The nonlinearity was from damping coefficient and geometric stretching of the messenger cable. The Stockbridge damper was modelled as two cantilevered beams with tip masses. Barry et al. (2015) used Hamilton's principle to derive the equation of motion and boundary conditions. Explicit expressions were presented for the frequency equation, modes shapes, nonlinear frequency, and modulation equations. The experimental setup and procedure were performed according to IEEE guide. The Stockbridge damper was mounted on an electrodynamic shaker (B & K 4802). Experiments were conducted to measure the damper resonant frequencies and to validate the proposed analytical model. The proposed model can be used on asymmetric and symmetric Stockbridge dampers. Numerical simulation showed that both the nonlinear frequency and vibration amplitude were significantly affected by the counterweight mass and rotary inertia. It was also noticed that the damping coefficient is an important factor in determining the influence of the geometric stretching of the messenger cable. It was discovered that the model can be used by design engineers to predict the dynamic behaviour of Stockbridge damper.

Kalombo et al. (2012) and Badibanga (2012) developed an effective mathematical model. It was describing the bending stress of a symmetrical Stockbridge damper's messenger cable close to the clamped end. During its operation, the damper's messenger cable vibrates and bending stress is developed. This can affect the performance of the Stockbridge damper. The aim of the study was to analyse the developed mathematical model describing the bending stress of the Stockbridge damper's messenger cable near the clamped end. Data from experiments agreed with that from theory (mathematical model) at resonance frequency.

Results show that the model can be used to predict the stress at resonance frequency (Kalombo et al., 2012, Badibanga, 2012) .

Standard Stockbridge dampers are designed so that their mechanical impedance matches as closely as possible the optimum damper impedance determined for the cable to be protected (Markiewicz, 1995). Since the optimum impedance is calculated assuming that the cable is clamped at its extremity, the optimally tuned standard dampers will work efficiently only when they are mounted near suspension clamps. In some spans, however, conductors are connected to the tower by means of special tension equipment which may affect the efficiency of the mounted standard damper. Analysis were done to show that the optimum damper impedance required for such spans (called Dead-end spans) differs significantly from the optimum impedance of the standard damper. Markiewicz (1995) presented a method and computational model for the evaluation of the optimum dynamic characteristics of Stockbridge dampers to be mounted near tension insulator assemblies. It also shows how the efficiency of a standard damper used in such spans may be improved by its proper location.

Experimental measurement campaign was conducted with a modified dynamometric Stockbridge damper clamped to a laboratory test span (Diana et al., 2003). The goal was to get the force and the torque exerted between the cable and the damper on a span. Three tests were done to get the needed parameters: cable self-damping tests, tests with the Stockbridge damper clamped on the shaker, and tests on the span equipped with the dynamometric damper (Diana et al., 2003).

All the design parameters that influenced the Stockbridge damper model were undertaken using the design sensitivity analysis of a Stockbridge damper (Kim, 2017). Using partial derivatives of the functions of two eigenvalues with respect to each design parameter the design sensitivity equations were formulated; the contribution of each variable was determined according to the partial derivatives with respect to the concerned variable. The possibility of the sensitivity analysis result was validated using a simple model of a Stockbridge damper and modifying the value of each parameter by up to 30 % from the baseline (Kim, 2017). Based on the simulation results the design guidelines for a Stockbridge damper were then established

Vaja et al. (2018) developed an analytical model of an unusual vibration damper with an increased number of resonant frequencies of the damper. The 3D finite element was also developed to validate the result of an analytical model. Experiments were not conducted (Vaja et al., 2018). This research focuses on doing experiments and the development of an analytical model of an asymmetric damper which was not done by the other researchers. Experiment is also conducted in changing the geometry of the counterweight of the damper.

# CHAPTER 4

# MATERIAL AND METHOD

## 4.1 Equipment

This chapter describes the equipment used and the procedure followed in conducting the tests carried out at the vibration research and testing facility at the University of KwaZulu-Natal. The vibration system is composed of important components shown in Figure 4.1. It consist of:

- An electro-dynamic shaker (TIRA Model, Type TV 56263/LS-340) for providing an input force to the damper.
- An amplifier to control the voltage or current to the shaker.
- A control system (known as a computer controlled data acquisition system)
- A compressor for load protection
- Ten (10) asymmetric Stockbridge dampers of various sizes.

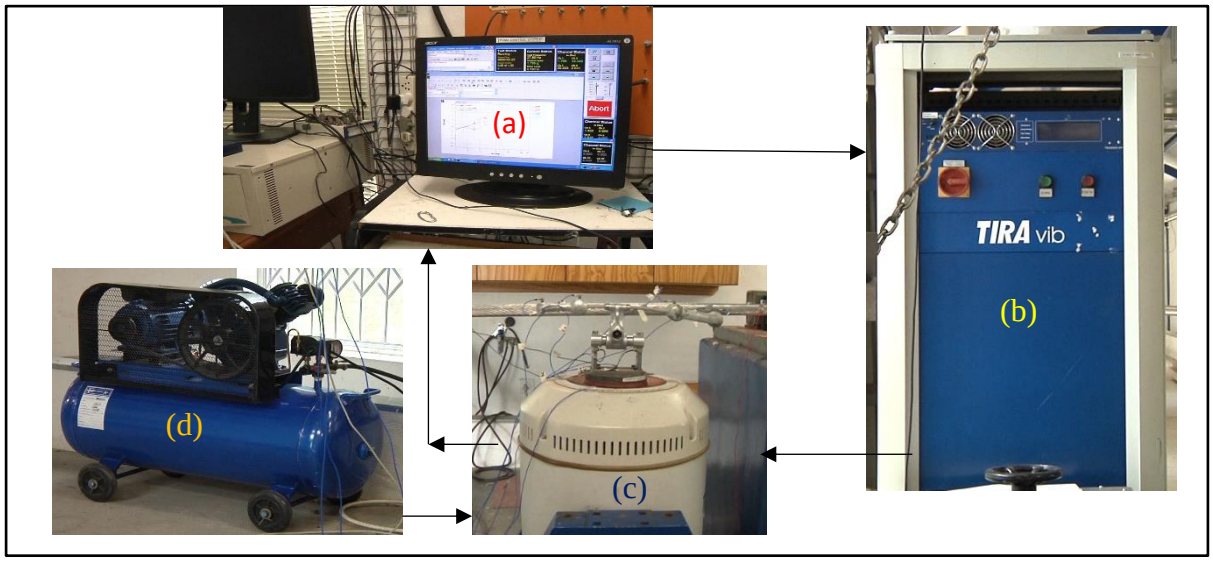


Figure 4. 1: Components of the vibration test system on the shaker base. (a) controller. (b) Amplifier. (c) Shaker, asymmetric damper and accelerometers. (d) Compressor.

## 4.2 Experimental setup

The procedure used for the force response test is presented in figure 4.3 and experimental setup made with the following units:

- Mount the jig on the shaker
- Mount two transducers on each support of the jig
- Mount the Damper in an upright position in the middle of the rigid bar of the jig
- Stick one accelerometer on the shaker base for control
- Stick two accelerometers using glue on each damper's weights as shown in figure 4.2
- Make a sweep at constant velocity of 0.1 m/s in the frequency range between 5 – 300 Hz (to cover a broad spectrum of frequencies) for 30 minutes.
- Repeat the experiment for each damper following the same procedure.
- 30 tests of Stockbridge Dampers will be tested and statistical methods will be used.
- After collecting the data obtain the graph of amplitude vs frequency representing the characteristic of asymmetrical Stockbridge Damper

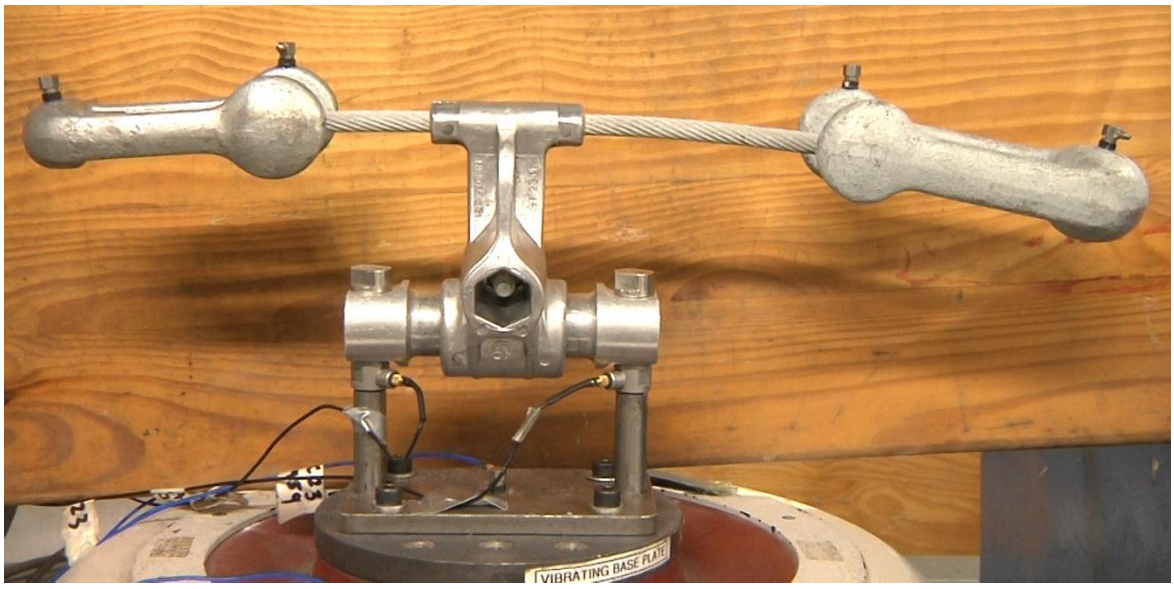


Figure 4. 2: Asymmetric Stockbridge damper with four accelerometers

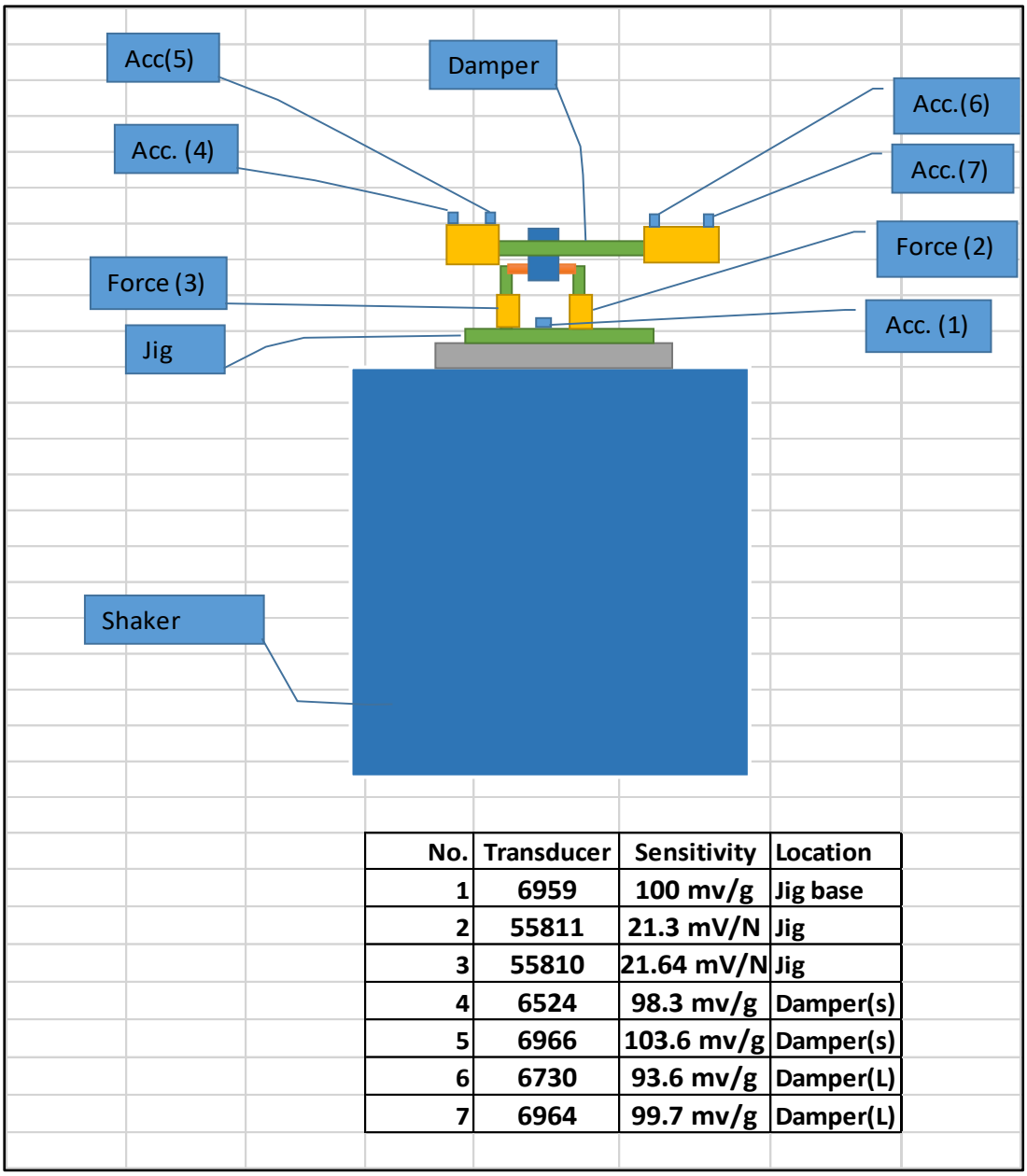


| No. | Transducer | Sensitivity | Location |
|---|---|---|---|
| 1 | 6959 | 100 mv/g | Jig base |
| 2 | 55811 | 21.3 mV/N | Jig |
| 3 | 55810 | 21.64 mV/N | Jig |
| 4 | 6524 | 98.3 mv/g | Damper(s) |
| 5 | 6966 | 103.6 mv/g | Damper(s) |
| 6 | 6730 | 93.6 mv/g | Damper(L) |
| 7 | 6964 | 99.7 mv/g | Damper(L) |

Figure 4. 3: Experimental setup used in the current study

# CHAPTER 5

# EXPERIMENTAL RESULTS AND DISCUSSIONS

## 5.1 Introduction

This chapter presents the results of the thirty tests conducted on three different sets of asymmetrical dampers and the analyses of the results obtained. The resonant frequencies and amplitudes were presented for the various configurations of asymmetrical damper.

The following three sets of dampers were tested:

- Damper (182 025-301) Ø31 – 39 mm :4 of them set A
- Damper (182 025-401) Ø39 – 47mm :3 of them set B
- Damper (182 025-101) Ø7 – 15 mm :3 of them set C
- In total the number of dampers is ten (10) and each damper to be tested three times which makes thirty tests to be done for statistical consideration

## 5.2 Experimental results for set A Stockbridge Damper no. 1 (182 025-301) Ø31 – 39 mm

The following results are related to the set A damper 1 (182 025-301) Ø31 – 39 mm. There were 4 of them as mentioned before; however in this section only one sample shown tested in triplicate. The remaining results of set A are attached in appendix A

### 5.2.1 Discussions for damper 1 (182 025-301) Ø31 – 39 mm of set A

5.2.1.1 There are effectively 4 masses on the Stockbridge damper therefore the damper is a four degrees of freedom as shown in Figure 5.1;

5.2.1.2 From the big mass, it is observed that it vibrates at 8 Hz with an amplitude of 0.6 G and 1 G as shown in Figure 5.2;

5.2.1.3 From the big mass, it is also observed to vibrate at 50 Hz with an amplitude of 1.9 G and 5 G as shown in Figure 5.2;

5.2.1.4 Each mass has a two degrees of freedom ( inner and outer part) as shown in Figure 5.1;

5.2.1.5 At resonance, or maximum peak it has a frequency of 8 Hz and 50 Hz corresponding to the bigger mass as shown in Figure 5.2;

5.2.1.6 Figure 5.5 and 5.6 show the first and second modes of the bigger mass during operation;

5.2.1.7 From the small mass, it is observed that it vibrates at 22 Hz with an amplitude of 1.9 G and 4 G (log) as shown is Figure 5.3;

5.2.1.8 From the same small mass it also vibrates at 70 Hz with an amplitude of 4 G and 10 G (log) as shown in Figure 5.3;

5.2.1.9 At resonance, or maximum peak it has 22 Hz, 70 Hz corresponding to the small mass;

5.2.1.10 Figure 5.7 and 5.8 show the first and second modes of the small mass during operation;

5.2.1.11 The Stockbridge damper has resonance frequencies at 8 Hz, 22 Hz, 50 Hz and 70 Hz;

5.2.1.12 The Stockbridge damper is a mass vibration absorber;

5.2.1.13 At any other frequencies except 8 Hz, 22 Hz, 50 Hz and 70 Hz the damper is not a mass absorber;

5.2.1.14 Statistics: 30 experiments to increase significant or confidence level of results or certainty, normal distribution.

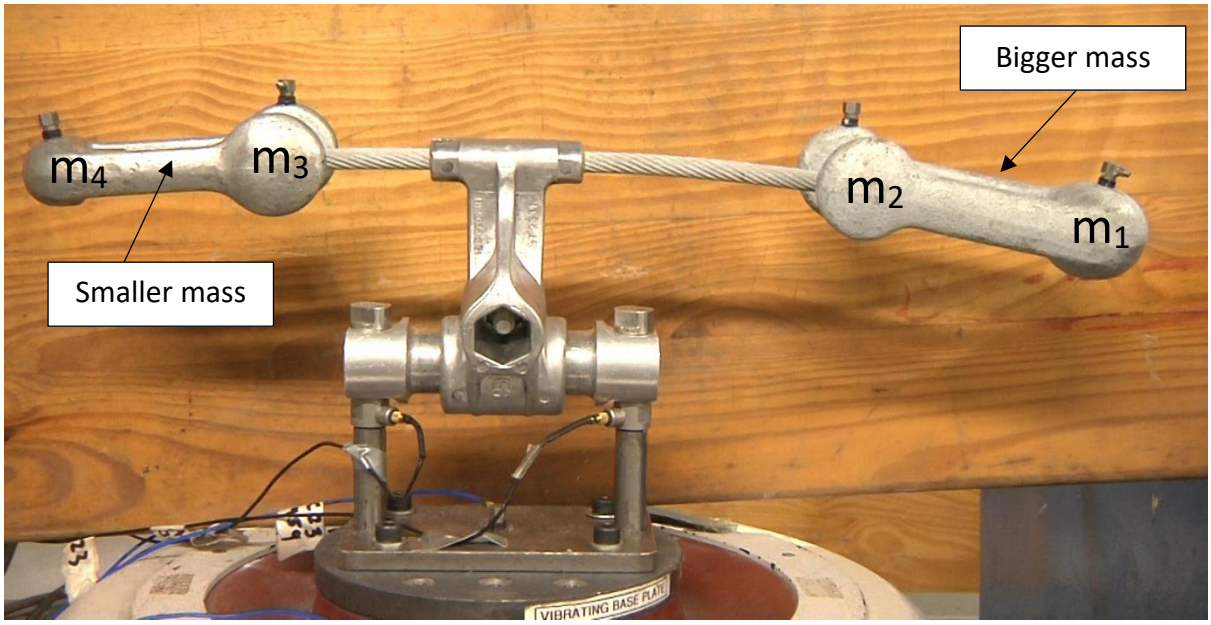


Figure 5. 1**:** The asymmetric Stockbridge damper is a four degrees of freedom

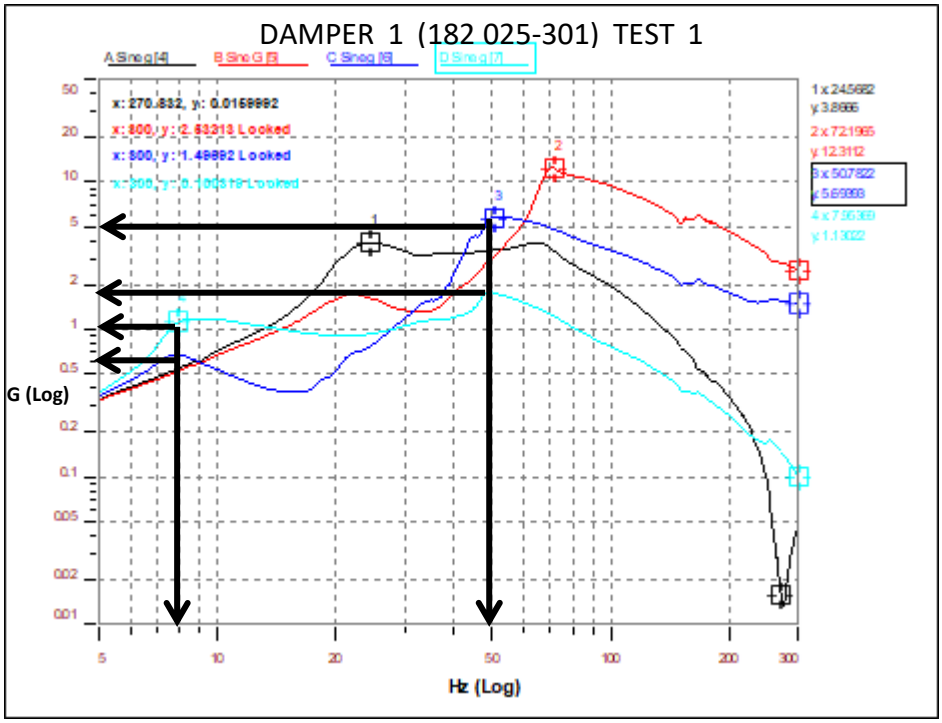


Figure 5. 2**:** The graph of acceleration amplitude G (log) vs Hz (log)

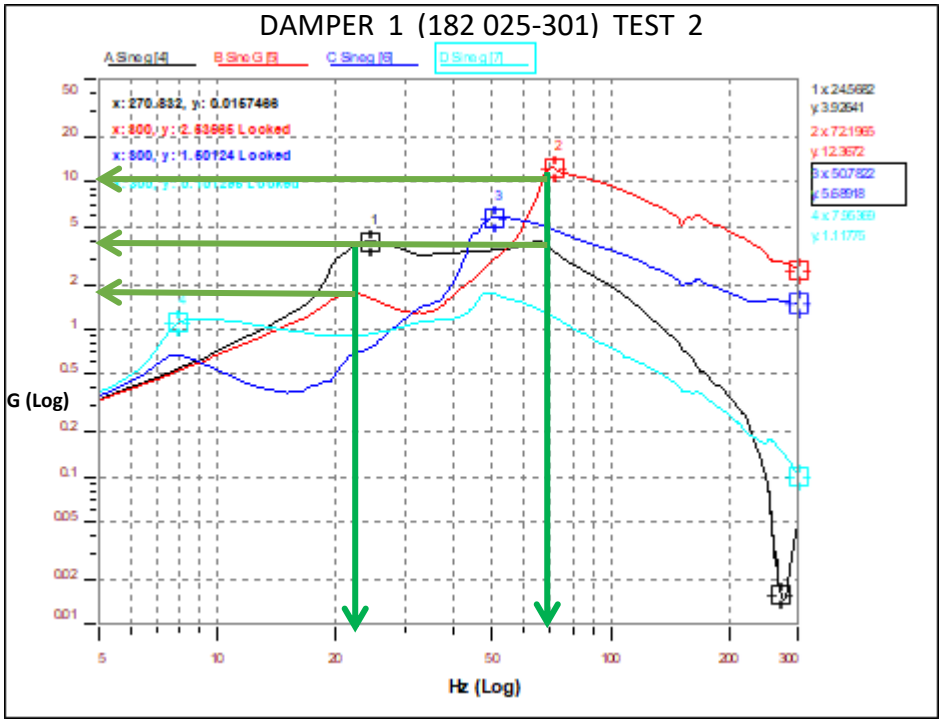


Figure 5. 3**:** The graph of acceleration amplitude G (log) vs Hz (log)

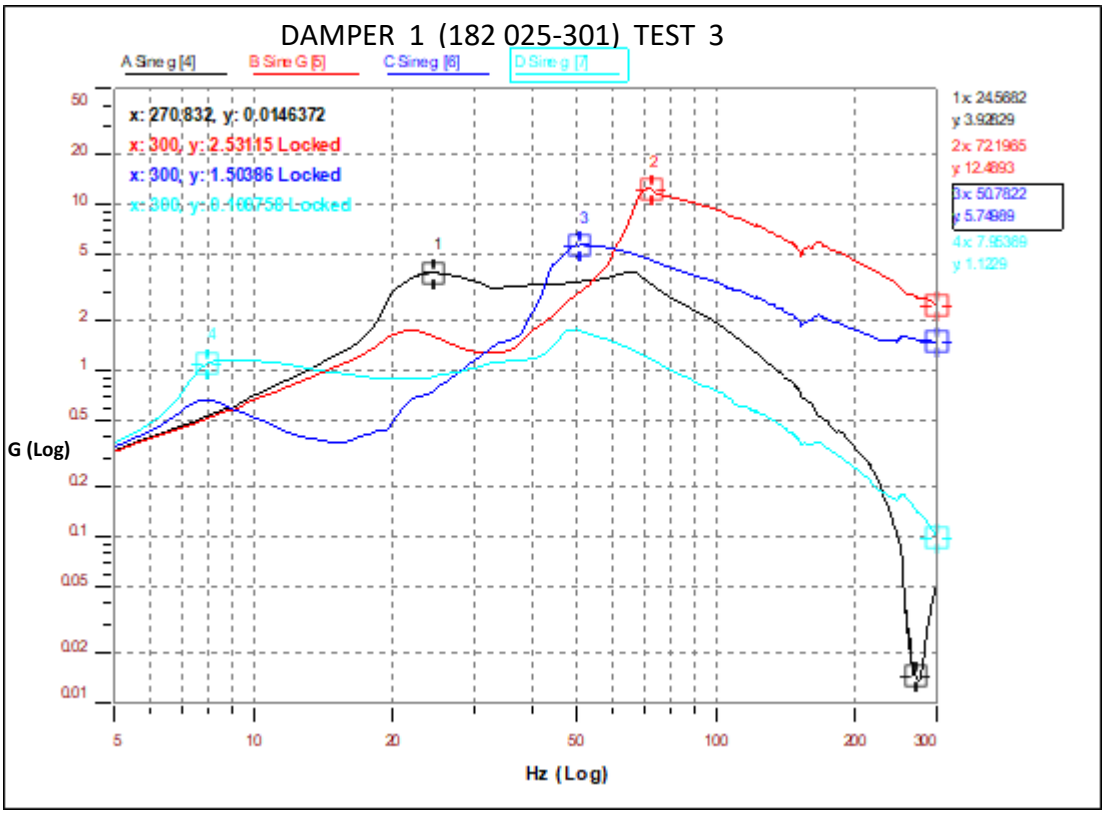


Figure 5. 4**:** The graph of acceleration amplitude G (log) vs Hz (log)

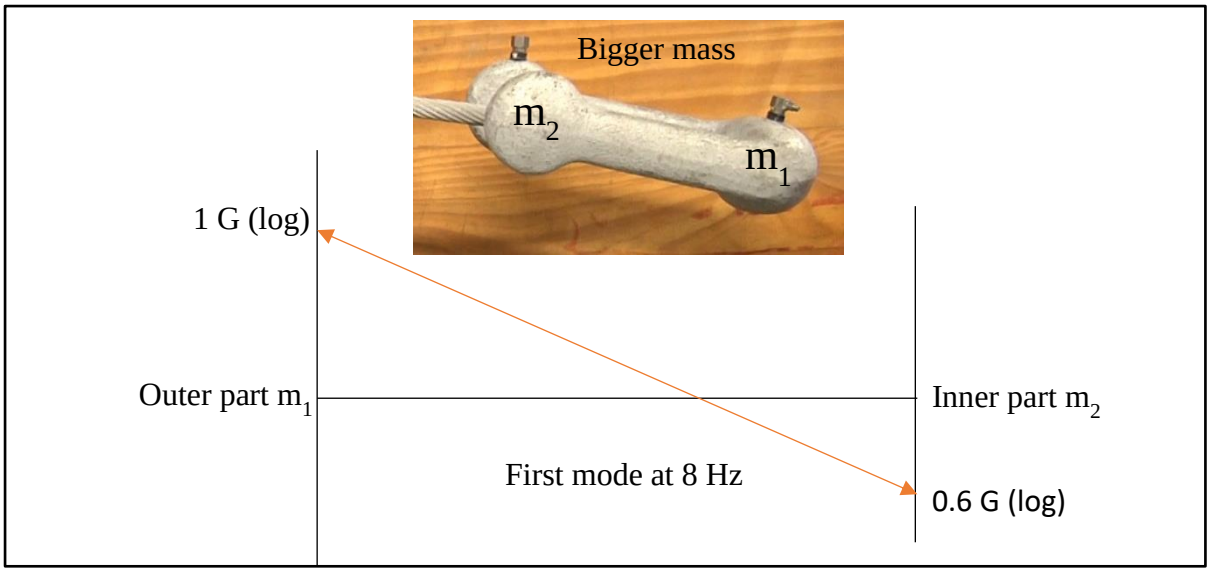


Figure 5. 5: Bigger mass of the Stockbridge damper (first mode at 8 Hz)

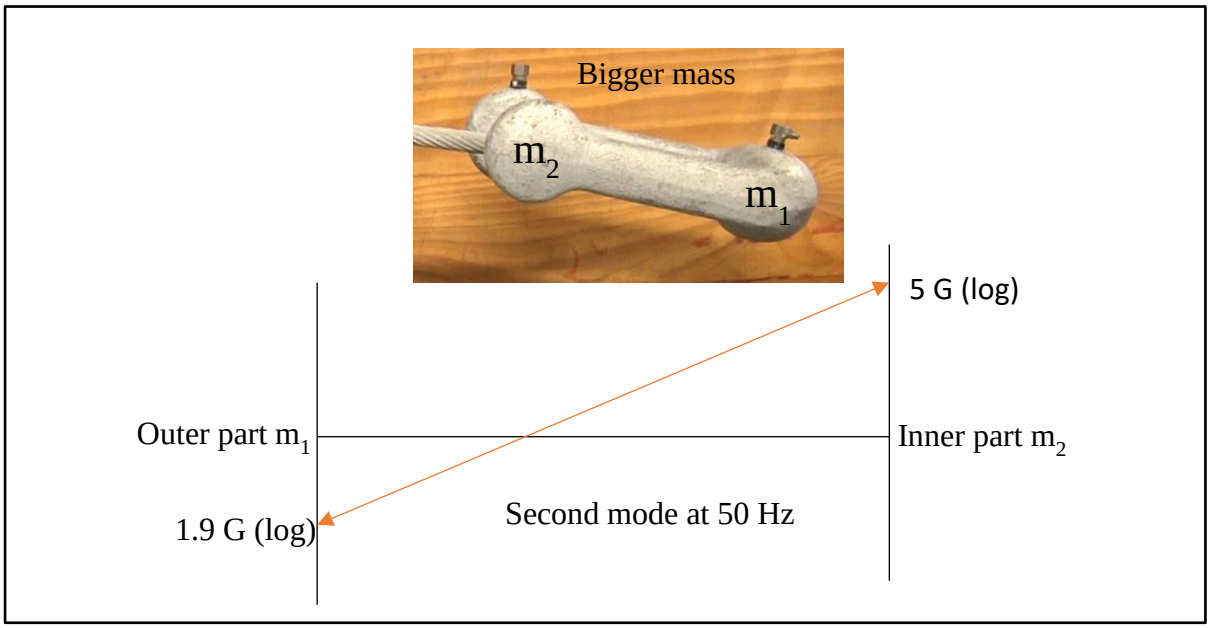


Figure 5. 6: Bigger mass of the Stockbridge damper (second mode at 50 Hz)

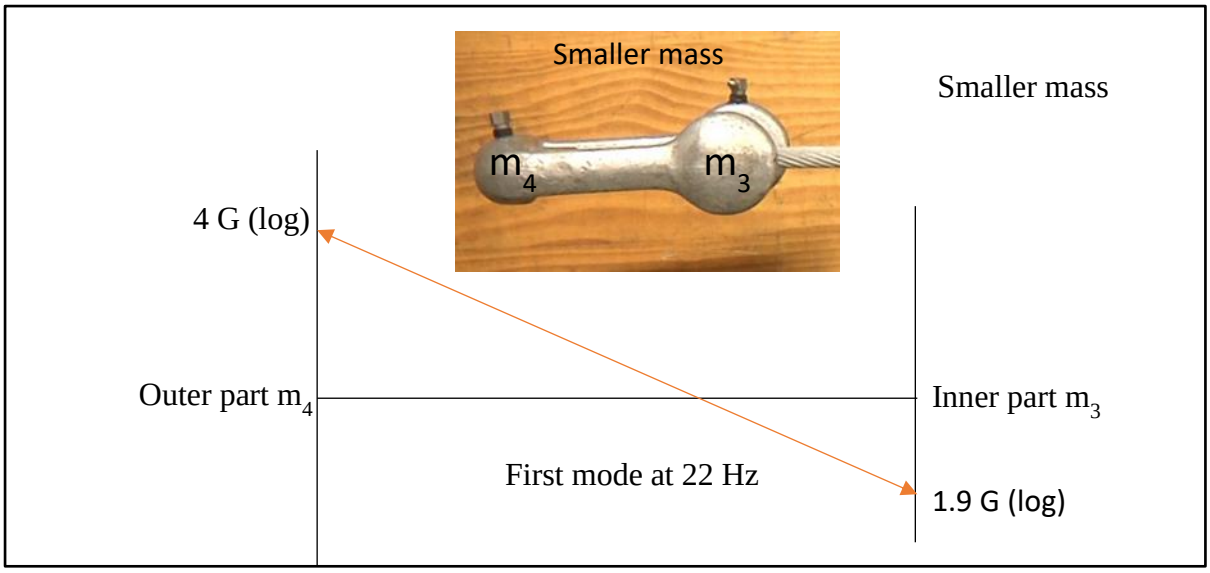


Figure 5. 7: Smaller mass of the Stockbridge damper (first mode at 22 Hz)

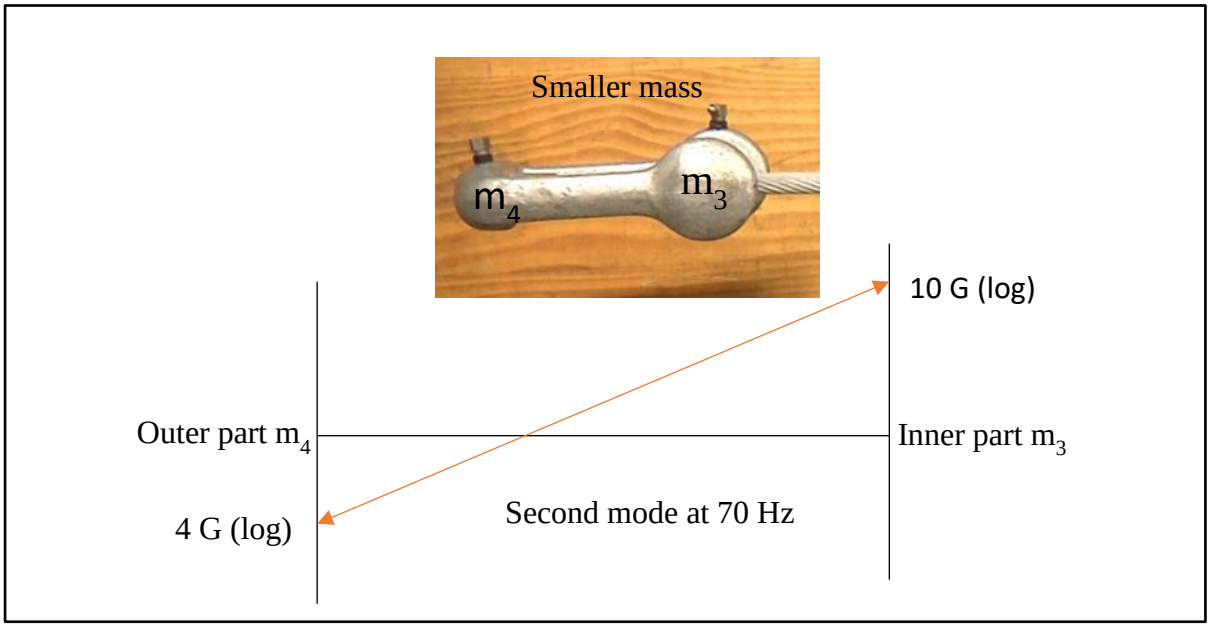


Figure 5. 8: Smaller mass of the Stockbridge damper (second mode at 70 Hz)

## 5.3 Experimental results for set B Stockbridge Damper no. 5 (182 025-401) Ø39 – 47mm

The following results are related to the set B of damper no.5 (182 025-401). There were 3 of them as mentioned before, however in this section only one sample of damper (182 025-401) tested in triplicate. The remaining results of set B are attached in appendix B

### 5.3.1 Discussions for set B damper 5 (182 025-401) Ø39 – 47mm

5.3.1.1 Everything is the same for damper 5 (182 025-401) Ø39 – 47 mm set B if it is compared to damper 1 (182 025-301) Ø31 – 39 mm set A discussed previously in terms of results. The only thing that differs is the frequency, the amplitude for the first mode and second mode of the bigger mass and the small mass.

5.3.1.2 From the big mass, it is observed that it vibrates at 6.2 Hz with an amplitude of 0.5 G and 1.2 G (log) as shown in Figure 5.9;

5.3.1.3 From the big mass, it is also observed to vibrate at 26 Hz with an amplitude of 1 G and 4 G (log) in Figure 5.9;

5.3.1.4 Table 5.1 presents the first and the second modes of the bigger mass;

5.3.1.5 From the small mass, it is observed that it vibrates at 14 Hz with an amplitude of 1 G and 2.8 G (log) as shown is Figure 5.10;

5.3.1.6 From the same small mass it also vibrates at 52 Hz with an amplitude of 1.8 G and 12 G (log) as shown in Figure 5.10;

5.3.1.7 Table 5.2 presents the first and the second modes of the smaller mass;

5.3.1.8 The Stockbridge damper has resonance frequencies at 6.2 Hz, 26 Hz, 14 Hz and 52 Hz;

5.3.1.9 At any other frequencies except 6.2 Hz, 14 Hz, 26Hz and 52 Hz the damper is not a mass absorber.

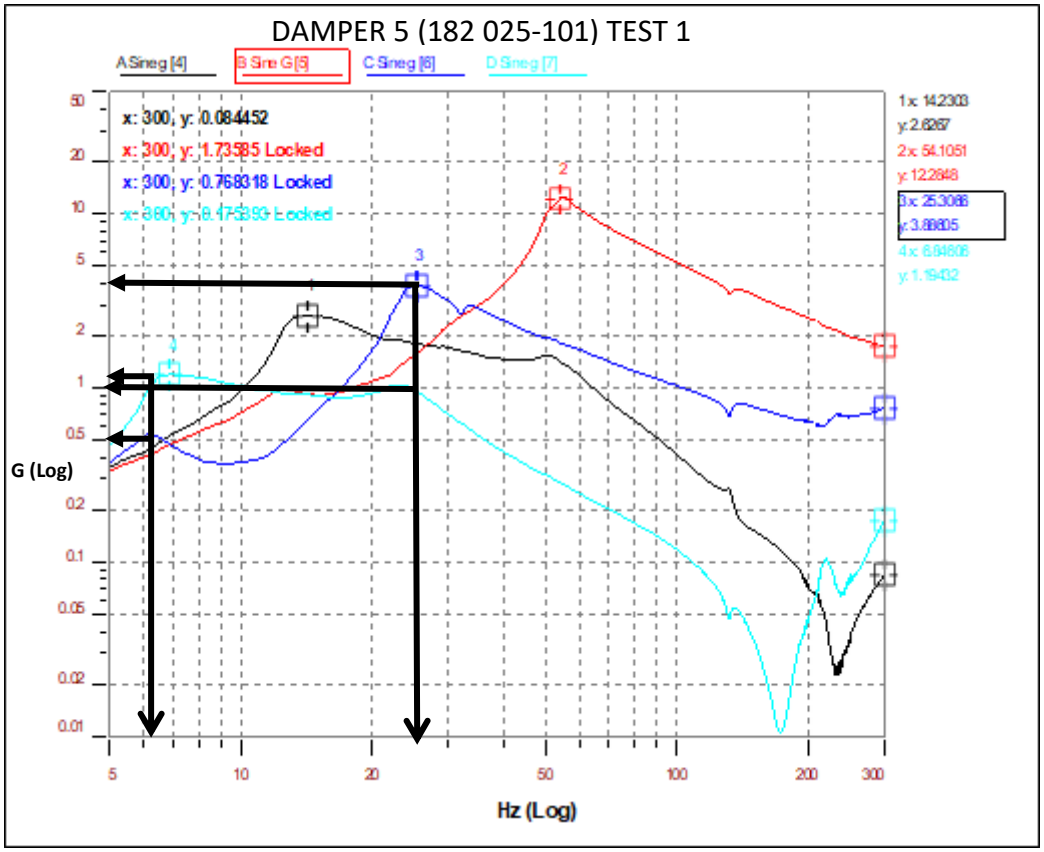


Figure 5. 9**:** The graph of acceleration amplitude G (log) vs Hz (log)

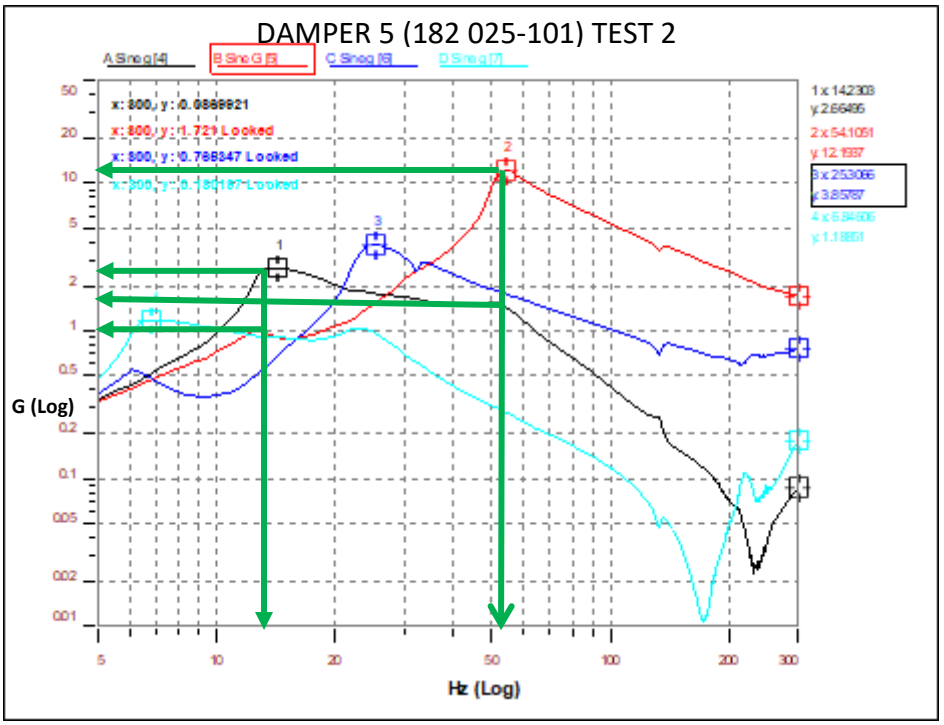


Figure 5. 10**:** The graph of acceleration amplitude G (log) vs Hz (log)

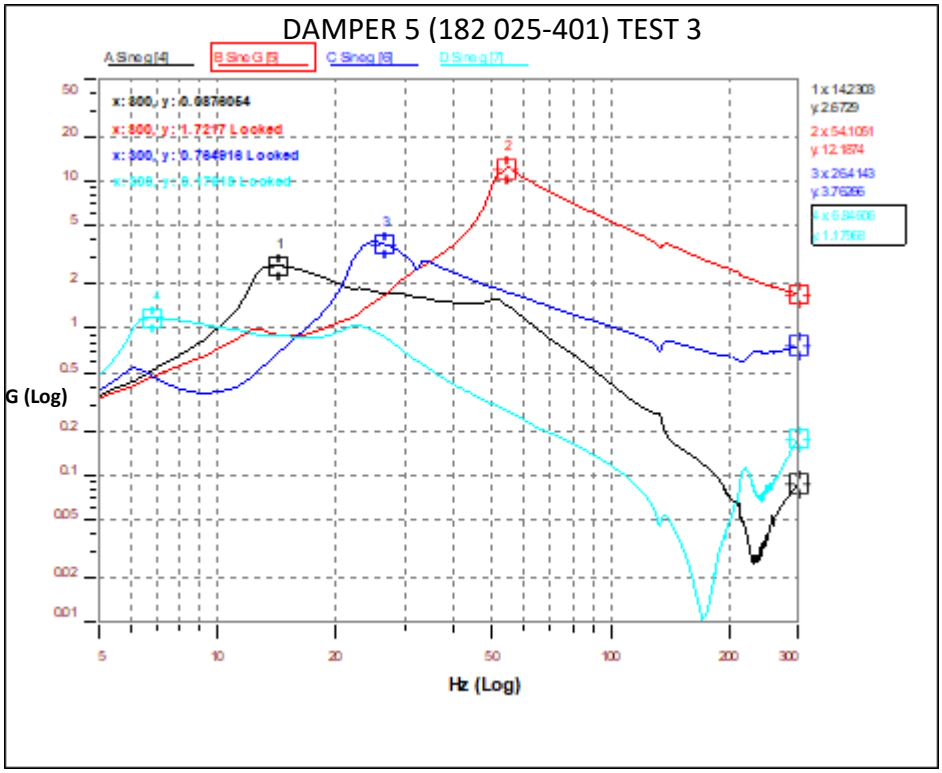


Figure 5. 11**:** The graph of acceleration amplitude G (log) vs Hz (log)

Table 5.1**:** Represents the first and second modes of the bigger mass of damper 5 (182 025-401) Ø39 – 47mm.

| **Bigger mass first mode** | |
|---|---|
| frequency | 6.2 Hz (log) |
| Amplitude | 0.5 G and 1.2 G (log) |
| **Bigger mass second mode** | |
| frequency | 26 Hz (log) |
| amplitude | 1 G and 4 G (log) |

Table 5.2**:** Represents the first and second modes of the smaller mass of damper 5 (182 025-401) Ø39 – 47mm.

| **Smaller mass first mode** | |
|---|---|
| frequency | 14 Hz (log) |
| Amplitude | 1 G and 2.8 G (log) |
| **Smaller mass second mode** | |
| frequency | 52 Hz (log) |
| amplitude | 1.8 G and 12 G (log) |

## 5.4 Experimental results for set C Stockbridge Damper no. 8 Damper (182 025-101) Ø7 – 15 mm

The following results are related to the set C of damper 10 (182 025-101). There were 3 of them as mentioned before, however in this section only one sample of damper (182 025-101) tested in triplicate. The remaining are attached in appendix C

### 5.4.1 Discussions for set C damper 8 (182 025-101) Ø7 – 15 mm

5.4.1.1 Everything is the same for damper no 8 (182 025-101) Ø7 – 15 mm set C if it is compared to sets A and B discussed previously in terms of results. The only thing that differs is the frequency, the amplitude for the first mode and second mode of the bigger mass and the small mass.

5.4.1.2 From the big mass, it is observed that it vibrates at 15 Hz with an amplitude of 1.1 G and 2 G (log) as shown in Figure 5.12

5.4.1.3 From the big mass, it is also observed to vibrate at 70 Hz with an amplitude of 3 G and 10 G (log) in Figure 5.12

5.4.1.4 Table 5.3 presents the first and the second modes of the bigger mass;

5.4.1.5 From the small mass, it is observed that it vibrates at 30 Hz with an amplitude of 2.4 G and 4 G (log) as shown is Figure 5.13;

5.4.1.6 From the same small mass it also vibrates at 190 Hz with an amplitude of 7 G and 40 G (log) as shown in Figure 5.13;

5.4.1.7 Table 5.4 presents the first and the second modes of the smaller mass;

5.4.1.8 The Stockbridge damper has resonance frequencies at 15 Hz, 30 Hz, 70 Hz and 190 Hz;

5.4.1.9 At any other frequencies except 15 Hz, 30 Hz, 70 Hz and 190 Hz the damper is not a mass absorber

DAMPER 8 (182 025-101) Ø7 – 15 mm

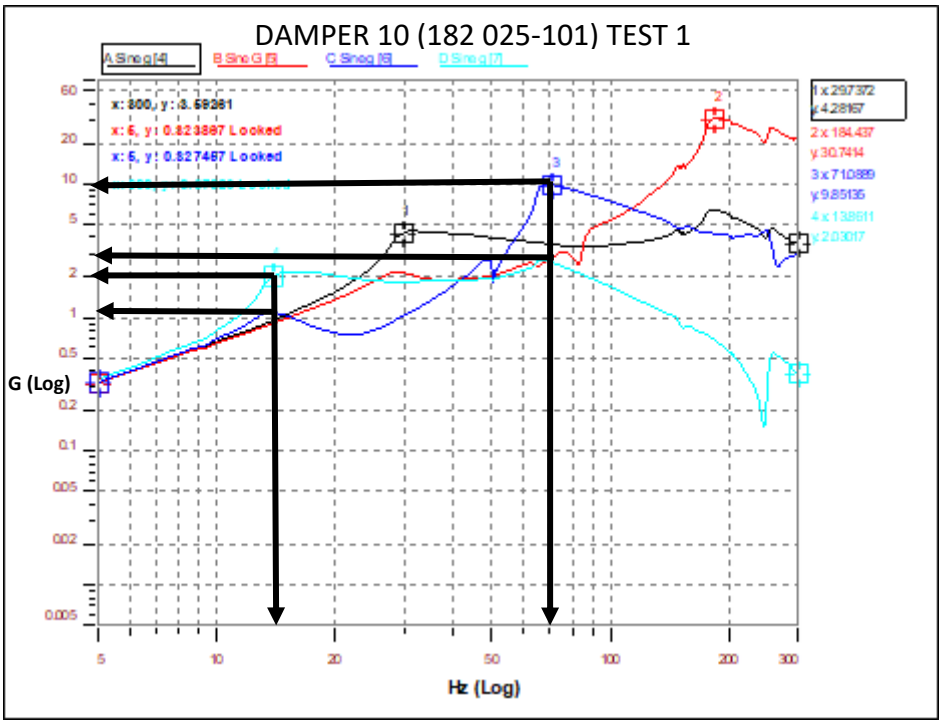


Figure 5. 12**:** The graph of acceleration amplitude G (log) vs Hz (log)

DAMPER 8 (182 025-101) Ø7 – 15 mm

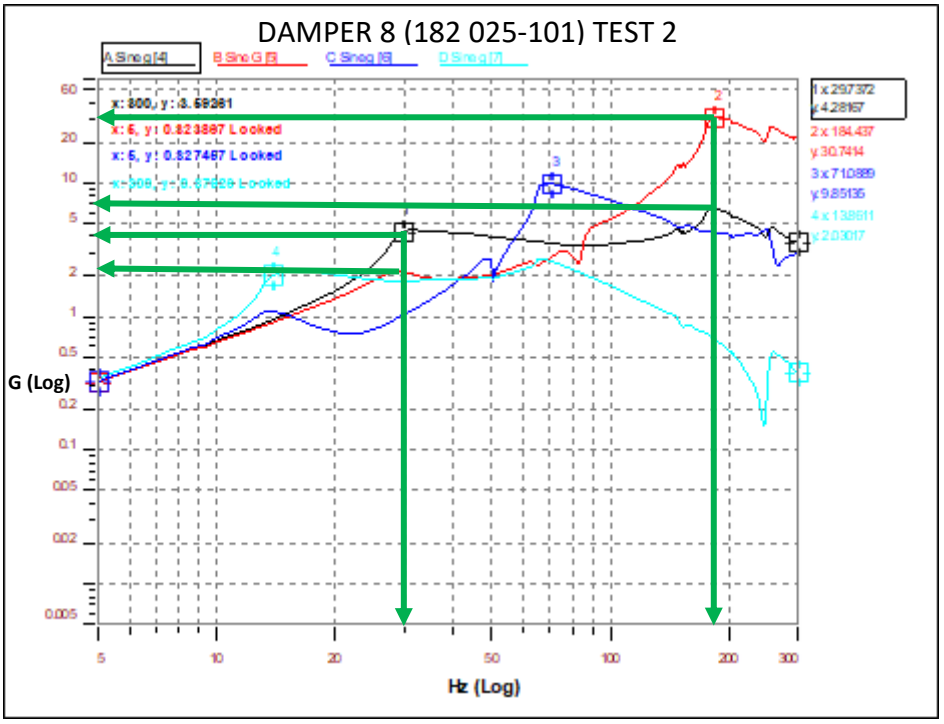


Figure 5. 13**:** The graph of acceleration amplitude G (log) vs Hz (log)

DAMPER 8C (182 025-101) Ø7 – 15 mm

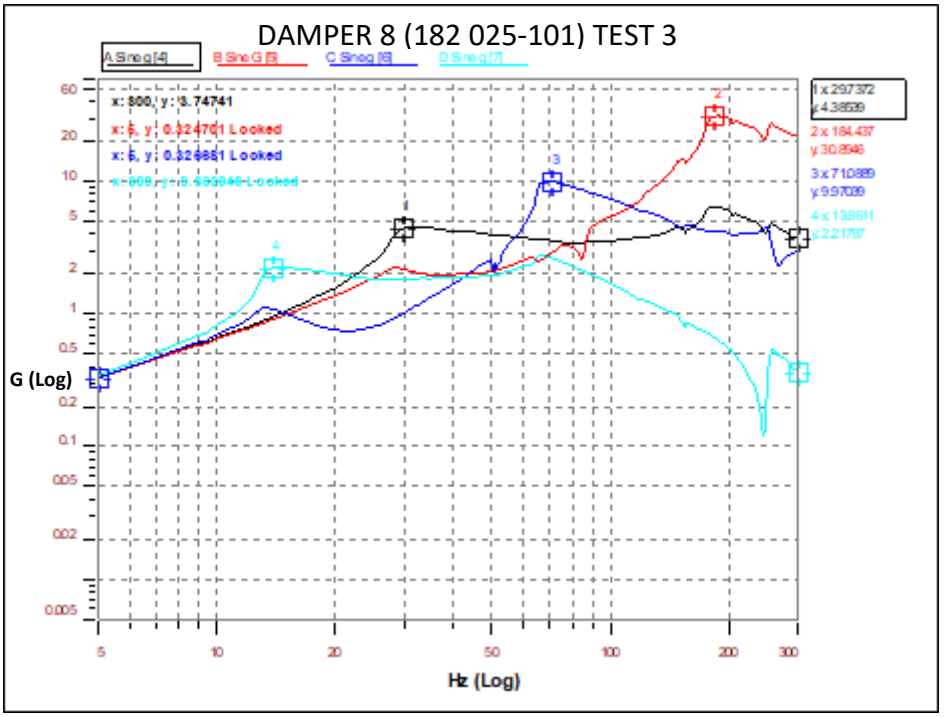


Figure 5. 14**:** The graph of acceleration amplitude G (log) vs Hz (log)

Table 5.3**:** Represents the first and second modes of the bigger mass of damper 8 (182 025-101) Ø7 – 15 mm.

| **Bigger mass first mode** | |
|---|---|
| frequency | 15 Hz (log) |
| Amplitude | 1.1 G and 2 G (log) |
| **Bigger mass second mode** | |
| frequency | 70 Hz (log) |
| amplitude | 3 G and 10 G (log) |

Table 5.4**:** Represents the first and second modes of the smaller mass of damper 8 (182 025-101) Ø7 – 15 mm.

| **Smaller mass first mode** | |
|---|---|
| frequency | 30 Hz (log) |
| Amplitude | 2.4 G and 4 G (log) |
| **Smaller mass second mode** | |
| frequency | 190 Hz (log) |
| amplitude | 7 G and 40 G (log) |

## 5.5 Additional experiments.

### 5.5.1 Introduction

Another set of experiments was conducted with two accelerometers on the inner part of each mass of the Stockbridge damper as shown in Figure 5.15. This was aiming to check if there is rotational motion on each mass of the Stockbridge damper during its operation. Three tests were conducted for each Stockbridge (182 025-301) and (182 025-401). The remaining results are attached in appendix D. The experimental procedure has not changed the only change is that each mass of the damper has two accelerometers on the inner part of the smaller and bigger mass.


Figure 5. 15**:** The asymmetric Stockbridge damper with two accelerometers on the inner part of each mass.

### 5.5.2 Discussion for damper (182 025-301) and (182 025-401)

On Figure 5.16 and 5.17 the graphs of the inner accelerometers are moving together showing that there is no rotational motion. This is to confirm that there was no rotation of the dampers about the messenger wire and only up and down vertical motion of the dampers due to the shaker applied force were observed and only vertical motion will be necessary for the mathematical models, thereby ignoring rotation.

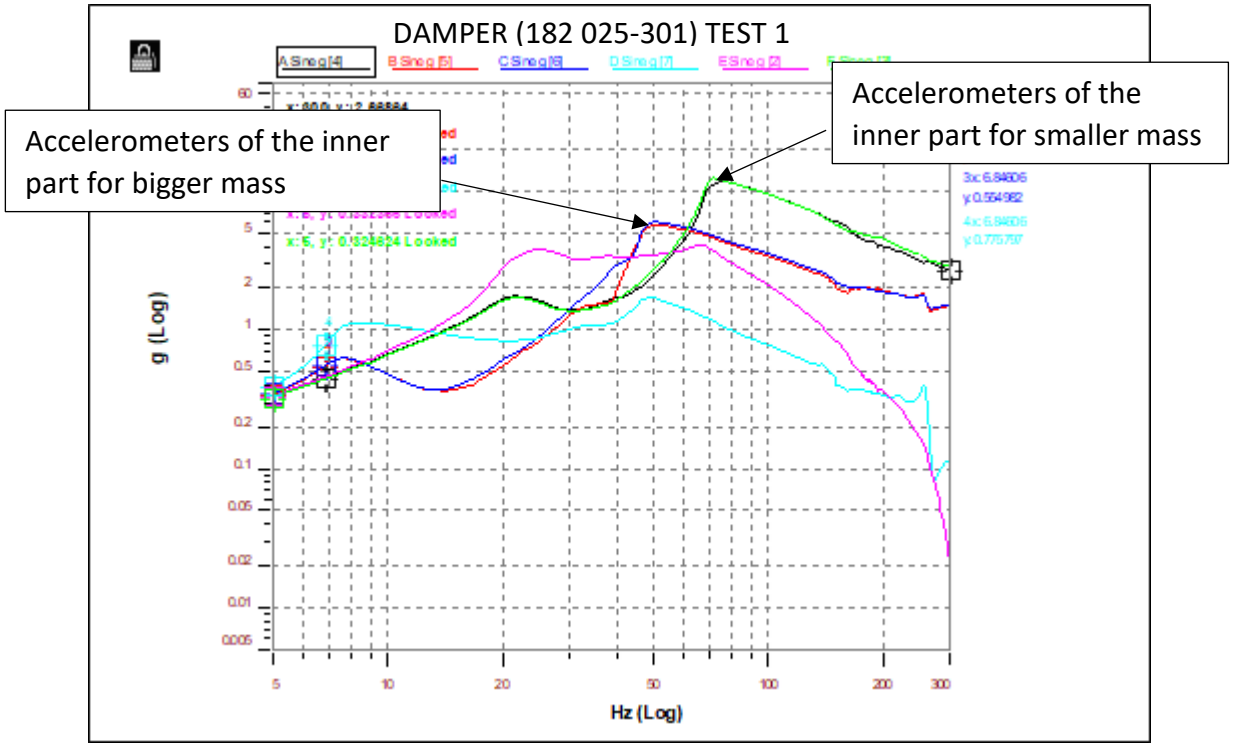


Figure 5. 16**:** The graph of acceleration amplitude G (log) vs Hz (log)

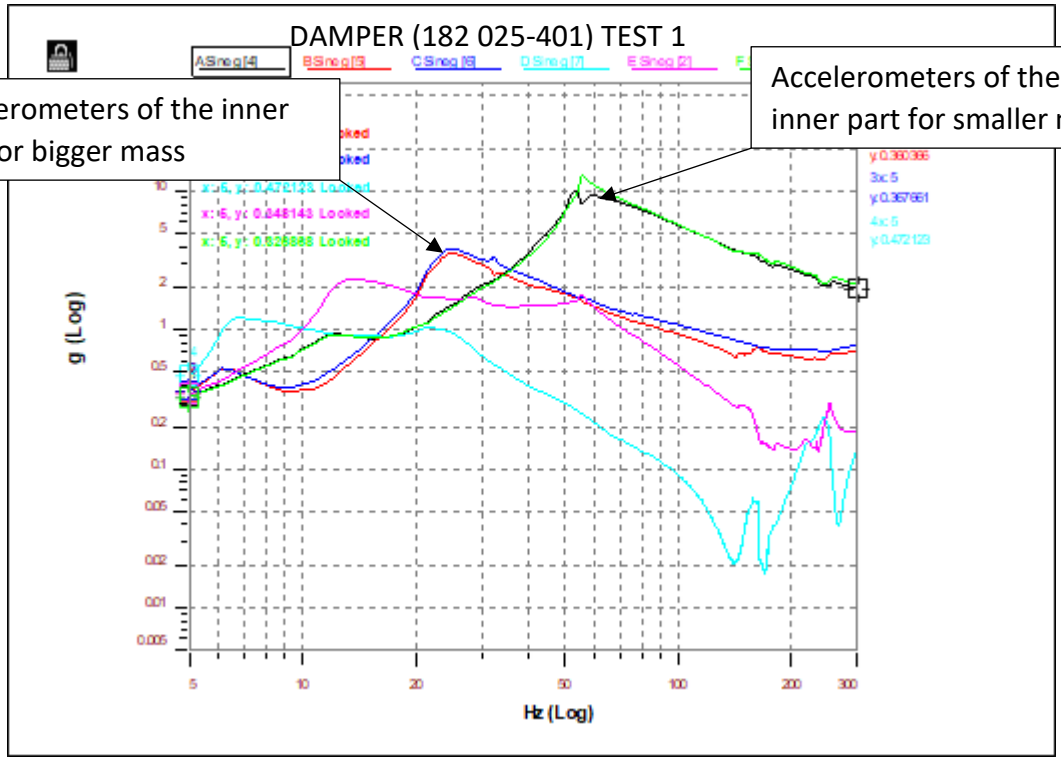


Figure 5. 17**:** The graph of acceleration amplitude G (log) vs Hz (log)

## 5.6 Introduction

The number of resonant frequencies produced by the Stockbrigde damper are very significant and they characterize the effectiveness of it. A set of experiments was conducted by adding a mass on each one side of the inner part of the damper as shown in Figure 5.18. The first experiment was conducted by adding a mass of 57.5 g and 100 g on each side of the inner part. The second experiment was done by doubling the masses.

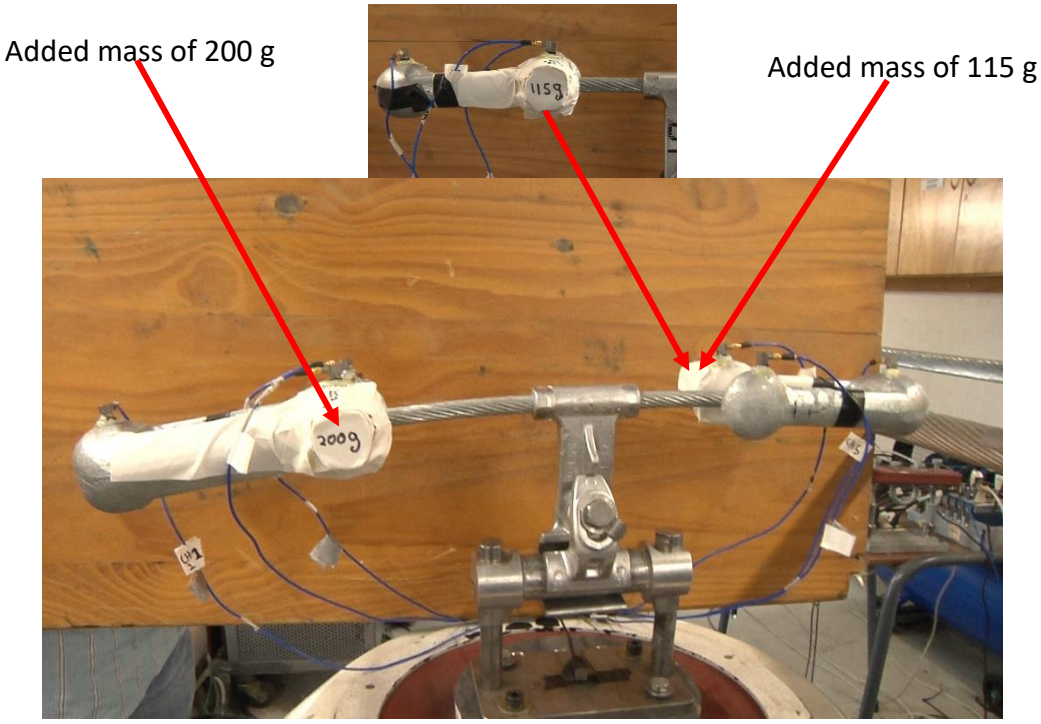


Figure 5. 18**:** The asymmetric Stockbridge damper with added masses on each side inner part of each mass.

### 5.6.1 Discussion for damper (182 025-401)

The two graphs on Figure 5.19 and 5.20 are the results of the experiment conducted when the inner part of the asymmetric Stockbrigde damper is changed by adding masses as shown in Figure 18. This shows that the damper is a six degree of freedom and has six resonant frequencies

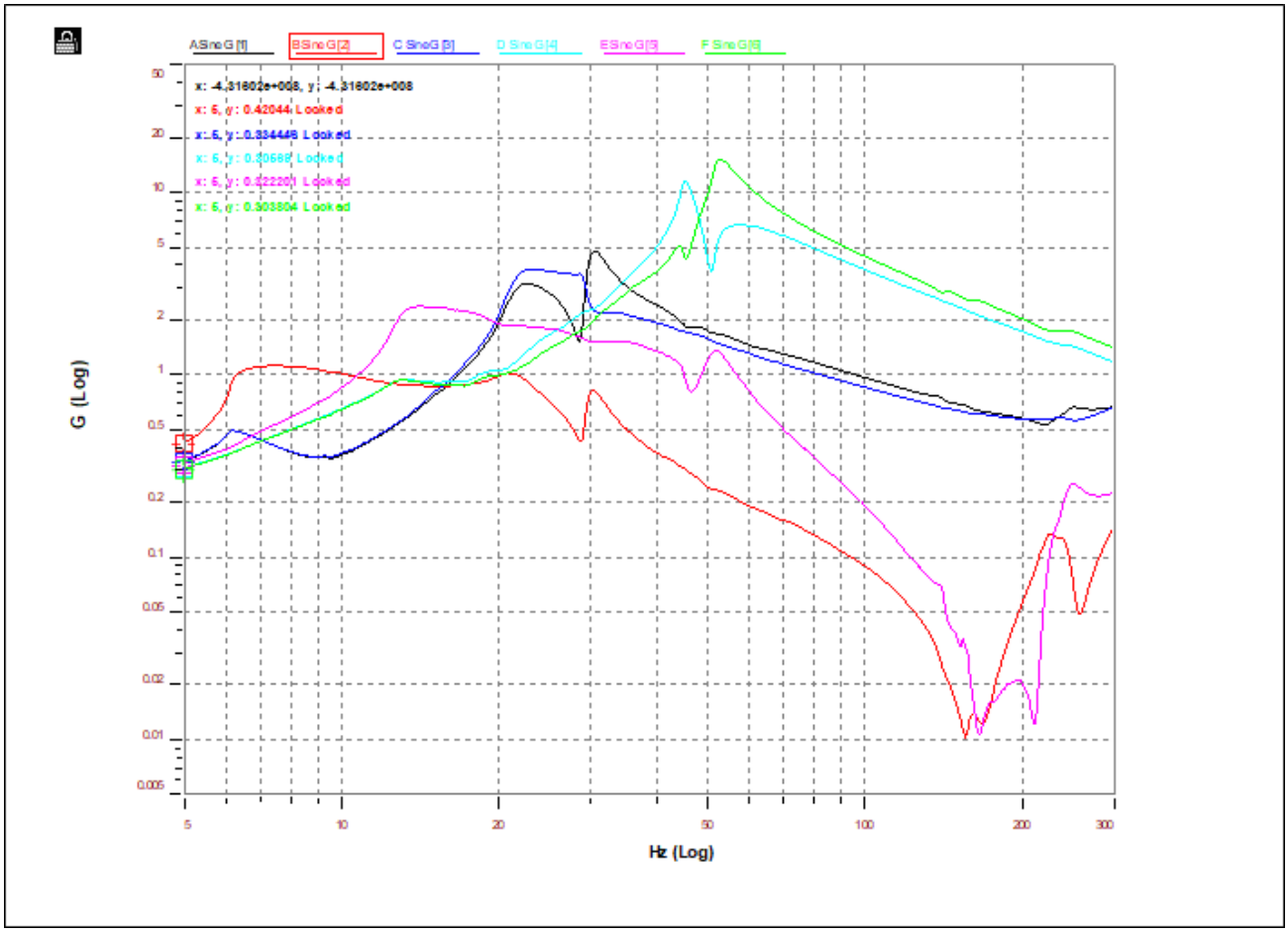


Figure 5. 19**:** The asymmetric Stockbridge damper with added masses of 57.5 g and 100 g on each side inner part of each mass.

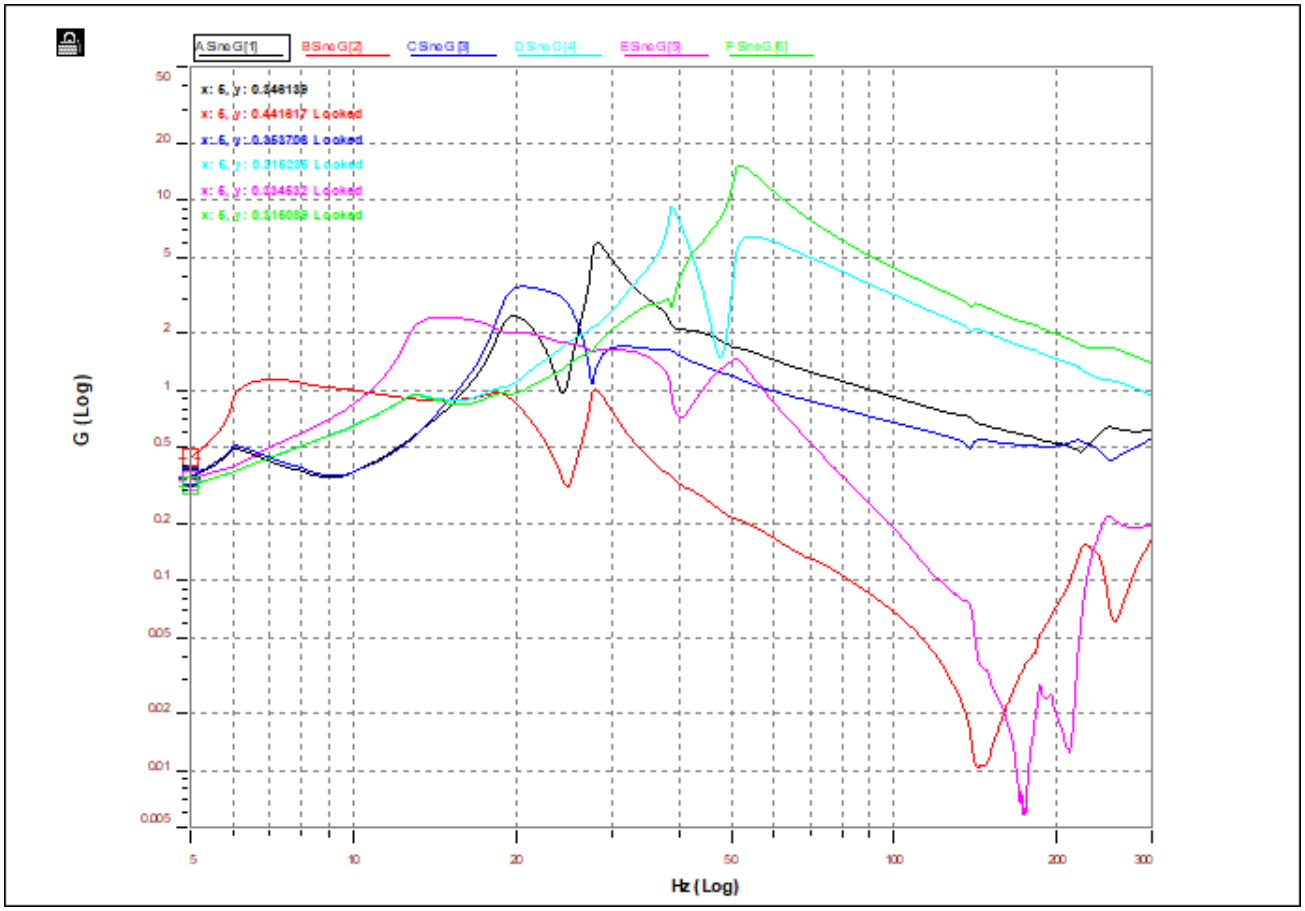


Figure 5. 20**:** The asymmetric Stockbridge damper with added masses of 115 g and 200 g on each side inner part of each mass.

# CHAPTER 6

# MODELLING AND DESIGN OF A NEW STOCKBRIDGE DAMPER

## 6.1 Introduction

The governing equations for the vibrating system represented by a half model of a vibration damper are presented. The purpose is to present theory for the design of Stockbridge dampers configured for better efficiency. The equations are overwhelming. An example case was presented for a two-degree-of-freedom modified damper to determine the frequencies and amplitudes of vibration. Material properties were assumed for a case, to obtain the frequencies and amplitudes of vibration for the damper.

## 6.2 Analytical model

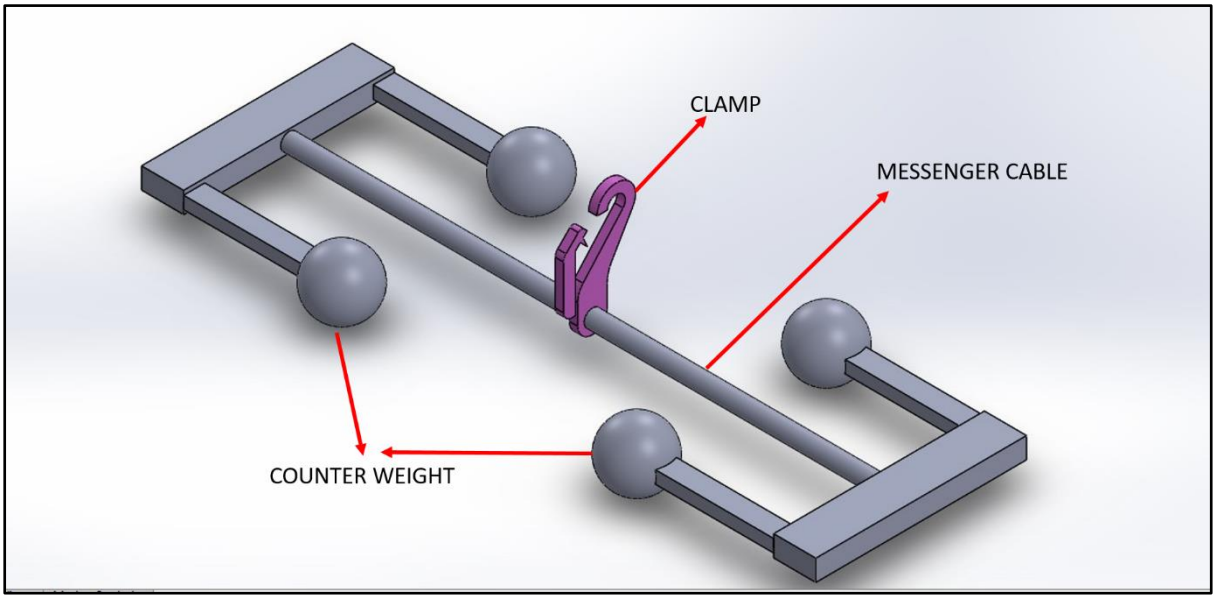


Figure 6. 1: Vibration damper (Vaja et al., 2018)

The mathematical model of the complete vibration damper will be large. The computation is simplified by looking at a half model of the vibration damper as shown in figure 6.2 (Vaja et al., 2018). Three coordinate systems ($O_1$ , $O_2$ $and$ $O_3$) are used. The model is treated as a three cantilever system each cantilever having a concentrated load at its end. The first

coordinate system $O_1$ is at the clamp of the damper with a mass $M_1$at the end of the messenger cable. The second coordinate is on the right side of mass $M_1$and has a mass $M_2$ at its end. The third coordinate is on the left side of $M_1$ with a mass $M_3$. The mass $M_1$ will have rotational motion during its operation while $M_2$ and $M_3$ are regarded to be concentrated masses acting at the ends of each beam. The masses $M_2$ and $M_3$ are equal in terms of mass and similar in shape. The vibration displacement along the $j$ coordinate is given as $Y_1, Y_2$, and $Y_3$ respectively in the first, second, and third coordinate system.

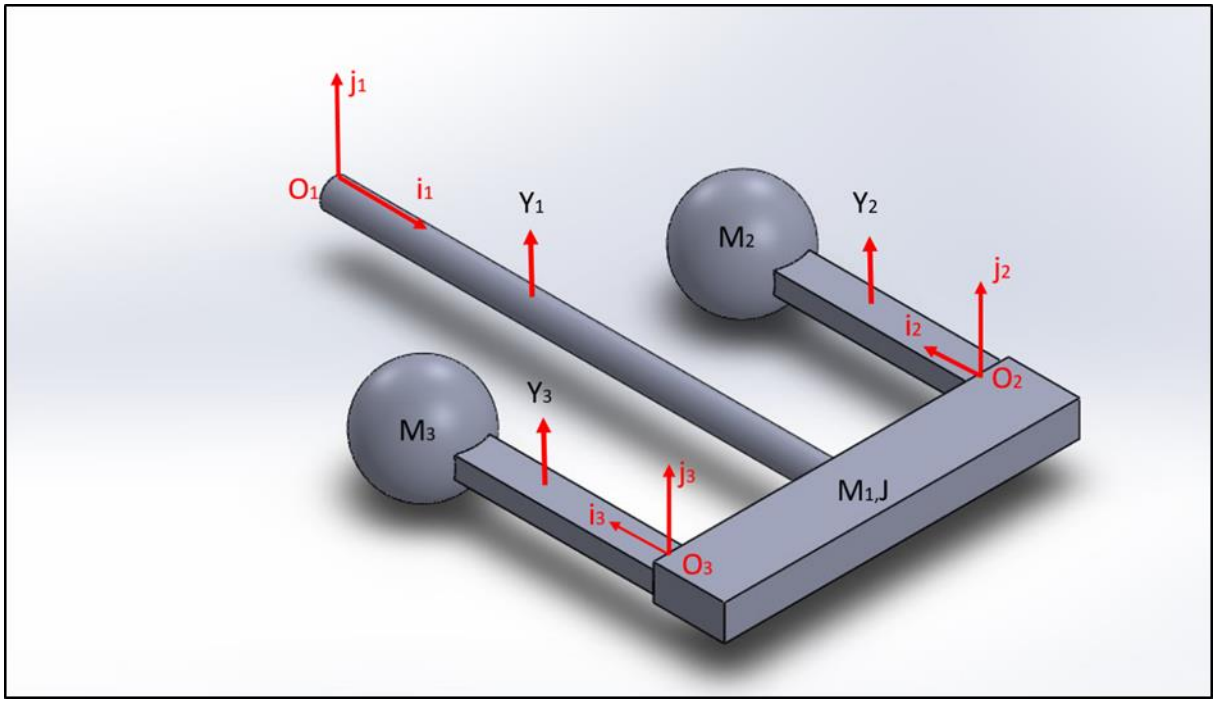


Figure 6. 2: Diagram of the half model of vibration damper (Vaja et al., 2018)

There are various parameters that need to be considered:

- Potential energy
- Kinetic energy
- Deflection of the beam
- Slope on the beam
- Bending moment of the beam
- Shear force acting in the beam
- Force per unit length

The following equations take all these parameters into consideration. The strain energy is considered as

$$U = \int_0^L \frac{M^2 dx}{2EI} \tag{6.1}$$

But the bending moment

$$M = EIY^{II} \tag{6.2}$$

Substitute equation 6.2 into 6.1

$$U = \int_0^L \frac{\left(EIY''\right)^2 dx}{2EI} \tag{6.3}$$

$$U = \frac{1}{2} EI \int_0^L Y''^2 \ dx \tag{6.4}$$

Equation 6.4 becomes the potential energy equation of the system because the beam after being strained has the strain energy converted to potential energy ($V$)

$$V = \frac{1}{2} EI \int_0^L Y''^2 \ dx \tag{6.5}$$

The kinetic and potential energy of the system are provided by equations 6.6 and 6.7 respectively. The derivation of the equation, the free body diagram, the resulting equations are adapted from (Vaja et al., 2018) and are conveniently repeated as follows:

$$T = \frac{1}{2} m_1 \int_0^{L_1} \dot{Y}_1^{\,2} (x_1, t)\, dx + \frac{1}{2} M_1 \dot{Y}_1^{\,2} (L_1, t) + J\dot{Y}_1' (L_1, t) + \frac{1}{2} m_2 \int_0^{L_2} \dot{Y}_2^{\,2} (x_2, t)\, dx + \frac{1}{2} M_2 \dot{Y}_2^{\,2} (L_2, t) + \frac{1}{2} m_3 \int_0^{L_3} \dot{Y}_3^{\,2} (x_3, t)\, dx + \frac{1}{2} M_3 \dot{Y}_3^{\,2} (L_3, t) \tag{6.6}$$

$$V = \frac{1}{2} EI_1 \int_0^{L_1} Y''^2 (x_1, t) \ dx + \frac{1}{2} EI_2 \int_0^{L_2} Y''^2 (x_2, t) \ dx + \frac{1}{2} EI_3 \int_0^{L_3} Y''^2 (x_3, t) \ dx \tag{6.7}$$

The highpoints in the above equations represent differentiation with respect to time which is represented by dots, and differentiation with respect to $x$. $E$ is Young's modulus of elasticity,

$I_1, I_2$ and $I_3$ are the second moments of area of the messenger cables and beams respectively. $J$ is the rotational moment of inertia of the mass $M_1$, $L_1$ is the length, $m_1$ is the mass per unit length of the cable. $L_2$, $L_3$ are the lengths and $m_2$, $m_3$ are the mass per unit length of the beams respectively. The rate of change of the shear force at any point on the axis of the beam is equal to the negative of the intensity of the distributed load at any point (Gere and Timoshenko, 1997). Using Hamilton's principle, Lagrange equations and Newton's second Laws, the equations of motions of the system are obtained as

$$EI_1 Y_1^{IV} + m_1 \ddot{Y}_1 = 0 \tag{6.8}$$

$$EI_2 Y_2^{IV} + m_2 \ddot{Y}_2 = 0 \tag{6.9}$$

$$EI_3 Y_3^{IV} + m_3 \ddot{Y}_3 = 0 \tag{6.10}$$

For harmonic motion the system shows the following equations as given below

$$Y_1(x_1, t) = F(x_1)e^{i\omega t} \tag{6.11}$$

$$Y_2(x_2, t) = G(x_2)e^{i\omega t} \tag{6.12}$$

$$Y_3(x_3, t) = H(x_3)e^{i\omega t} \tag{6.13}$$

The natural frequency is represented by $\omega$ and the mode shapes at these frequencies is given as

$$F(x_1) = a_1 \sin \beta_1 x_1 + a_2 \cos \beta_1 x_1 + a_3 \sinh \beta_1 x_1 + a_4 \cosh \beta_1 x_1 \tag{6.14}$$

$$G(x_2) = a_5 \sin \beta_2 x_2 + a_6 \cos \beta_2 x_2 + a_7 \sinh \beta_2 x_2 + a_8 \cosh \beta_2 x_2 \tag{6.15}$$

$$H(x_3) = a_9 \sin \beta_3 x_3 + a_{10} \cos \beta_3 x_3 + a_{11} \sinh \beta_3 x_3 + a_{12} \cosh \beta_3 x_3 \tag{6.16}$$

The equations 6.14, 6.15 and 6.16 into equation 6.11, 6.12 and 6.13 respectively give:

$$Y_1(x_1, t) = (a_1 \sin \beta_1 x_1 + a_2 \cos \beta_1 x_1 + a_3 \sinh \beta_1 x_1 + a_4 \cosh \beta_1 x_1)e^{i\omega t} \tag{6.17}$$

$$Y_2(x_2, t) = (a_5 \sin \beta_2 x_2 + a_6 \cos \beta_2 x_2 + a_7 \sinh \beta_2 x_2 + a_8 \cosh \beta_2 x_2)e^{i\omega t} \tag{6.18}$$

$$Y_3(x_3,t) = (a_9 \sin\beta_3 x_3 + a_{10}\cos\beta_3 x_3 + a_{11}\sinh\beta_3 x_3 + a_{12}\cosh\beta_3 x_3)e^{i\omega t} \quad (6.19)$$

So that:

$$Y_1'(x_1,t) = (a_1 \cos\beta_1 x_1 - a_2 \sin\beta_1 x_1 + a_3 \cosh\beta_1 x_1 + a_4 \sinh\beta_1 x_1)\beta_1 e^{i\omega t} \quad (6.20)$$

$$Y_2'(x_2,t) = (a_5 \cos\beta_2 x_2 - a_6 \sin\beta_2 x_2 + a_7 \cosh\beta_2 x_2 + a_8 \sinh\beta_2 x_2)\beta_2 e^{i\omega t} \quad (6.21)$$

$$Y_3'(x_3,t) = (a_9 \cos\beta_3 x_3 - a_{10} \sin\beta_3 x_3 + a_{11} \cosh\beta_3 x_3 + a_{12} \sinh\beta_3 x_3)\beta_3 e^{i\omega t} \quad (6.22)$$

$$Y_1''(x_1,t) = (-a_1 \sin\beta_1 x_1 - a_2 \cos\beta_1 x_1 + a_3 \sinh\beta_1 x_1 + a_4 \cosh\beta_1 x_1)\beta_1^2 e^{i\omega t} \quad (6.23)$$

$$Y_2''(x_2,t) = (-a_5 \sin\beta_2 x_2 - a_6 \cos\beta_2 x_2 + a_7 \sinh\beta_2 x_2 + a_8 \cosh\beta_2 x_2)\beta_2^2 e^{i\omega t} \quad (6.24)$$

$$Y_3''(x_3,t) = \left(-a_9 \sin\beta_3 x_3 - a_{10} \cos\beta_3 x_3 + a_{11} \sinh\beta_3 x_3 + a_{12} \cosh\beta_3 x_3\right)\beta_3^2 e^{i\omega t} \quad (6.25)$$

$$Y_1'''(x_1,t) = (-a_1 \cos\beta_1 x_1 + a_2 \sin\beta_1 x_1 + a_3 \cosh\beta_1 x_1 + a_4 \sinh\beta_1 x_1)\beta_1^3 e^{i\omega t} \quad (6.26)$$

$$Y_2'''(x_1,t) = (-a_5 \cos\beta_2 x_2 + a_6 \sin\beta_2 x_2 + a_7 \cosh\beta_2 x_2 + a_8 \sinh\beta_2 x_2)\beta_2^3 e^{i\omega t} \quad (6.27)$$

$$Y_3'''(x_1,t) = (-a_9 \cos\beta_3 x_3 + a_{10} \sin\beta_3 x_3 + a_{11} \cosh\beta_3 x_3 + a_{12} \sinh\beta_3 x_3)\beta_3^3 e^{i\omega t} \quad (6.28)$$

$$\dot{Y}_1(x_1,t) = (a_1 \sin\beta_1 x_1 + a_2 \cos\beta_1 x_1 + a_3 \sinh\beta_1 x_1 + a_4 \cosh\beta_1 x_1)\omega i e^{i\omega t} \quad (6.29)$$

$$\ddot{Y}_1(x_1,t) = -(a_1 \sin\beta_1 x_1 + a_2 \cos\beta_1 x_1 + a_3 \sinh\beta_1 x_1 + a_4 \cosh\beta_1 x_1)\omega^2 e^{i\omega t} \quad (6.30)$$

$$\dot{Y}_2(x_2,t) = (a_5 \sin\beta_1 x_1 + a_6 \cos\beta_1 x_1 + a_7 \sinh\beta_1 x_1 + a_8 \cosh\beta_1 x_1)\omega i e^{i\omega t} \quad (6.31)$$

$$\ddot{Y}_2(x_2,t) = -(a_5 \sin\beta_1 x_1 + a_6 \cos\beta_1 x_1 + a_7 \sinh\beta_1 x_1 + a_8 \cosh\beta_1 x_1)\omega^2 e^{i\omega t} \quad (6.32)$$

$$\dot{Y}_3(x_3,t) = (a_9 \sin\beta_1 x_1 + a_{10} \cos\beta_1 x_1 + a_{11} \sinh\beta_1 x_1 + a_{12} \cosh\beta_1 x_1)\omega i e^{i\omega t} \quad (6.33)$$

$$\ddot{Y}_3(x_3,t) = -(a_9 \sin\beta_1 x_1 + a_{10} \cos\beta_1 x_1 + a_{11} \sinh\beta_1 x_1 + a_{12} \cosh\beta_1 x_1)\omega^2 e^{i\omega t} \quad (6.34)$$

Using the boundary conditions the messenger cable is fixed at the left end, therefore the slope and deflection at this point are zero. Therefore $x_1 = 0$

$$Y_1(0,t) = 0; \tag{6.35}$$

$$Y_1'(0,t) = 0; \tag{6.36}$$

At $x_1 = L_1$ at the right end of the cable there is the mass $M_1$. At this point the displacement is expected to be equal, but the slope is opposite in direction due to the choice of reference coordinates. Therefore,

$$Y_1(L_1,t) = Y_2(0,t) = Y_3(0,t) \tag{6.37}$$

$$Y_1'(L_1,t) = -Y_2'(0,t) = -Y_3'(0,t) \tag{6.38}$$

The bending moment and the shear force are going to be the continuity conditions at

$x_1 = L_1, x_2 = 0$ and $x_3 = 0$. Figure 6.3 below shows the free body diagram of moments

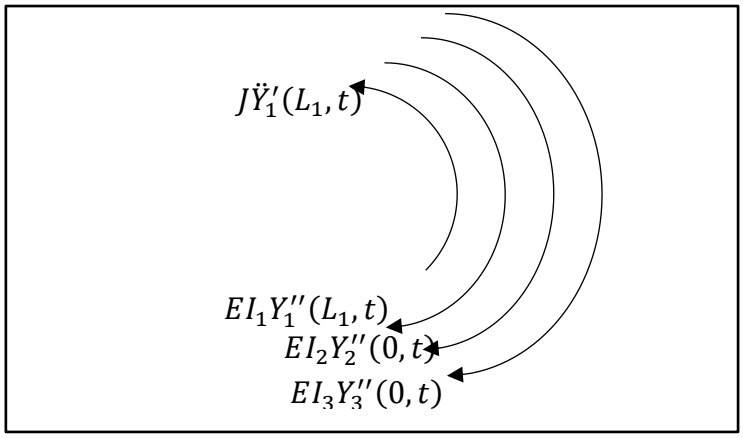


Figure 6. 3**:** The free body diagram of the beam for equating moments

$$EI_1Y_1''(L_1,t) - J\ddot{Y}_1'(L_1,t) + EI_2Y_2''(0,t) + EI_3Y_3''(0,t) = 0 \tag{6.39}$$

$$-EI_1Y_1'''(L_1,t) - EI_2Y_2'''(0,t) - EI_3Y_3'''(0,t) = M_1\ddot{Y}_1(L_1,t) \tag{6.40}$$

There are two beams attached to mass $M_1$, the first beam is free at the end; therefore the boundary conditions at $x_2 = L_2$ are:

$$Y_2''(L_2,t) = 0 \tag{6.41}$$

$$M_2\ddot{Y}_2(L_2,t) - EI_2Y_2'''(L_2,t) = 0 \qquad (6.42)$$

The same thing will happen to the second beam because it is also free at the end. Therefore the boundary conditions at the free end at $x_3 = L_3$ are:

$$Y_3''(L_3,t) = 0 \qquad (6.43)$$

$$M_3\ddot{Y}_3(L_3,t) - EI_3Y_3'''(L_3,t) = 0 \qquad (6.44)$$

All the calculations for the boundary conditions for each point are shown in the appendix E. Applying the boundary condition $Y_1(0,t) = 0$ to equation 6.17 gives

$$0 = (a_1\sin(0) + a_2\cos(0) + a_3\sinh(0) + a_4\cosh(0))e^{i\omega t}$$

$$0 = (a_2 + a_4)e^{i\omega t}$$

This implies that either $e^{i\omega t} = 0$ for all values of $t$, or $a_2 + a_4 = 0$. The first statement is clearly not true, so it must be the case that

$$\boldsymbol{a_2 + a_4 = 0} \qquad (6.45)$$

Applying the boundary condition $Y_1'(0,t) = 0$ to equation 6.20 gives

$$0 = (a_1\cos(0) - a_2\sin(0) + a_3\cosh(0) + a_4\sinh(0))\beta_1 e^{i\omega t}$$

$$(a_1 + a_3)\beta_1 e^{i\omega t} = 0$$

$$\boldsymbol{a_1 + a_3 = 0} \qquad 6.46)$$

At $x_1 = L_1$ at the cable there is the mass $M_1$; at this point the displacement is expected to be equal, but the slope is opposite in direction due to the choice of reference coordinates. Therefore,

$$Y_1(L_1,t) = Y_2(0,t) = Y_3(0,t)$$

$$Y_1'(L_1,t) = -Y_2'(0,t) = -Y_3'(0,t)$$

Applying the boundary condition $Y_1(L_1,t) = Y_2(0,t) = Y_3(0,t)$ to equations 6.17, 6.18 and 6.19 gives

$Y_1(L_1, t) = Y_2(0, t)$

$$\boldsymbol{a_1 \sin \beta_1 L_1 + a_2 \cos \beta_1 L_1 + a_3 \sinh \beta_1 L_1 + a_4 \cosh \beta_1 L_1 - a_6 - a_8 = 0} \quad (6.47)$$

Same procedure applies

$Y_1(L_1, t) = Y_3(0, t)$

$$\boldsymbol{a_1 \sin \beta_1 L_1 + a_2 \cos \beta_1 L_1 + a_3 \sinh \beta_1 L_1 + a_4 \cosh \beta_1 L_1 - a_{10} - a_{12} = 0} \quad (6.48)$$

Applying the boundary condition $Y_1'(L_1, t) = -Y_2'(0, t) = -Y_3'(0, t)$ to equations 6.20, 6.21 and 6.22 gives

$Y_1'(L_1, t) = -Y_2'(0, t)$

$$\boldsymbol{a_1 \beta_1 \cos \beta_1 L_1 - a_2 \beta_1 \sin \beta_1 L_1 + a_3 \beta_1 \cosh \beta_1 L_1 + a_4 \beta_1 \sinh \beta_1 L_1 + a_5 \beta_2 + a_7 \beta_2 = 0} \quad (6.49)$$

$Y_1'(L_1, t) = -Y_3'(0, t)$

$$\boldsymbol{a_1 \beta_1 \cos \beta_1 L_1 - a_2 \beta_1 \sin \beta_1 L_1 + a_3 \beta_1 \cosh \beta_1 L_1 + a_4 \beta_1 \sinh \beta_1 L_1 + a_9 \beta_3 + a_{11} \beta_3 = 0} \quad (6.50)$$

$EI_1 Y_1''(L_1, t) - J\ddot{Y}_1'(L_1, t) + EI_2 Y_2''(0, t) + EI_3 Y_3''(0, t) = 0$

For $x_1 = L_1, x_2 = 0$ and $x_3 = 0$. We have from 6.23, 6.24, 6.25 and 6.30 the following:

$Y_1''(L_1, t) = (-a_1 \sin \beta_1 L_1 - a_2 \cos \beta_1 L_1 + a_3 \sinh \beta_1 L_1 + a_4 \cosh \beta_1 L_1) \beta_1^2 e^{i\omega t}$

$\ddot{Y}_1'(L_1, t) = -(a_1 \beta_1 \cos \beta_1 L_1 - a_2 \beta_1 \sin \beta_1 L_1 + a_3 \beta_1 \cosh \beta_1 L_1 + a_4 \beta_1 \sinh \beta_1 L_1) \omega^2 e^{i\omega t}$

$Y_2''(0, t) = (-a_6 + a_8) \beta_2^2 e^{i\omega t}$

$Y_3''(0, t) = (-a_{10} + a_{12}) \beta_3^2 e^{i\omega t}$

Substitute the above equations to equation 6.39, we obtain

$$\boldsymbol{a_1(-EI_1 \beta_1^2 \sin \beta_1 L_1 + J\omega^2 \beta_1 \cos \beta_1 L_1) + a_2(-EI_1 \beta_1^2 \cos \beta_1 L_1 - J\omega^2 \beta_1 \sin \beta_1 L_1) + a_3(EI_1 \beta_1^2 \sinh \beta_1 L_1 + J\omega^2 \beta_1 \cosh \beta_1 L_1) + a_4(EI_1 \beta_1^2 \cosh \beta_1 L_1 + J\omega^2 \beta_1 \sinh \beta_1 L_1) - a_6 EI_2 \beta_2^2 + a_8 EI_2 \beta_2^2 - a_{10} EI_3 \beta_3^2 + a_{12} EI_3 \beta_3^2 = 0} \quad (6.51)$$

$$-EI_1Y_1'''(L_1,t) - EI_2Y_2'''(0,t) - EI_3Y_3'''(0,t) = M_1\ddot{Y}_1(L_1,t)$$

Applying the boundary conditions to equation 6.40 lead to the following

$$\boldsymbol{a_1\left(-EI_1\beta_1^3\cos\beta_1 L_1 - M_1\omega^2\sin\beta_1 L_1\right) + a_2\left(EI_1\beta_1^3\sin\beta_1 L_1 - M_1\omega^2\cos\beta_1 L_1\right) + a_3\left(EI_1\beta_1^3\cosh\beta_1 L_1 - M_1\omega^2\sinh\beta_1 L_1\right) + a_4\left(EI_1\beta_1^3\sinh\beta_1 L_1 - M_1\omega^2\cosh\beta_1 L_1\right) - a_5EI_2\beta_2^3 + a_7EI_2\beta_2^3 - a_9EI_3\beta_3^3 + a_{11}EI_3\beta_3^3 = 0} \quad (6.52)$$

There are two beams attached to mass $M_1$, the first beam is free at the end. Therefore the boundary conditions at $x_2 = L_2$ are:

$$Y_2''(L_2,t) = 0$$

$$M_2\ddot{Y}_2(L_2,t) - EI_2Y_2'''(L_2,t) = 0$$

Applying the boundary condition to equation 6.41 gives

$$(-a_5\sin\beta_2 L_2 - a_6\cos\beta_2 L_2 + a_7\sinh\beta_2 L_2 + a_8\cosh\beta_2 L_2)\beta_2^2 e^{i\omega t} = 0$$

Therefore

$$\boldsymbol{-a_5\beta_2^2\sin\beta_2 L_2 - a_6\beta_2^2\cos\beta_2 L_2 + a_7\beta_2^2\sinh\beta_2 L_2 + a_8\beta_2^2\cosh\beta_2 L_2 = 0} \quad (6.53)$$

Applying the boundary condition to equation 6.42 gives

$$\boldsymbol{a_5\left(M_2\omega^2\sin\beta_2 L_2 - \beta_2^3 EI_2\cos\beta_2 L_2\right) + a_6\left(M_2\omega^2\cos\beta_2 L_2 + \beta_2^3 EI_2\sin\beta_2 L_2\right) + a_7\left(M_2\omega^2\sinh\beta_2 L_2 + \beta_2^3 EI_2\cosh\beta_2 L_2\right) + a_8\left(M_2\omega^2\cosh\beta_2 L_2 + \beta_2^3 EI_2\sinh\beta_2 L_2\right) = 0} \quad (6.54)$$

The second beam is also free at the end at $x_3 = L_3$, apply the boundary conditions in equation 6.43 and 6.44

$$\boldsymbol{-a_9\beta_3^2\sin\beta_3 L_3 - a_{10}\beta_3^2\cos\beta_3 L_3 + a_{11}\beta_3^2\sinh\beta_3 L_3 + a_{12}\beta_3^2\cosh\beta_3 L_3 = 0} \quad (6.55)$$

$$\boldsymbol{a_9\left(M_3\omega^2 \sin \beta_3 L_3 - \beta_3^3 EI_3 \cos \beta_3 L_3\right) + a_{10}\left(M_3\omega^2 \cos \beta_3 L_3 + \beta_3^3 EI_3 \sin \beta_3 L_3\right) + a_{11}\left(M_3\omega^2 \sinh \beta_3 L_3 + \beta_3^3 EI_3 \cosh \beta_3 L_3\right) + a_{12}\left(M_3\omega^2 \cosh \beta_3 L_3 + \beta_3^3 EI_3 \sinh \beta_3 L_3\right) = 0} \quad (6.56)$$

The characteristic equation is created by subjecting the general solution to the above boundary conditions. Twelve simultaneous homogeneous equations are determined and arranged to form the coefficient matrix shown in the appendix F. The characteristic equation is obtained by equating the determinant of the coefficient matrix to zero.

By referring to equation 3.102 and figure 3.10, the frequency equation is formed because solutions of this equation produce the frequencies of the characteristic values of system. The determinant of coefficient of $Y_1$ and $Y_2$ must be equal to zero.

$$[-m_1\omega^2 + (k_1 + k_2)]\,[-m_2\omega^2 + k_2] - [-k_2][-k_2] = 0$$

$$[-m_1\omega^2 + (k_1 + k_2)]\,[-m_2\omega^2 + k_2] - k_2^2 = 0$$

$$m_1m_2\omega^4 - m_1\omega^2k_2 - m_2\omega^2(k_1 + k_2) + k_2(k_1 + k_2) - k_2^2 = 0$$

$$m_1m_2\omega^4 - \omega^2[m_1k_2 + m_2(k_1 + k_2)] + k_1k_2 = 0$$

Let $\boldsymbol{a_0} = k_1k_2 = (12.6770\,x10^4)(26.1736\,x10^5) = 331.803\,x\,10^9$ See appendix G

$\boldsymbol{a_1} = m_1k_2 + m_2(k_1 + k_2) = (0.25)(26.1736\,x10^5) + (0.25)(12.6770\,x10^4 + 26.1736\,x10^5) = 1340372.5$ See appendix G

$\boldsymbol{a_2} = m_1m_2 = (0.25)(0.25) = 0.0625$ See appendix G

$$a_2\omega^4 - a_1\omega^2 + a_0 = 0$$

Let $\Lambda = \omega^2$ therefore

$$a_2\Lambda^2 - a_1\Lambda + a_0 = 0$$

$$\Lambda_{1,2} = \frac{a_1 \pm \sqrt{{a_1}^2 - 4a_2a_0}}{2a_2}$$

$$\Lambda_{1,2} = \frac{1340372.5 \pm \sqrt{(1340372.5)^2 - 4(0.0625)(331.803\,x\,10^9)}}{2(0.0625)}$$

$\Lambda_1 = 21195489.35$ or $\Lambda_2 = 250470.6503$

Therefore $\omega_1 = \pm 4603.855922\ {}^{rad}/_{sec}$ or $\omega_2 = \pm 500.470429\ {}^{rad}/_{sec}$

# CHAPTER 7

# CONCLUSION AND RECOMMENDATIONS

## 7.1 Conclusion

The main objective of this study was to conduct a set of experiments aiming to identify the characteristics of an asymmetric damper and to develop a mathematical model for the design of a modified damper. The experiments involved the investigation of the characteristics of an asymmetric damper, the rotational motion of the damper and the degrees of freedom for the masses attached to the messenger cable. From these investigations the following were established after conducting experiments:

- From the graphs it was found that the damper is a four degrees of freedom
- Resonance frequencies for each damper are not the same depending on the size of the damper.
- One of the dampers had resonant frequencies at 8Hz, 22 Hz, 50 Hz and 70 Hz. At any other frequency except the above resonance frequencies, the damper is not a mass absorber
- There is no rotation of the damper about the messenger wire, only up and down vertical motion of the damper due to the shaker during operation.
- If the two masses or weight of the damper are modified for operation, it changes from being a four degree of freedom to a six degree of freedom. It means it has six resonance frequencies.
- The mathematical model was developed and the theoretical or computational results were validated by experimental results.
- The results were presented at three conferences and were well received by the audience. At the Thirteenth International Conference on Computational Structures Technology in Spain, The South African Conference on Computational and Applied Mechanics (SACAM) at VUT and SAIMechE Postgraduate Conference on Mechanical, Materials, Manufacturing and Biomedical Engineering at CPUT.

## 7.2 Recommendations

From the findings of this study the following suggestions for future investigations are recommended for further research on dampers:

- The design and manufacturing of a prototype which may be tested at VRTC for more relevant data and improvements.
- For the mathematical model it is required to include rotation of damper about the messenger wire for further computational data and predictions.

# APPENDIX A

# GRAPHS OF DAMPER (182 025-301) Ø31 – 39 mm

DAMPER 2 (182 025-301) TEST 1

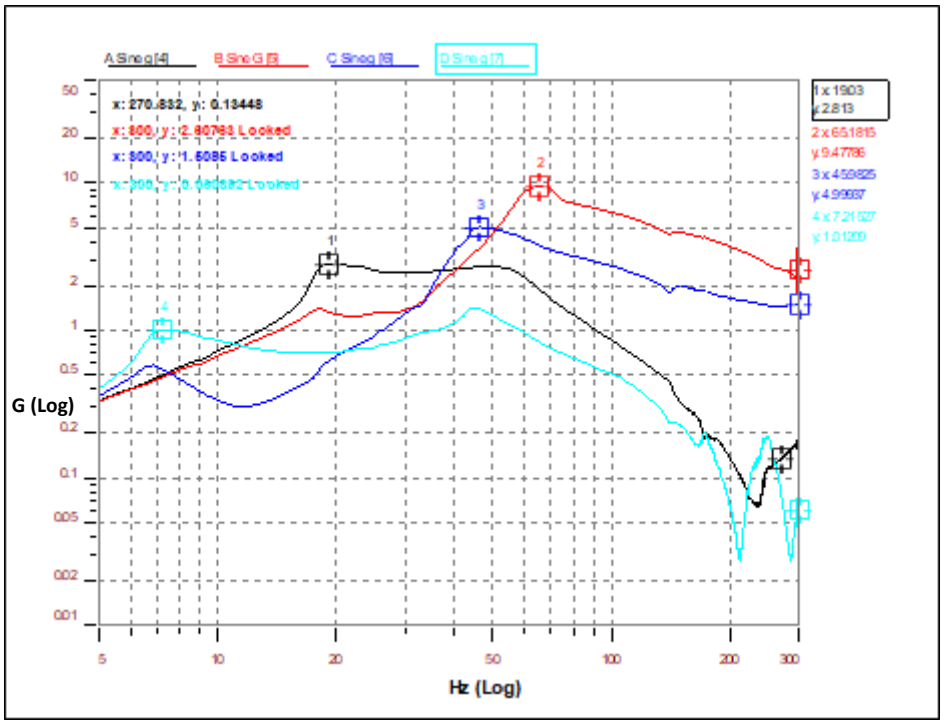


**Figure A.1:** The graph of acceleration amplitude G (log) vs frequency Hz (log)

DAMPER 2 (182 025-301) TEST 2

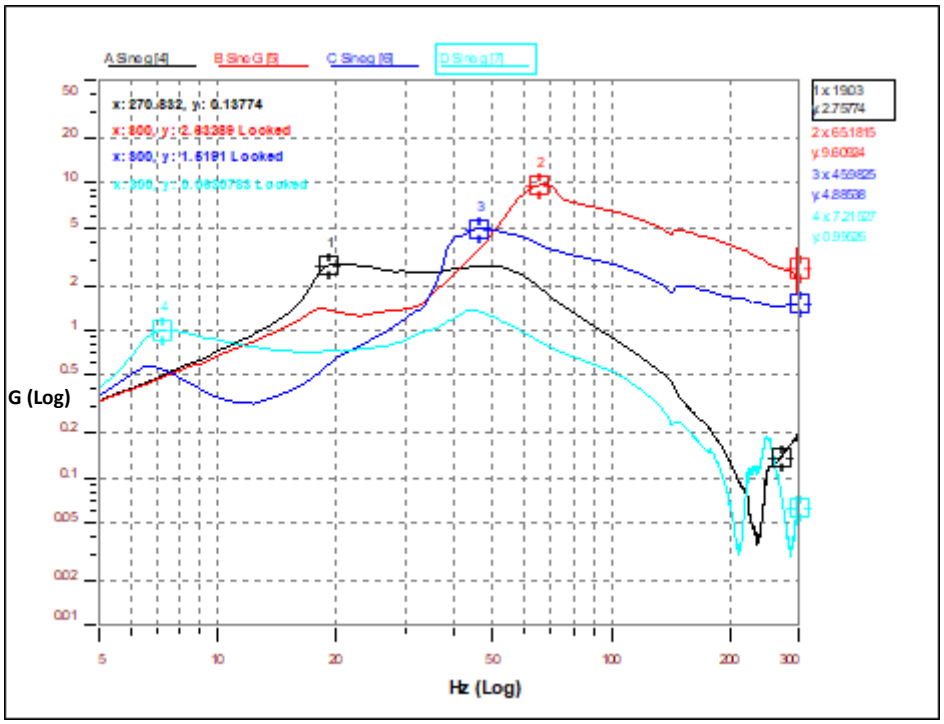


**Figure A.2:** The graph of acceleration amplitude G (log) vs frequency Hz (log)

DAMPER 2 (182 025-301) TEST 3

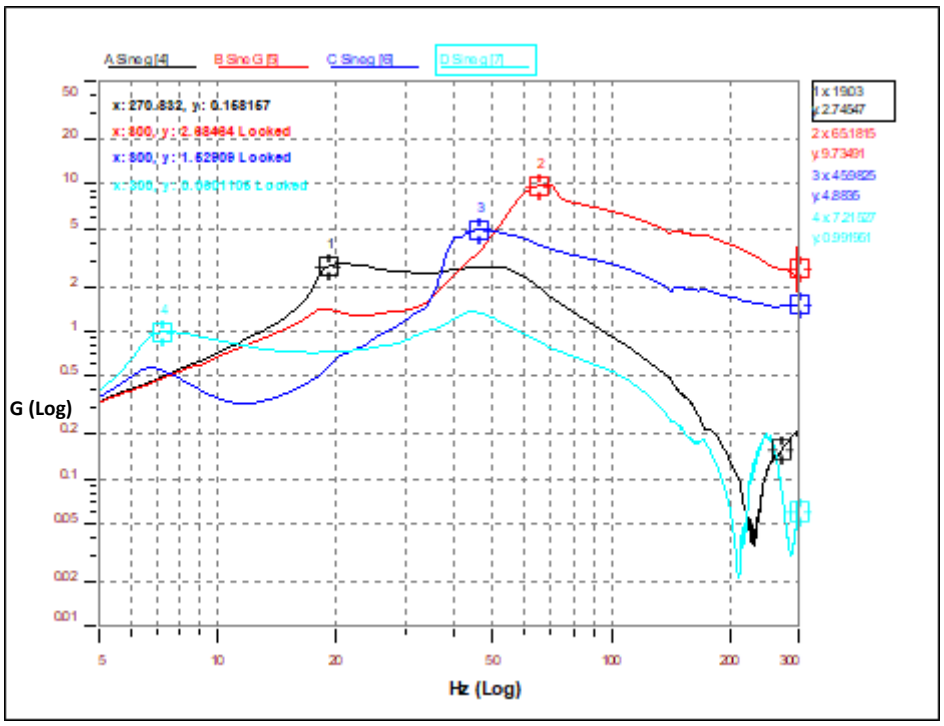

**Figure A.3:** The graph of acceleration amplitude G (log) vs frequency Hz (log)

DAMPER 3 (182 025-301) TEST 1

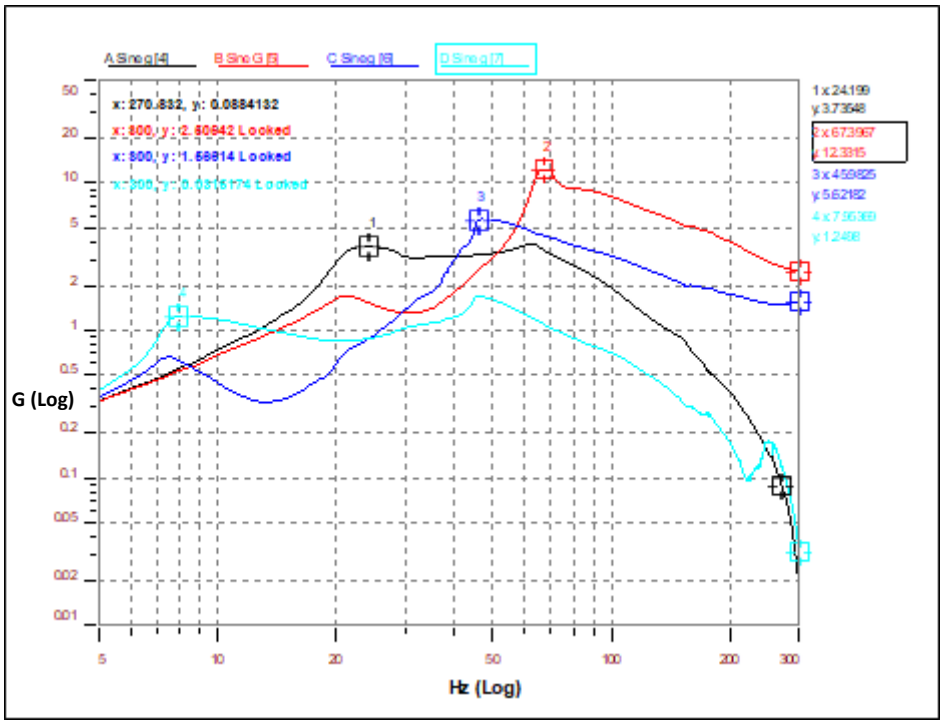


**Figure A.4:** The graph of acceleration amplitude G (log) vs frequency Hz (log)

DAMPER 3 (182 025-301) TEST 2

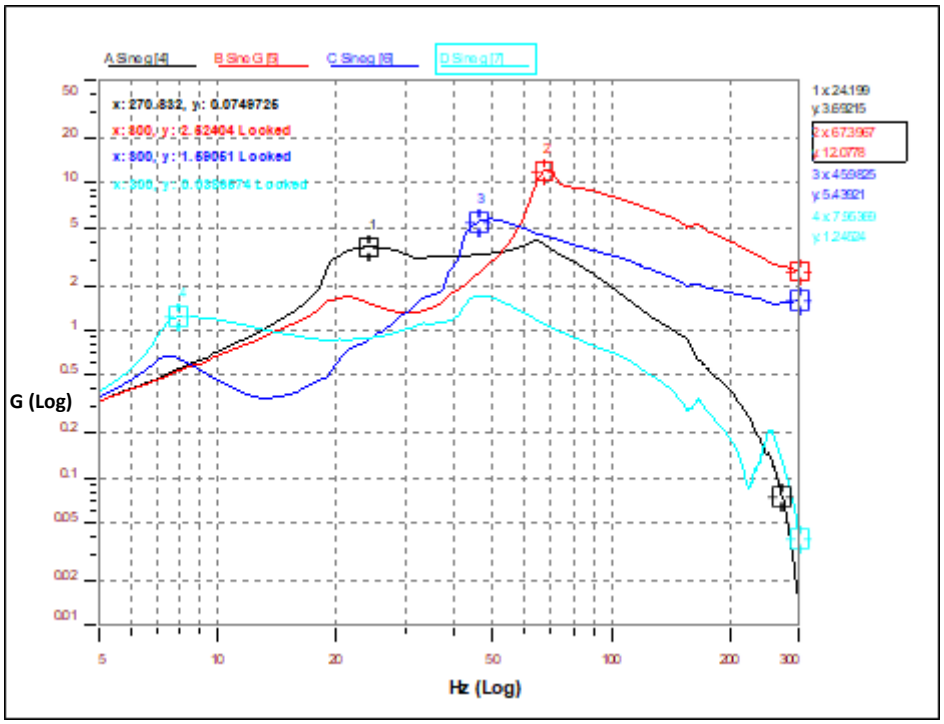


**Figure A.5:** The graph of acceleration amplitude G (log) vs frequency Hz (log)

DAMPER 3 (182 025-301) TEST 3

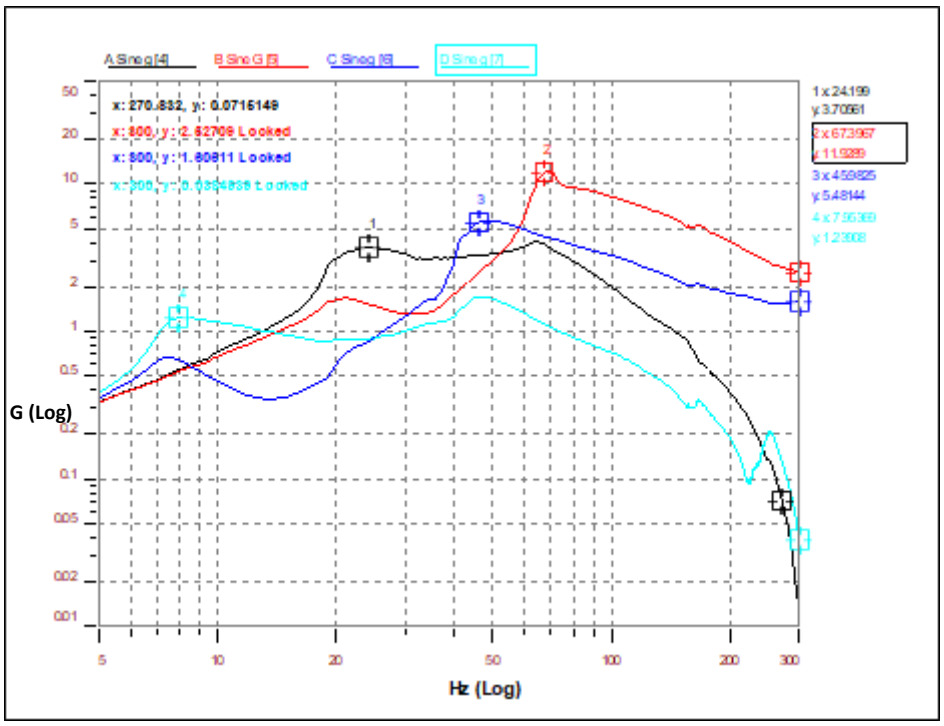


**Figure A.6:** The graph of acceleration amplitude G (log) vs frequency Hz (log)

DAMPER 4 (182 025-301) TEST1

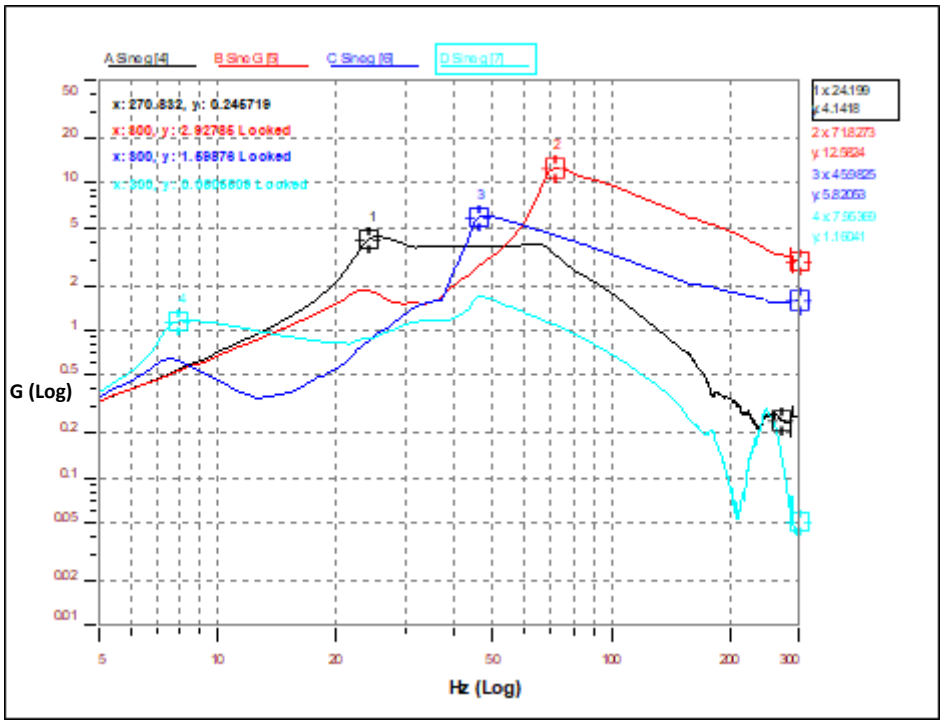


**Figure A.7:** The graph of acceleration amplitude G (log) vs frequency Hz (log)

DAMPER 4 (182 025-301) TEST 2

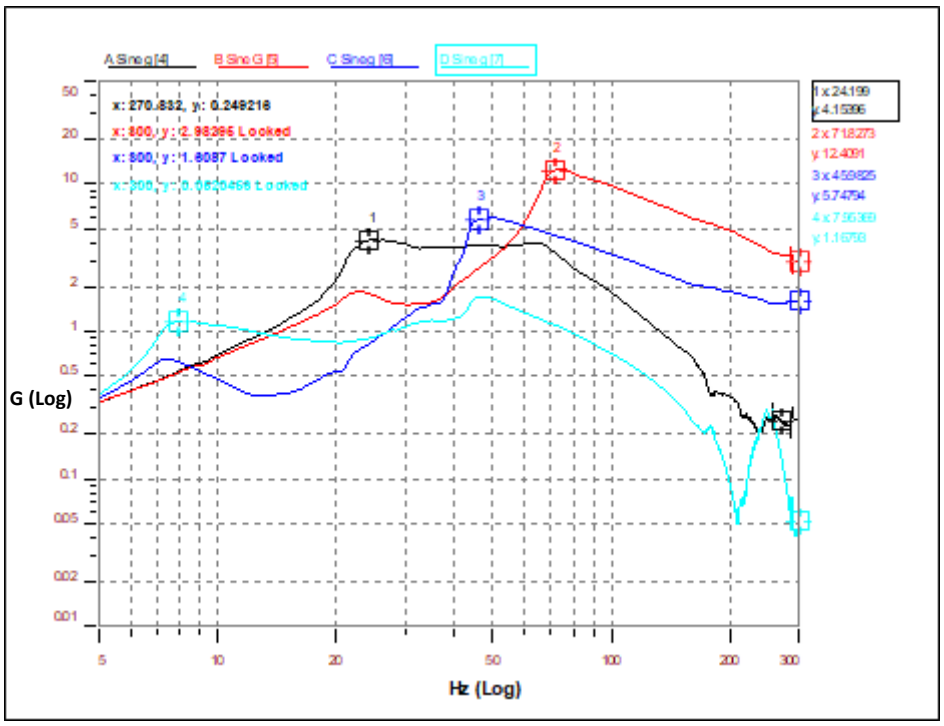


**Figure A.8:** The graph of acceleration amplitude G (log) vs frequency Hz (log)

DAMPER 4 (182 025-301) TEST 3

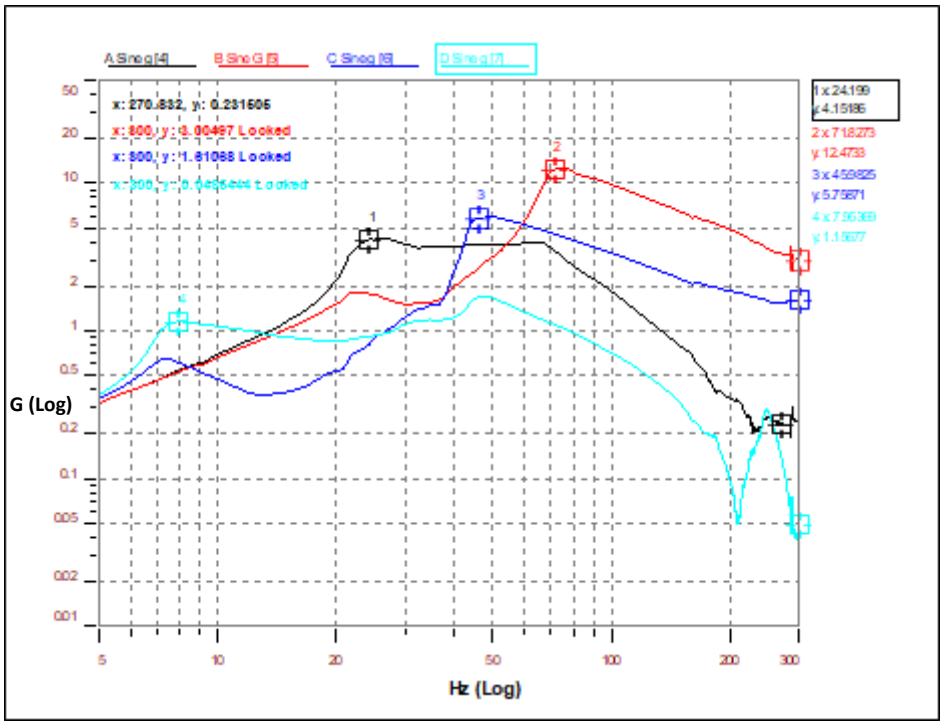

**Figure A.9:** The graph of acceleration amplitude G (log) vs frequency Hz (log)

# APPENDIX B

# GRAPHS OF DAMPER (182 025-401) Ø39 – 47 mm

DAMPER 6 (182 025-401) TEST 1

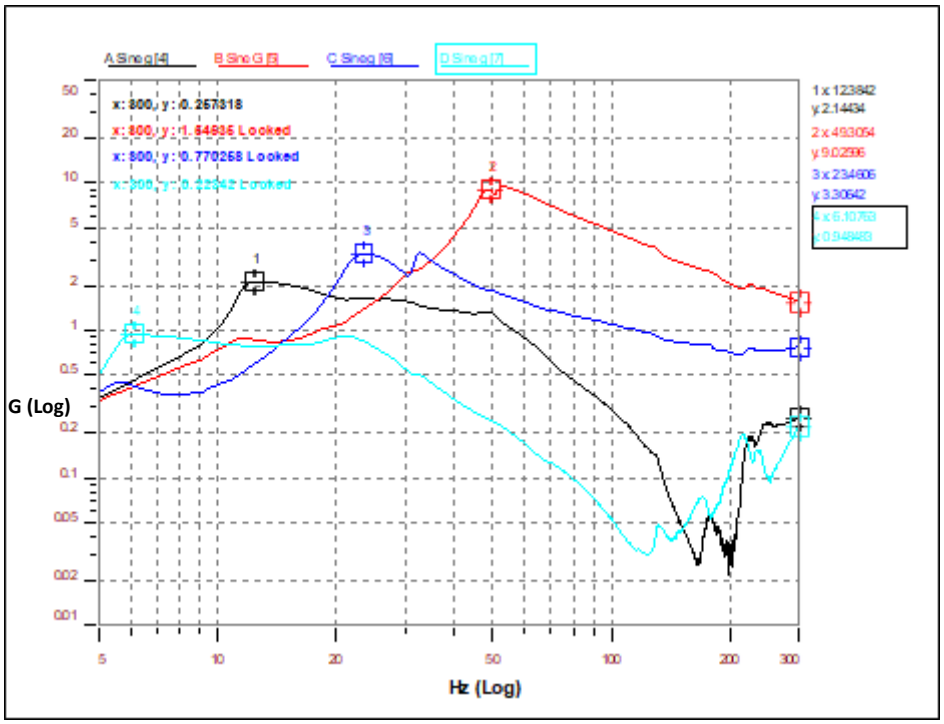


**Figure B.1:** The graph of acceleration amplitude G (log) vs frequency Hz (log)

DAMPER 6 (182 025-401) TEST 2

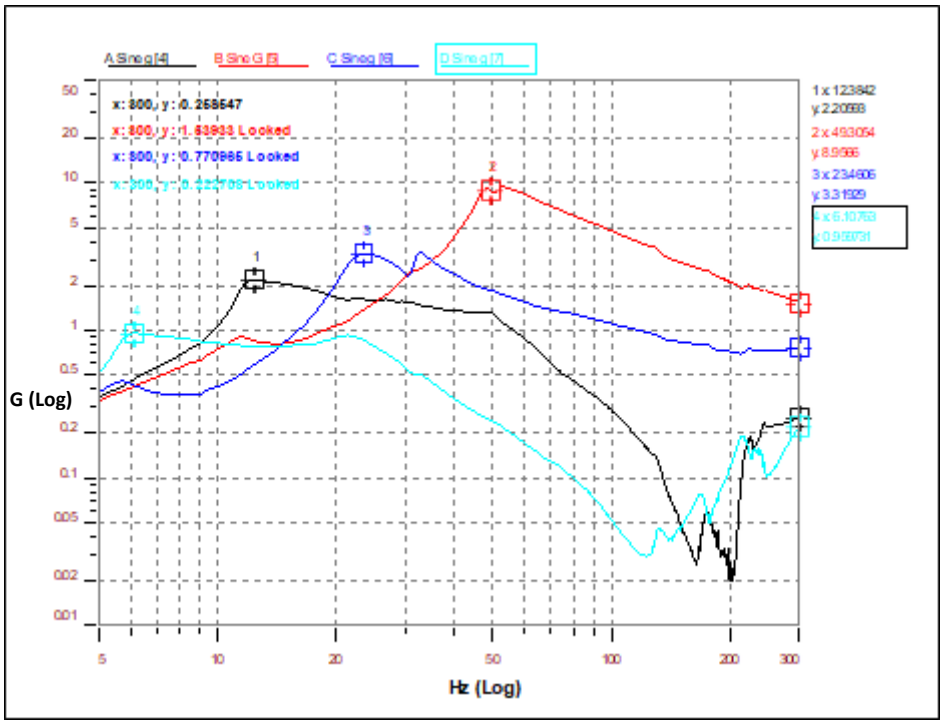


**Figure B.2:** The graph of acceleration amplitude G (log) vs frequency Hz (log)

DAMPER 6 (182 025-401) TEST 3

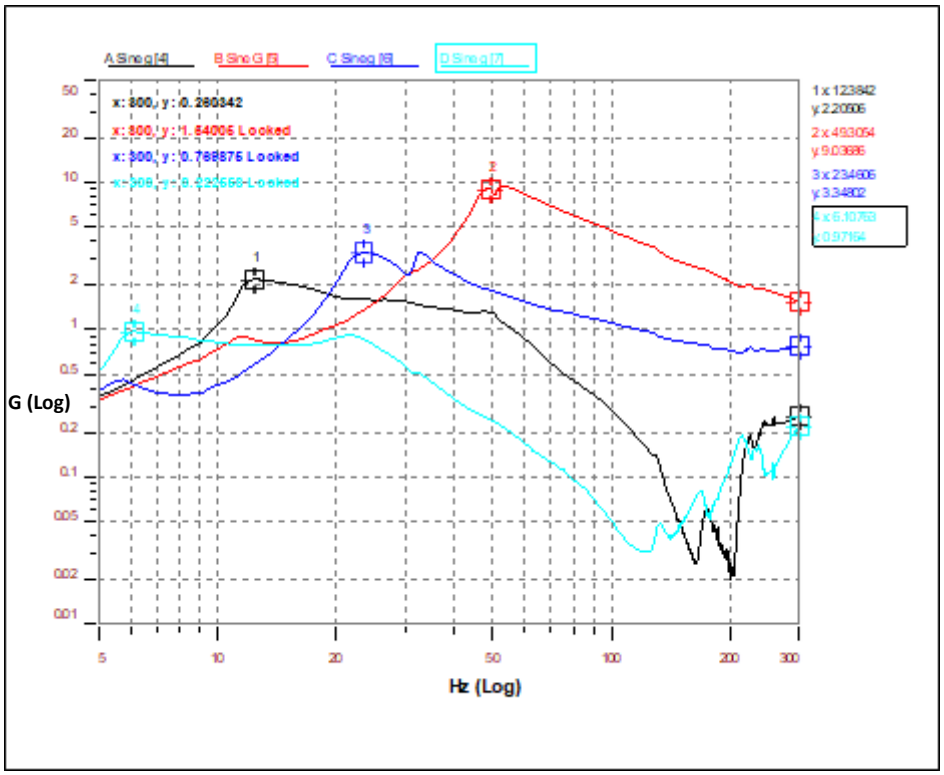

**Figure B.3:** The graph of acceleration amplitude G (log) vs frequency Hz (log)

DAMPER 7 (182 025-401) TEST 1

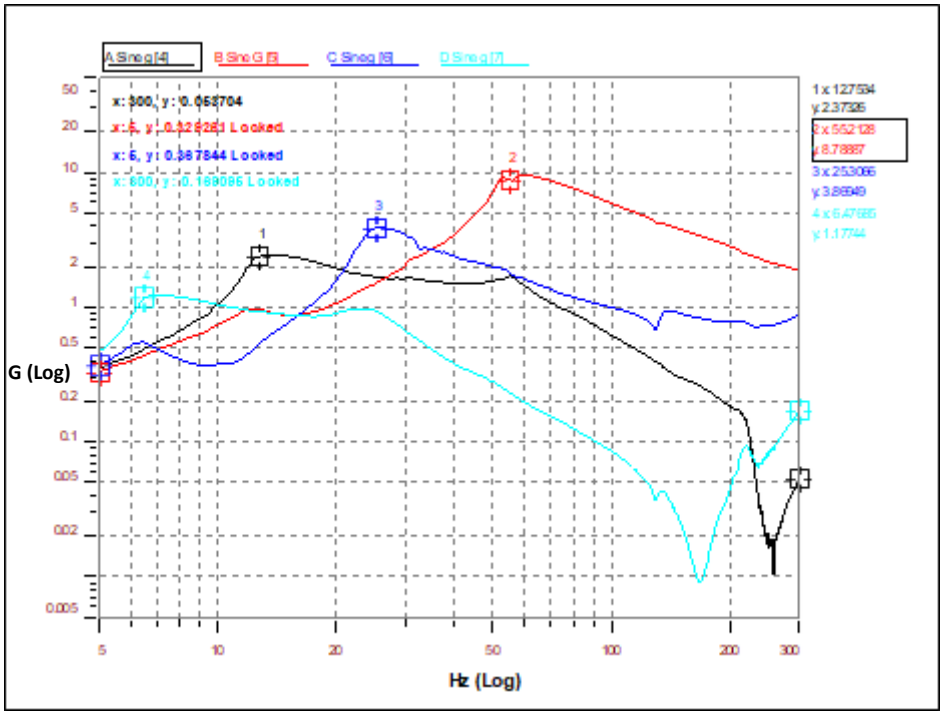


**Figure B.4:** The graph of acceleration amplitude G (log) vs frequency Hz (log)

DAMPER 7 (182 025-401) TEST2

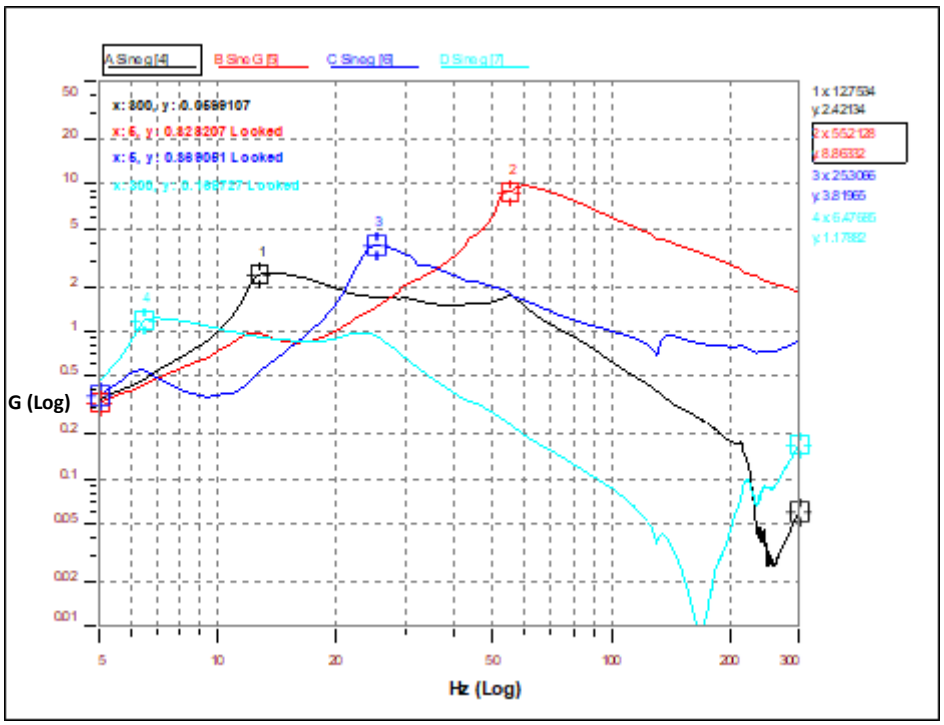


**Figure B.5:** The graph of acceleration amplitude G (log) vs frequency Hz (log)

DAMPER 7 (182 025-401) TEST 3

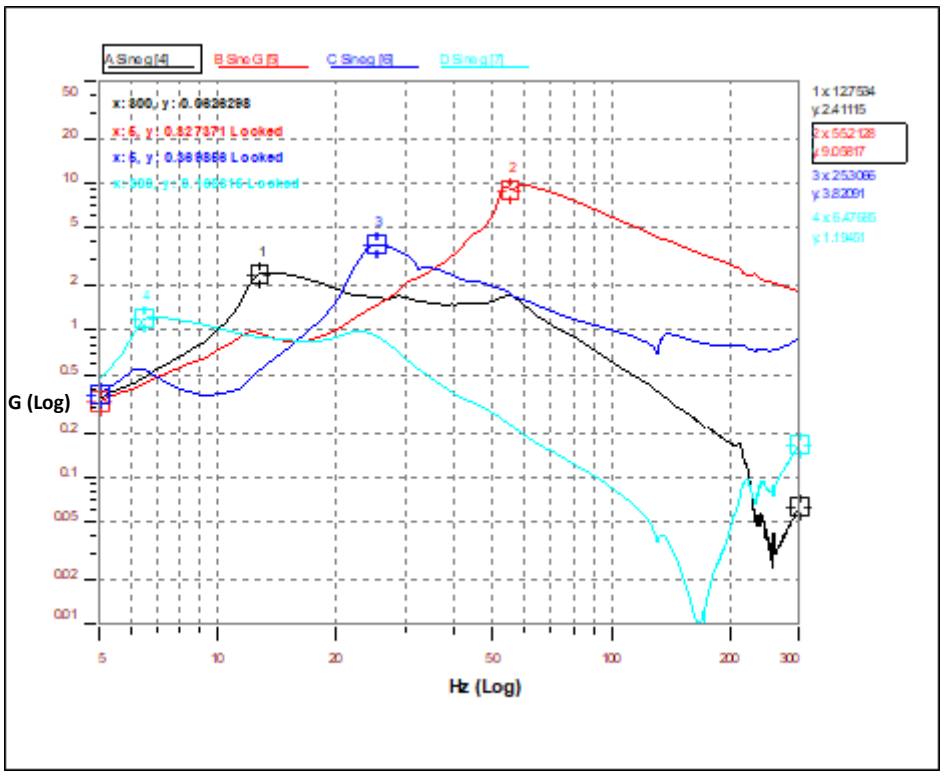


**Figure B.6:** The graph of acceleration amplitude G (log) vs frequency Hz (log)

# APPENDIX C

# GRAPHS OF DAMPER (182 025-101) Ø7 – 15 mm

DAMPER 9 (182 025-101) TEST 1

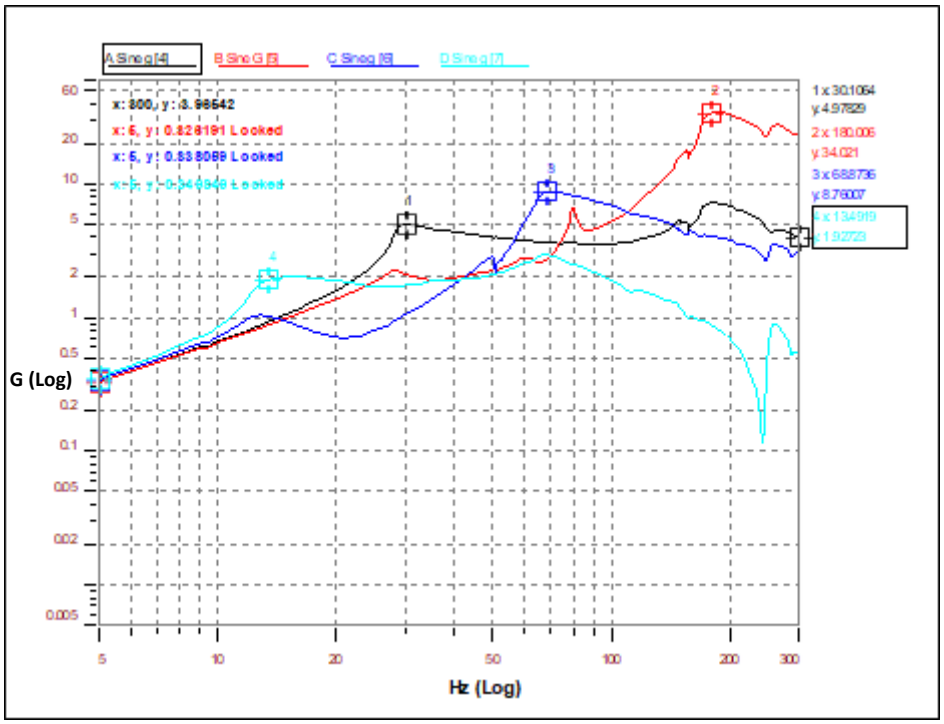


**Figure C.1:** The graph of acceleration amplitude G (log) vs frequency Hz (log)

DAMPER 9 (182 025-101) TEST 2

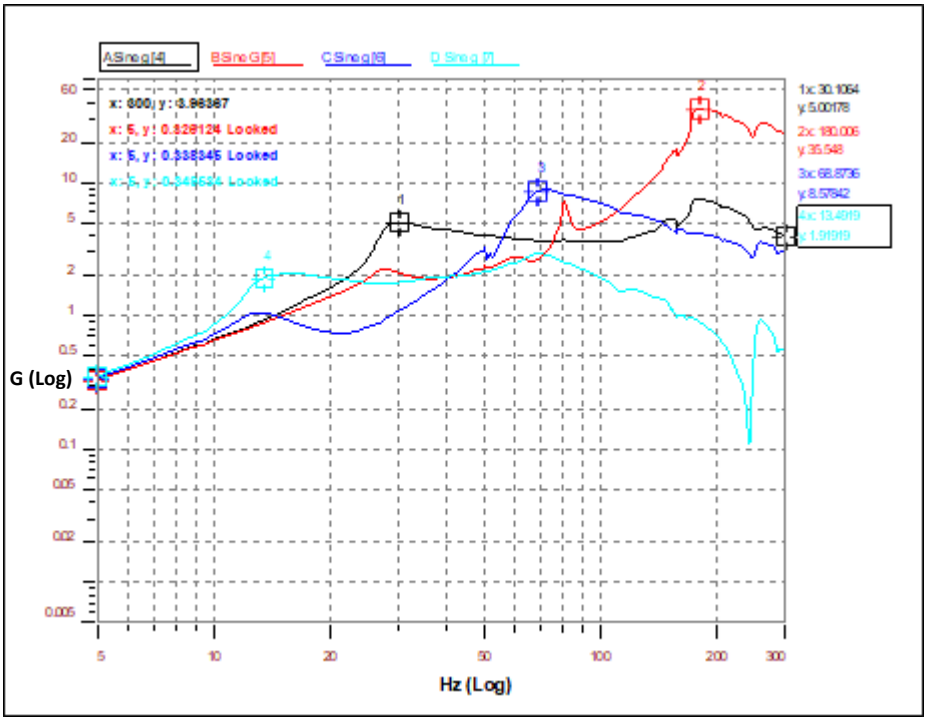


**Figure C.2:** The graph of acceleration amplitude G (log) vs frequency Hz (log)

DAMPER 9 (182 025-101) TEST 3

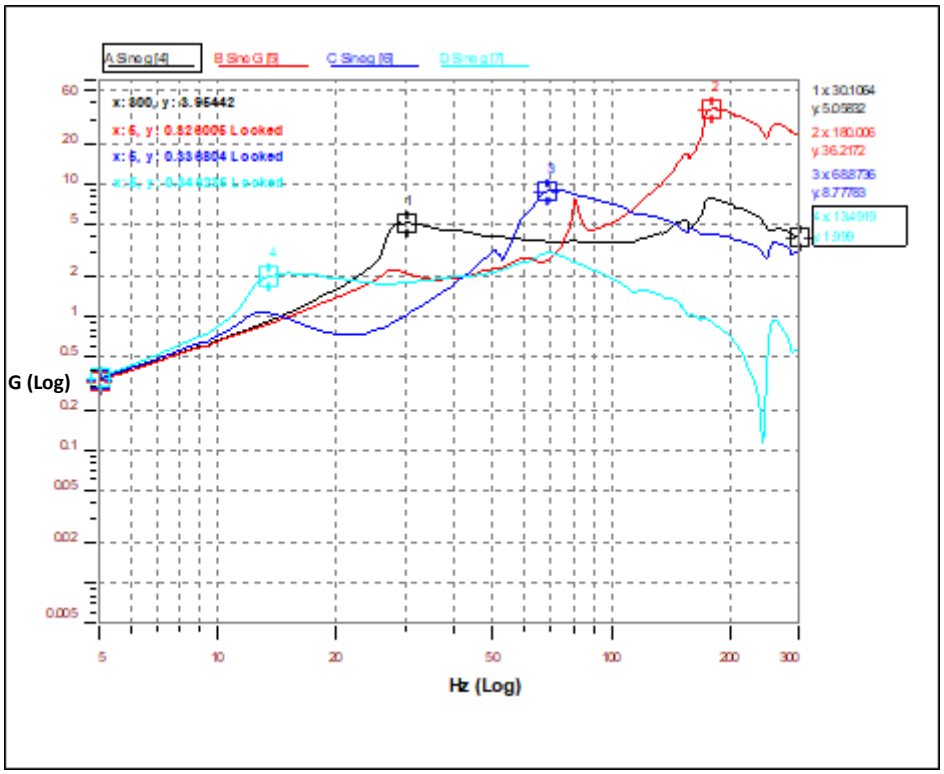


**Figure C.3:** The graph of acceleration amplitude G (log) vs frequency Hz (log

DAMPER 10 (182 025-101) TEST 1

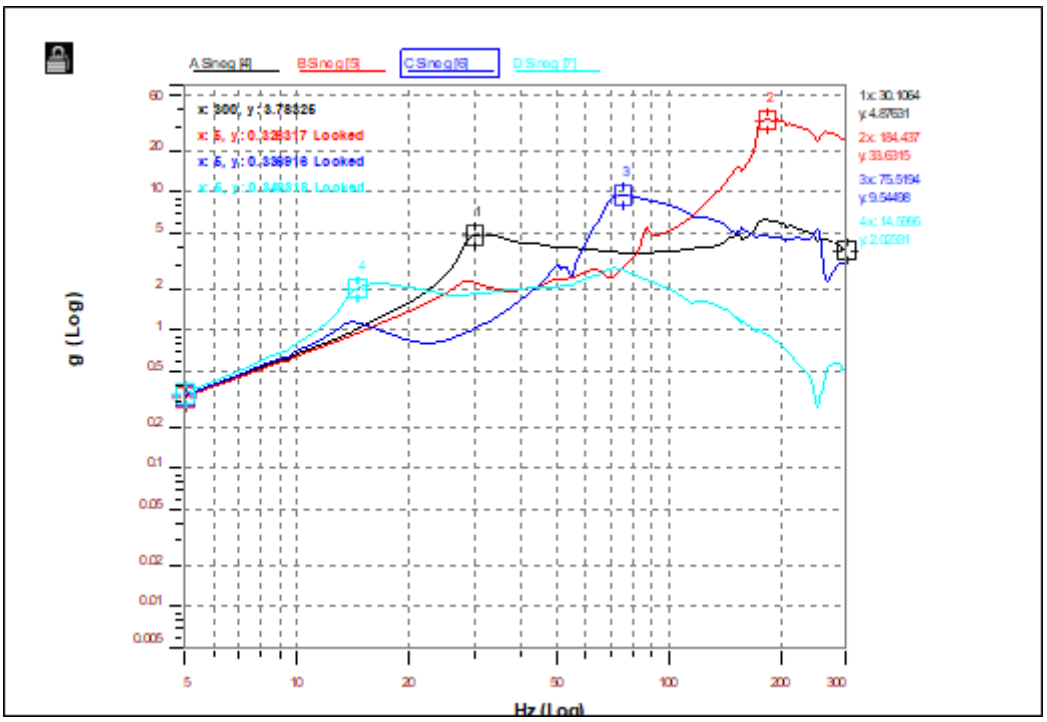


**Figure C.4:** The graph of acceleration amplitude G (log) vs frequency Hz (log)

DAMPER 10 (182 025-101) TEST 2

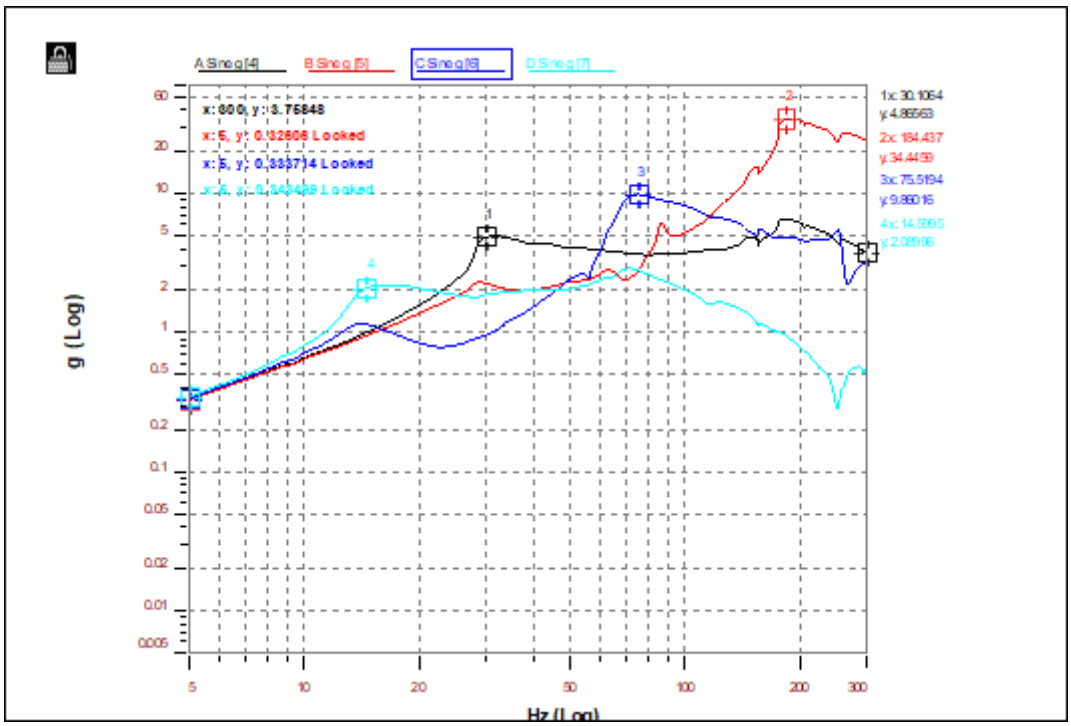


**Figure C.5:** The graph of acceleration amplitude G (log) vs frequency Hz (log)

DAMPER 10 (182 025-101) TEST 3

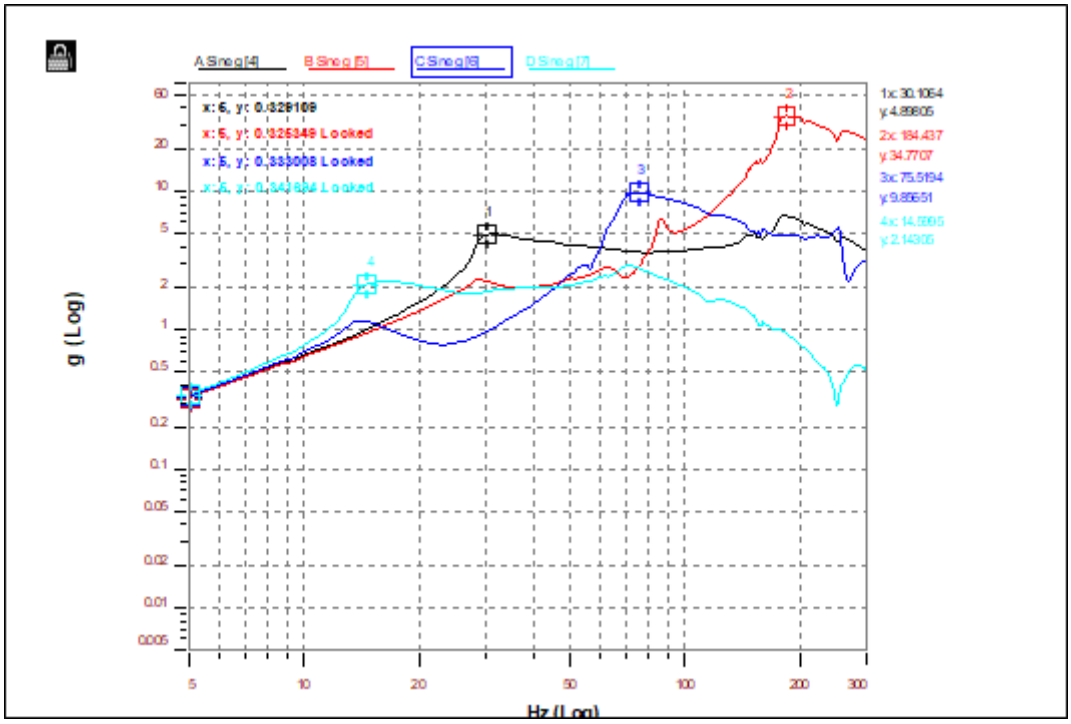


**Figure C.6:** The graph of acceleration amplitude G (log) vs frequency Hz (log)

# APPENDIX D

# GRAPHS OF DAMPER (182 025-301) AND (182 025-401)

DAMPER (182 025-301) TEST2

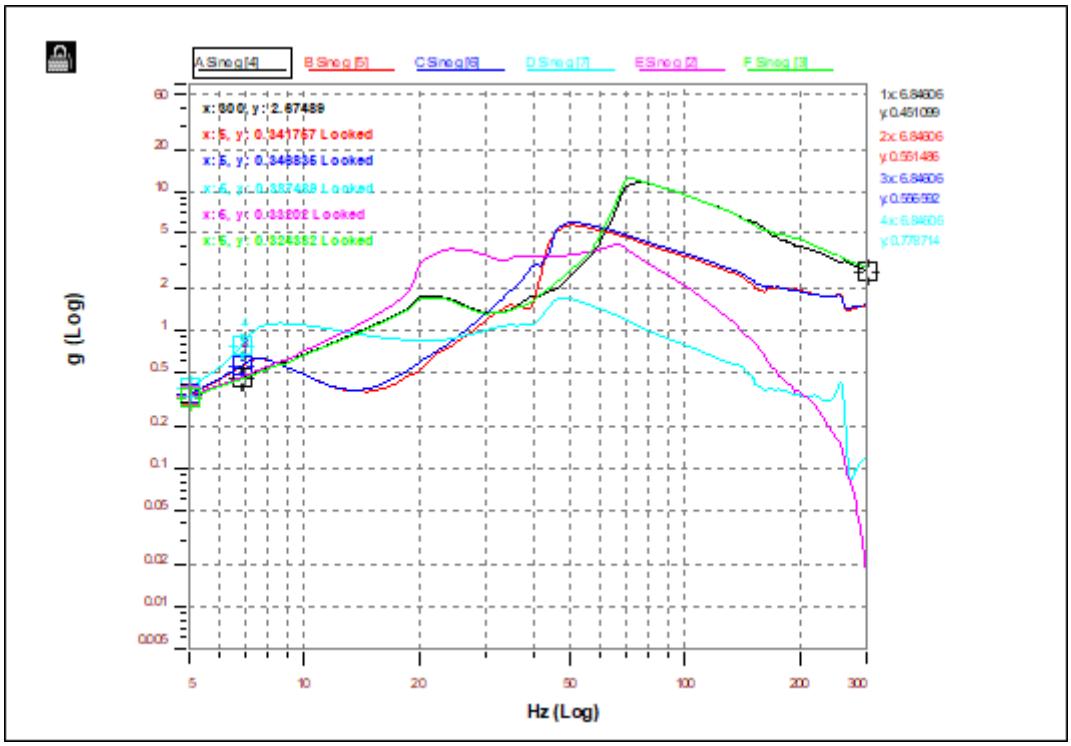


**Figure D.1:** The graph of acceleration amplitude G (log) vs frequency Hz (log)

DAMPER (182 025-301) TEST3

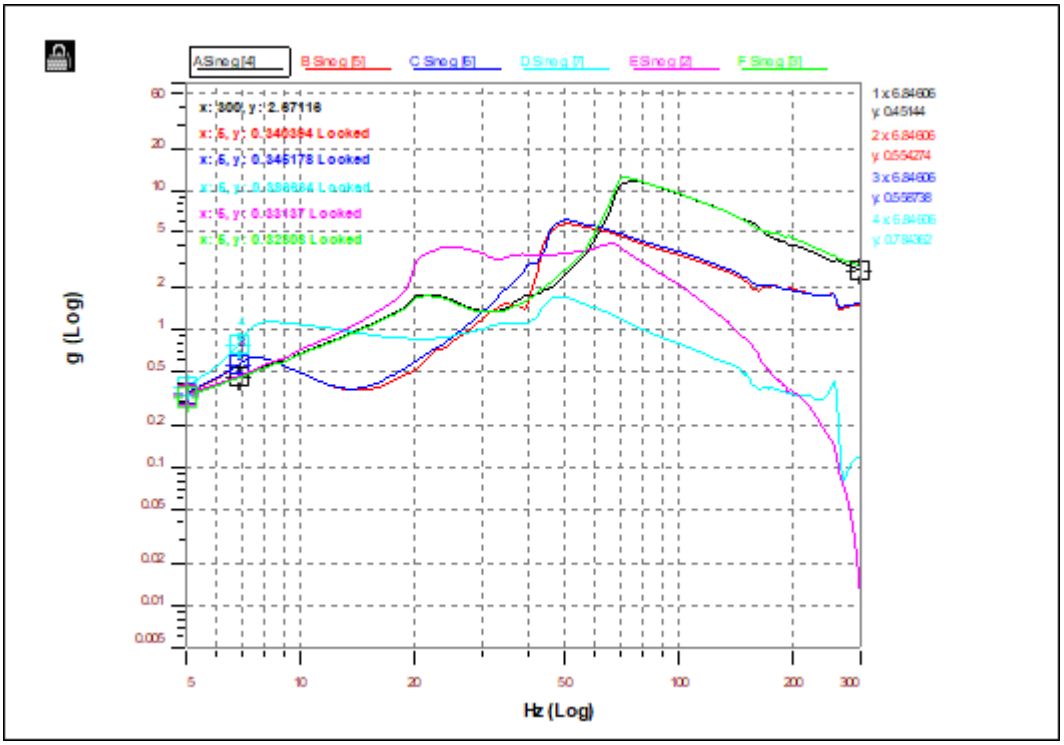


**Figure D.2:** The graph of acceleration amplitude G (log) vs frequency Hz (log)

DAMPER (182 025-401) TEST2

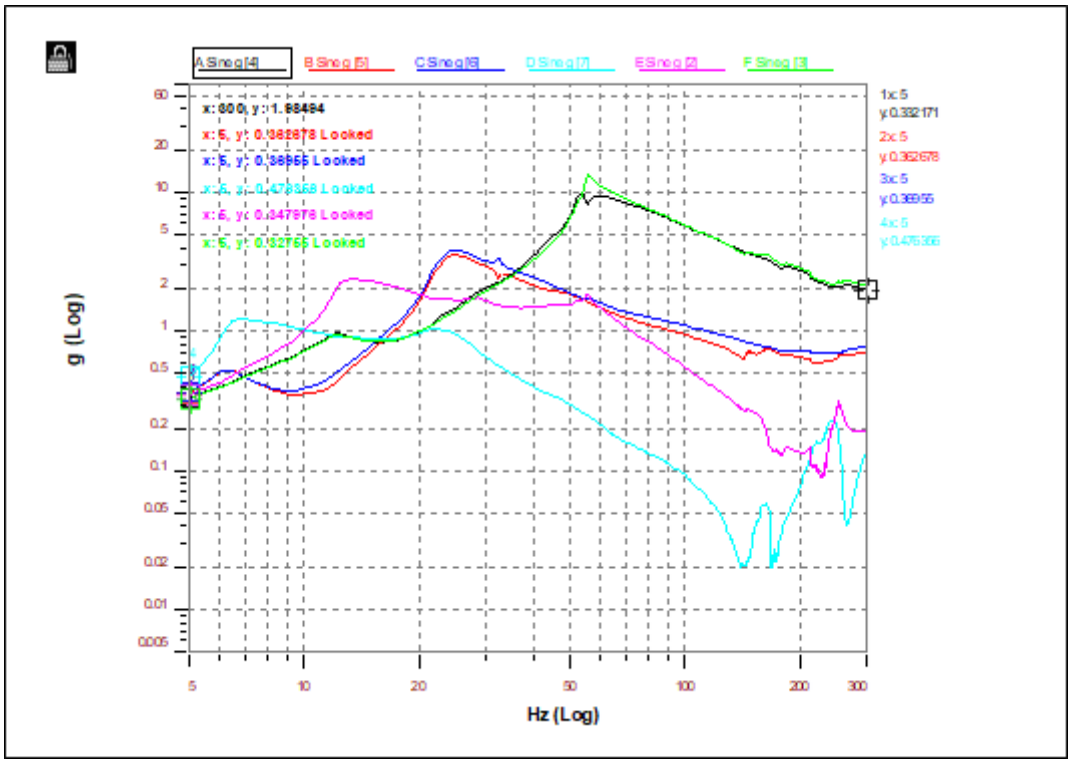


**Figure D.3:** The graph of acceleration amplitude G (log) vs frequency Hz (log)

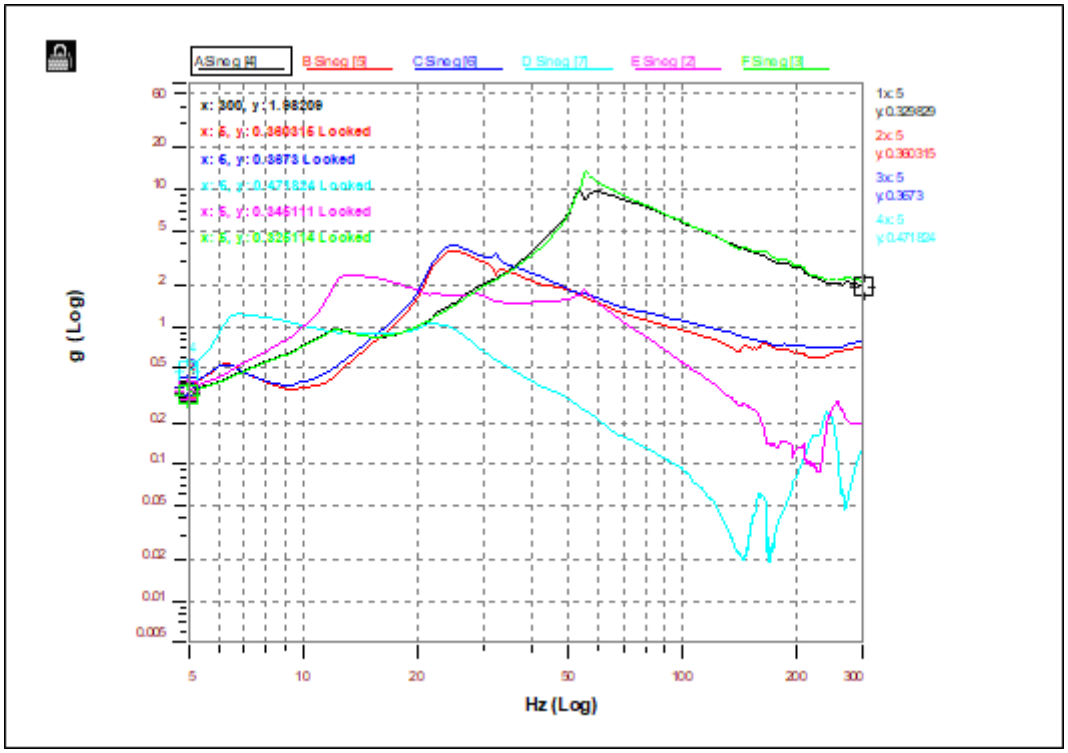


**Figure D.4:** The graph of acceleration amplitude G (log) vs frequency Hz (log)

# APPENDIX E

Applying the boundary condition $Y_1(0,t) = 0$ to equation 6.17 gives

$$0 = (a_1 \sin(0) + a_2 \cos(0) + a_3 \sinh(0) + a_4 \cosh(0))e^{i\omega t}$$

$$0 = (a_2 + a_4)e^{i\omega t}$$

This implies that either $e^{i\omega t} = 0$ for all values of $t$, or $a_2 + a_4 = 0$. The first statement is clearly not true, so it must be the case that

$$\boldsymbol{a_2 + a_4 = 0} \qquad \text{(E.1)}$$

Applying the boundary condition $Y_1'(0,t) = 0$ to equation 6.20 gives

$$0 = (a_1 \cos(0) - a_2 \sin(0) + a_3 \cosh(0) + a_4 \sinh(0))\beta_1 e^{i\omega t}$$

$$(a_1 + a_3)\beta_1 e^{i\omega t} = 0$$

$$\boldsymbol{a_1 + a_3 = 0} \qquad \text{(E.2)}$$

At $x_1 = L_1$ at the right end of the cable there is the mass $M_1$. At this point the displacement is expected to be equal, but the slope is opposite in direction due to the choice of reference coordinates. Therefore,

$$Y_1(L_1,t) = Y_2(0,t) = Y_3(0,t)$$

$$Y_1'(L_1,t) = -Y_2'(0,t) = -Y_3'(0,t)$$

Applying the boundary condition $Y_1(L_1,t) = Y_2(0,t) = Y_3(0,t)$ to equation 6.17, 6.18 and 6.19 gives

$Y_1(L_1,t) = Y_2(0,t)$

$(a_1 \sin\beta_1 L_1 + a_2 \cos\beta_1 L_1 + a_3 \sinh\beta_1 L_1 + a_4 \cosh\beta_1 L_1)e^{i\omega t} = \big(a_5 \sin\beta_2(0) + a_6 \cos\beta_2(0) + a_7 \sinh\beta_2(0) + a_8 \cosh\beta_2(0)\big)e^{i\omega t}$

$$\boldsymbol{a_1 \sin\beta_1 L_1 + a_2 \cos\beta_1 L_1 + a_3 \sinh\beta_1 L_1 + a_4 \cosh\beta_1 L_1 - a_6 - a_8 = 0} \quad \text{(E.3)}$$

Same procedure applies

$Y_1(L_1,t) = Y_3(0,t)$

$(a_1 \sin\beta_1 L_1 + a_2 \cos\beta_1 L_1 + a_3 \sinh\beta_1 L_1 + a_4 \cosh\beta_1 L_1)e^{i\omega t} = \big(a_9 \sin\beta_3(0) + a_{10} \cos\beta_3(0) + a_{11} \sinh\beta_3(0) + a_{12} \cosh\beta_3(0)\big)e^{i\omega t}$

$$\boldsymbol{a_1 \sin\beta_1 L_1 + a_2 \cos\beta_1 L_1 + a_3 \sinh\beta_1 L_1 + a_4 \cosh\beta_1 L_1 - a_{10} - a_{12} = 0} \quad \text{(E.4)}$$

Applying the boundary condition $Y_1'(L_1, t) = -Y_2'(0, t) = -Y_3'(0, t)$ to equation (6.20), (6.21) and (6.22) gives

$Y_1'(L_1, t) = -Y_2'(0, t)$

$$(a_1 \cos\beta_1 L_1 - a_2 \sin\beta_1 L_1 + a_3 \cosh\beta_1 L_1 + a_4 \sinh\beta_1 L_1)\beta_1 e^{i\omega t} = -\big(a_5 \cos\beta_2(0) - a_6 \sin\beta_2(0) + a_7 \cosh\beta_2(0) + a_8 \sinh\beta_2(0)\big)\beta_2 e^{i\omega t}$$

$$\boldsymbol{a_1\beta_1 \cos\beta_1 L_1 - a_2\beta_1 \sin\beta_1 L_1 + a_3\beta_1 \cosh\beta_1 L_1 + a_4\beta_1 \sinh\beta_1 L_1 + a_5\beta_2 + a_7\beta_2 = 0} \quad \text{(E.5)}$$

$Y_1'(L_1, t) = -Y_3'(0, t)$

$(a_1 \cos\beta_1 L_1 - a_2 \sin\beta_1 L_1 + a_3 \cosh\beta_1 L_1 + a_4 \sinh\beta_1 L_1)\beta_1 e^{i\omega t} = -(a_9 \cos\beta_3(0) - a_{10} \sin\beta_3(0) + a_{11} \cosh\beta_3(0) + a_{12} \sinh\beta(0)_3)\beta_3 e^{i\omega t}$

$$\boldsymbol{a_1\beta_1 \cos\beta_1 L_1 - a_2\beta_1 \sin\beta_1 L_1 + a_3\beta_1 \cosh\beta_1 L_1 + a_4\beta_1 \sinh\beta_1 L_1 + a_9\beta_3 + a_{11}\beta_3 = 0} \quad \text{(E.6)}$$

$EI_1 Y_1''(L_1, t) - J\ddot{Y}_1'(L_1, t) + EI_2 Y_2''(0, t) + EI_3 Y_3''(0, t) = 0$

For $x_1 = L_1, x_2 = 0$ and $x_3 = 0$. We have from 6.23, 6.24, 6.25 and 6.30 the following:

$Y_1''(L_1, t) = (-a_1 \sin\beta_1 L_1 - a_2 \cos\beta_1 L_1 + a_3 \sinh\beta_1 L_1 + a_4 \cosh\beta_1 L_1)\beta_1^2 e^{i\omega t}$

$\ddot{Y}_1'(L_1, t) = -(a_1 \beta_1 \cos\beta_1 L_1 - a_2 \beta_1 \sin\beta_1 L_1 + a_3 \beta_1 \cosh\beta_1 L_1 + a_4 \beta_1 \sinh\beta_1 L_1)\omega^2$

$Y_2''(0, t) = (-a_6 + a_8)\beta_2^2 e^{i\omega t}$

$Y_3''(0, t) = (-a_{10} + a_{12})\beta_3^2 e^{i\omega t}$

Substitute the above equations to equation 6.39, we obtain

$$EI_1(-a_1 \sin\beta_1 L_1 - a_2 \cos\beta_1 L_1 + a_3 \sinh\beta_1 L_1 + a_4 \cosh\beta_1 L_1)\beta_1^2 e^{i\omega t} + J(a_1 \beta_1 \cos\beta_1 L_1 - a_2\beta_1 \sin\beta_1 L_1 + a_3 \beta_1 \cosh\beta_1 L_1 + a_4 \beta_1 \sinh\beta_1 L_1)\omega^2 e^{i\omega t} + EI_2(-a_6 + a_8)\beta_2^2 e^{i\omega t} + EI_3(-a_{10} + a_{12})\beta_3^2 e^{i\omega t} = 0$$

$$-a_1 EI_1\beta_1^2 \sin\beta_1 L_1 + a_1 J\omega^2\beta_1 \cos\beta_1 L_1 - a_2 EI_1\beta_1^2 \cos\beta_1 L_1 - a_2 J\omega^2\beta_1 \sin\beta_1 L_1 + a_3 EI_1\beta_1^2 \sinh\beta_1 L_1 + a_3 J\omega^2\beta_1 \cosh\beta_1 L_1 + a_4 EI_1\beta_1^2 \cosh\beta_1 L_1 + a_4 J\omega^2\beta_1 \sinh\beta_1 L_1 - a_6 EI_2\beta_2^2 + a_8 EI_2\beta_2^2 - a_{10} EI_3\beta_3^2 + a_{12} EI_3\beta_3^2 = 0$$

$$\boldsymbol{a_1(-EI_1\beta_1^2 \sin\beta_1 L_1 + J\omega^2 \beta_1 \cos\beta_1 L_1) + a_2(-EI_1\beta_1^2 \cos\beta_1 L_1 - J\omega^2\beta_1 \sin\beta_1 L_1) + a_3(EI_1\beta_1^2 \sinh\beta_1 L_1 + J\omega^2\beta_1 \cosh\beta_1 L_1) + a_4(EI_1\beta_1^2 \cosh\beta_1 L_1 + J\omega^2\beta_1 \sinh\beta_1 L_1) - a_6 EI_2\beta_2^2 + a_8 EI_2\beta_2^2 - a_{10} EI_3\beta_3^2 + a_{12} EI_3\beta_3^2 = 0} \quad \text{(E.7)}$$

$$-EI_1 Y_1'''(L_1, t) - EI_2 Y_2'''(0, t) - EI_3 Y_3'''(0, t) = M_1 \ddot{Y}_1(L_1, t)$$

Applying the boundary conditions to equation 6.40 lead to the following

$$-EI_1(-a_1 \beta_1^3 \cos\beta_1 L_1 + a_2 \beta_1^3 \sin\beta_1 L_1 + a_3 \beta_1^3 \cosh\beta_1 L_1 + a_4 \beta_1^3 \sinh\beta_1 L_1)e^{i\omega t} - EI_2(-a_5 \beta_2^3 \cos\beta_1(0) + a_6 \beta_2^3 \sin\beta_1(0) + a_7 \beta_2^3 \cosh\beta_1(0) + a_8 \beta_2^3 \sinh\beta_1(0))e^{i\omega t} - EI_3(-a_9 \beta_3^3 \cos\beta_1(0) + a_{10} \beta_3^3 \sin\beta_1(0) + a_{11} \beta_3^3 \cosh\beta_1(0) + a_{12} \beta_3^3 \sinh\beta_1(0))e^{i\omega t} + M_1(a_1 \omega^2 \sin\beta_1 L_1 + a_2 \omega^2 \cos\beta_1 L_1 + a_3 \omega^2 \sinh\beta_1 L_1 + a_4 \omega^2 \cosh\beta_1 L_1)e^{i\omega t} = 0$$

$$-EI_1(-a_1 \beta_1^3 \cos\beta_1 L_1 + a_2 \beta_1^3 \sin\beta_1 L_1 + a_3 \beta_1^3 \cosh\beta_1 L_1 + a_4 \beta_1^3 \sinh\beta_1 L_1)e^{i\omega t} - EI_2(-a_5\beta_2^3 + a_7\beta_2^3)e^{i\omega t} - EI_3(-a_9\beta_3^3 + a_{11}\beta_3^3)e^{i\omega t} + M_1(a_1 \omega^2 \sin\beta_1 L_1 + a_2 \omega^2 \cos\beta_1 L_1 + a_3 \omega^2 \sinh\beta_1 L_1 + a_4 \omega^2 \cosh\beta_1 L_1)e^{i\omega t} = 0$$

$$-a_1 EI_1\beta_1^3 \cos\beta_1 L_1 + a_2 EI_1\beta_1^3 \sin\beta_1 L_1 + a_3 EI_1\beta_1^3 \cosh\beta_1 L_1 + a_4 EI_1\beta_1^3 \sinh\beta_1 L_1 - a_5 EI_2\beta_2^3 + a_7 EI_2\beta_2^3 - a_9 EI_3\beta_3^3 + a_{11} EI_3\beta_3^3 - a_1 M_1\omega^2 \sin\beta_1 L_1 - a_2 M_1 \omega^2 \cos\beta_1 L_1 - a_3 M_1\omega^2 \sinh\beta_1 L_1 - a_4 M_1 \omega^2 \cosh\beta_1 L_1 = 0$$

$$\boldsymbol{a_1(-EI_1\beta_1^3 \cos\beta_1 L_1 - M_1\omega^2 \sin\beta_1 L_1) + a_2(EI_1\beta_1^3 \sin\beta_1 L_1 - M_1 \omega^2 \cos\beta_1 L_1) + a_3(EI_1\beta_1^3 \cosh\beta_1 L_1 - M_1\omega^2 \sinh\beta_1 L_1) + a_4(EI_1\beta_1^3 \sinh\beta_1 L_1 - M_1 \omega^2 \cosh\beta_1 L_1) - a_5 EI_2\beta_2^3 + a_7 EI_2\beta_2^3 - a_9 EI_3\beta_3^3 + a_{11} EI_3\beta_3^3 = 0} \quad \text{(E.8)}$$

There are two beams attached to mass $M_1$, the first beam is free at the end. Therefore the boundary conditions at $x_2 = L_2$ are:

$$Y_2''(L_2, t) = 0$$

$$M_2\ddot{Y}_2(L_2, t) - EI_2 Y_2'''(L_2, t) = 0$$

Applying the boundary condition to equation 6.41 gives

$$(-a_5 \sin\beta_2 L_2 - a_6 \cos\beta_2 L_2 + a_7 \sinh\beta_2 L_2 + a_8 \cosh\beta_2 L_2)\beta_2^2 e^{i\omega t} = 0$$

Therefore

$$\boldsymbol{-a_5\beta_2^2 \sin\beta_2 L_2 - a_6 \beta_2^2 \cos\beta_2 L_2 + a_7 \beta_2^2 \sinh\beta_2 L_2 + a_8 \beta_2^2 \cosh\beta_2 L_2 = 0} \quad \text{(E.9)}$$

Applying the boundary condition to equation 6.42 gives

$$-M_2(a_5 \sin\beta_2 L_2 + a_6 \cos\beta_2 L_2 + a_7 \sinh\beta_2 L_2 + a_8 \cosh\beta_2 L_2)\omega^2 e^{i\omega t} - EI_2(-a_5 \cos\beta_2 x_2 + a_6 \sin\beta_2 x_2 + a_7 \cosh\beta_2 x_2 + a_8 \sinh\beta_2 x_2)\beta_2^3 e^{i\omega t} = 0$$

$$\boldsymbol{a_5(M_2\omega^2 \sin\beta_2 L_2 - \beta_2^3 EI_2 \cos\beta_2 x_2) + a_6(M_2\omega^2 \cos\beta_2 L_2 + \beta_2^3 EI_2 \sin\beta_2 x_2) + a_7(M_2\omega^2 \sinh\beta_2 L_2 + \beta_2^3 EI_2 \cosh\beta_2 x_2) + a_8(M_2\omega^2 \cosh\beta_2 L_2 + \beta_2^3 EI_2 \sinh\beta_2 x_2) = 0} \quad \text{(E.10)}$$

The second beam is also free at the end. Therefore the boundary conditions at the free end at $x_3 = L_3$, apply the boundary conditions in equation 6.43 and 6.44

$$\boldsymbol{-a_9\beta_3^2 \sin\beta_3 L_3 - a_{10} \beta_3^2 \cos\beta_3 L_3 + a_{11} \beta_3^2 \sinh\beta_3 L_3 + a_{12} \beta_3^2 \cosh\beta_3 L_3 = 0} \quad \text{(E.11)}$$

$$\boldsymbol{a_9(M_3\omega^2 \sin\beta_3 L_3 - \beta_3^3 EI_3 \cos\beta_3 x_3) + a_{10}(M_3\omega^2 \cos\beta_3 L_3 + \beta_3^3 EI_3 \sin\beta_3 x_3) + a_{11}(M_3\omega^2 \sinh\beta_3 L_3 + \beta_3^3 EI_3 \cosh\beta_3 x_3) + a_{12}(M_3\omega^2 \cosh\beta_3 L_3 + \beta_3^3 EI_3 \sinh\beta_3 x_3) = 0} \quad \text{(E.12)}$$

# APPENDIX F

$$\begin{bmatrix} 0 & A_2 & 0 & A_4 & 0 & 0 & 0 & 0 & 0 & 0 & 0 & 0 \\ B_1 & 0 & B_3 & 0 & 0 & 0 & 0 & 0 & 0 & 0 & 0 & 0 \\ C_1 & C_2 & C_3 & C_4 & 0 & C_6 & 0 & C_8 & 0 & 0 & 0 & 0 \\ D_1 & D_2 & D_3 & D_4 & 0 & 0 & 0 & 0 & 0 & D_{10} & 0 & D_{12} \\ E_1 & E_2 & E_3 & E_4 & E_5 & 0 & E_7 & 0 & 0 & 0 & 0 & 0 \\ F_1 & F_2 & F_3 & F_4 & 0 & 0 & 0 & 0 & F_9 & 0 & F_{11} & 0 \\ G_1 & G_2 & G_3 & G_4 & 0 & G_6 & 0 & G_8 & 0 & G_{10} & 0 & G_{12} \\ H_1 & H_2 & H_3 & H_4 & H_5 & 0 & H_7 & 0 & H_9 & 0 & H_{11} & 0 \\ 0 & 0 & 0 & 0 & I_5 & I_6 & I_7 & I_8 & 0 & 0 & 0 & 0 \\ 0 & 0 & 0 & 0 & J_5 & J_6 & J_7 & J_8 & 0 & 0 & 0 & 0 \\ 0 & 0 & 0 & 0 & 0 & 0 & 0 & 0 & K_9 & K_{10} & K_{11} & K_{12} \\ 0 & 0 & 0 & 0 & 0 & 0 & 0 & 0 & L_9 & L_{10} & L_{11} & L_{12} \end{bmatrix} \cdot \begin{bmatrix} a_1 \\ a_2 \\ a_3 \\ a_4 \\ a_5 \\ a_6 \\ a_7 \\ a_8 \\ a_9 \\ a_{10} \\ a_{11} \\ a_{12} \end{bmatrix} = 0$$

Where

$$A_2 = 1; A_4 = 1$$

$$B_1 = 1; B_3 = 1$$

$$C_1 = \sin \beta_1 L_1 \, ; C_2 = \cos \beta_1 \, L_1;$$

$$C_3 = \sinh \beta_1 L_1 \, ; C_4 = \cosh \beta_1 \, L_1$$

$$C_6 = -1; C_8 = -1$$

$$D_1 = \sin \beta_1 L_1 \, ; D_2 = \cos \beta_1 \, L_1;$$

$$D_3 = \sinh \beta_1 L_1 \, ; D_4 = \cosh \beta_1 \, L_1$$

$$D_{10} = -1; D_{12} = -1$$

$$E_1 = \beta_1 \cos \beta_1 \, L_1; \; E_2 = \beta_1 \sin \beta_1 L_1$$

$$E_3 = \beta_1 \cosh \beta_1 \, L_1 \; ; \; E_4 = \beta_1 \sinh \beta_1 L_1$$

$$E_5 = \beta_2; \; E_7 = \beta_2$$

$$F_1 = \beta_1 \cos \beta_1 L_1;\ F_2 = -\beta_1 \sin \beta_1 L_1$$

$$F_3 = \beta_1 \cosh \beta_1 L_1\ ;\ F_4 = = \beta_1 \sinh \beta_1 L_1$$

$$F_9 = \beta_3;\ F_{11} = \beta_3$$

$$G_1 = -EI_1\beta_1^2 \sin \beta_1 L_1 + J\omega^2\, \beta_1 \cos \beta_1 L_1;\ G_2 = -EI_1\beta_1^2 \cos \beta_1 L_1 - J\omega^2 \beta_1 \sin \beta_1\, L_1$$

$$G_3 = \ EI_1\beta_1^2 \sinh \beta_1 L_1 + J\omega^2 \beta_1 \cosh \beta_1 L_1\ ;\ G_4 = EI_1\beta_1^2\, \cosh \beta_1 L_1 + J\omega^2 \beta_1 \sinh \beta_1 L_1$$

$$G_6 = EI_2\beta_2^2\ ;\ G_8 = EI_2\beta_2^2$$

$$G_{10} = EI_3\beta_3^2\ ;\ G_{12} = EI_3\beta_3^2$$

$$H_1 = -\ EI_1\beta_1^3 \cos \beta_1\, L_1 - M_1\omega^2 \sin \beta_1 L_1\ ;\ H_2 = EI_1\beta_1^3 \sin \beta_1 L_1 - M_1\, \omega^2 \cos \beta_1 L_1$$

$$H_3 = EI_1\beta_1^3 \cosh \beta_1 L_1 - M_1\omega^2 \sinh \beta_1\, L_1\ ;\ H_4 = EI_1\beta_1^3 \sinh \beta_1 L_1 - M_1\, \omega^2 \cosh \beta_1 L_1$$

$$H_5 = \ EI_2\beta_2^3\ ;\ H_7 = \ EI_2\beta_2^3$$

$$H_9 = \ -EI_3\beta_3^3\ ;\ H_{11} = \ EI_3\beta_3^3$$

$$I_5 = -\beta_2^2 \sin \beta_2\, L_2\ ;\ I_6 = -\beta_2^2\, \sin \beta_2\, L_2$$

$$I_7 = \beta_2^2 \sinh \beta_2 L_2\ ;\ I_8 = \beta_2^2 \cosh \beta_2 L_2$$

$$J_5 = M_2\omega^2 \sin \beta_2 L_2 - \beta_2^3\, EI_2 \cos \beta_2 L_2\ ;\ J_6 = M_2\omega^2\, \cos \beta_2 L_2 + \beta_2^3 EI_2 \sin \beta_2 L_2$$

$$J_7 = M_2\omega^2 \sinh \beta_2\, L_2 + \beta_2^3 EI_2 \cosh \beta_2 L_2\ ;\ J_8 = M_2\omega^2\, \cosh \beta_2\, L_2 + \beta_2^3 EI_2 \sinh \beta_2 L_2$$

$$K_9 = -\beta_3^2 \sin \beta_3\, L_3;\ K_{10} = -\ \beta_3^2 \cos \beta_3\, L_3$$

$$K_{11} = \beta_3^2 \sinh \beta_3 L_3\ ;K_{12} = \ \beta_3^2 \cosh \beta_3 L_3$$

$$L_9 = M_3\omega^2 \sin\beta_3 L_3 - \beta_3^3\, EI_3 \cos\beta_3 L_3\ ;\ L_{10} = M_3\omega^2 \cos\beta_3 L_3 + \beta_3^3 EI_3 \sin\beta_3\, L_3$$

$$L_{11} = M_3\omega^2 \sinh\beta_3\, L_3 + \beta_3^3 EI_3 \cosh\beta_3 L_3\ ;\ L_{12} = M_3\omega^2 \cosh\beta_3\, L_3 + \beta_3^3 EI_3 \sinh\beta_3 L_3$$

# APPENDIX G

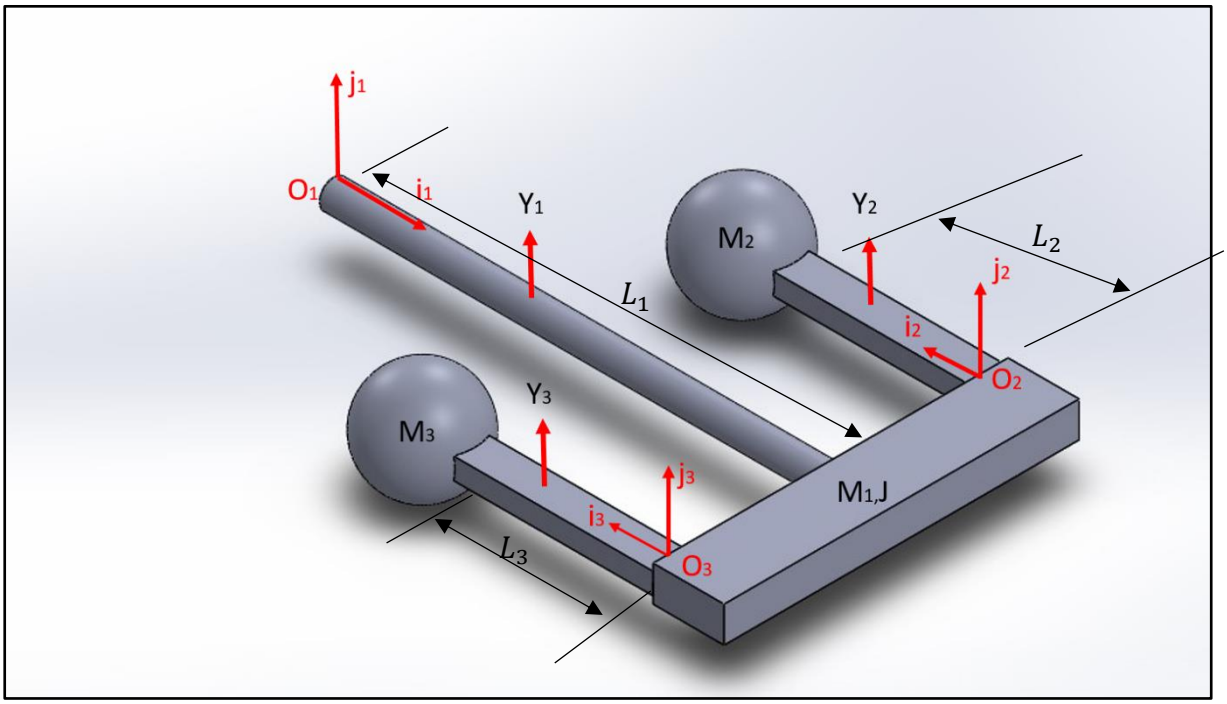


**Figure G.1**: Diagram of the half model of vibration damper (Vaja et al., 2018)

**Messenger cable with a mass ($M_1$)**

$M_1 = 0.5\ kg$

$Diamete\ of\ the\ messenger\ cable\ is\ 9\ mm$

$I_1 = \frac{\pi(D)^4}{32} = \frac{\pi(0.009)^4}{32} = 6.4412\ x\ 10^{-10} m^4$

$L_1 = 0.145\ m$

$\cos(L_1\beta_1) = \cos\theta\ \ (\theta\ could\ be\ \frac{\pi}{2}, \frac{\pi}{4}, \frac{\pi}{8}, \frac{\pi}{16}, \frac{\pi}{32}, \frac{\pi}{64})$

$\cos(0.145\beta_1) = \cos\frac{\pi}{2}$

$\beta_1 = 10.833$

$G = 200\ GPa\ for\ steel$

$J_{total} = \frac{M_{cable}L_{cable}^2}{3} + M_1 r^2 = \frac{(0.05352)(0.145)^2}{3} + (0.25)(0.145)^2 = 5.631\ x\ 10^{-3} kgm^4$

$k_1 = \frac{3EI_1}{l_1} = \frac{(3)(200)(10^9)(6.4412\ x\ 10^{-10})}{0.145^3} = 12.6770\ x10^4\ {}^{N}/_{m}$ (The messenger cable is considered as the cantilever beam with a load acting at the end)

**Cantilever beam with a concentrated load ($M_2$)**

$A_2 =$ Cross sectional area of the cantilever beam

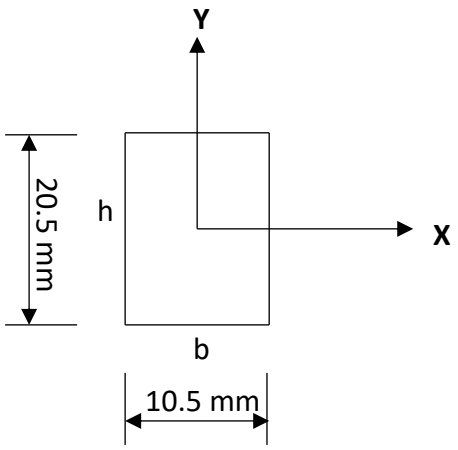


$M_2 = 0.25\ kg$

$I_2 = \frac{bh^3}{12} = \frac{(0.0105)(0.0205)^3}{12} = 7.538\ x\ 10^{-9}\ m^4$

$L_2 = 0.12\ m$

$\cos(L_2\beta_2) = \cos\frac{\pi}{2}$

$\cos(0.12\beta_2) = \cos\frac{\pi}{2}$ ( $\theta$ *could be* $\frac{\pi}{2}, \frac{\pi}{4}, \frac{\pi}{8}, \frac{\pi}{16}, \frac{\pi}{32}, \frac{\pi}{64}$ )

$\beta_2 = 13.0899$

$E = 200\ GPa\ for\ steel$

$k_2 = \frac{3EI_2}{L_2^3} = \frac{(3)(200)(10^9)(7.538\ x\ 10^{-9})}{0.12^3} = 26.1736\ x10^5\ {}^{N}/_{m}$

## Cantilever beam with a concentrated load ($M_3$)

$M_3 = 0.25\ kg$

$I_3 = I_2 = \frac{bh^3}{12} = 7.538\ x\ 10^{-9}\ m^4$

$L_3 = 0.12\ m$

$\cos(L_3\beta_3) = \cos\frac{\pi}{2}$ ( $\theta$ *could be* $\frac{\pi}{2}, \frac{\pi}{4}, \frac{\pi}{8}, \frac{\pi}{16}, \frac{\pi}{32}, \frac{\pi}{64}$ )

$\cos(0.12\beta_3) = \cos\frac{\pi}{2}$

$\beta_3 = 13.0899$

$E = 200\ GPa\ for\ steel$

$k_3 = \frac{3EI_3}{L_3^3} = \frac{(3)(200)(10^9)(7.538\ x\ 10^{-9})}{0.12^3} = 26.1736\ x10^5\ {}^{N}/_{m}$

# References


Ayres, F. J. 1962. *Theory and problems matrices,* United State of America, Schaum Publishing Company.

Badibanga, K. R. 2012. *Life prediction of power line damper.*

Brownjohn, J. M. W. 2005. *Single degree of freedom* [Online]. University of Plymouth. Available: www.tech.plym.ac.uk/soe/james/my_papers/STRC201_SDOF_JMWB.pd [Accessed June 2017].

Chan, J. 2006. *EPRI transmission line reference book: Wind induced-induced conductor motion motion,* Palo Alto, California, Electric Power Research Institute

Diana, G., Cigada, A., Belloli, M. & Vanali, M. 2003. Stockbridge-type damper effectiveness evaluation. I. Comparison between tests on span and on the shaker. *IEEE Transactions on Power Delivery,* 18**,** 1462-1469.

Gere, M. J. & Timoshenko, S. P. 1997. *Mechanical of material,* Boston, MA 02116-4324, PWS Publishing Company.

Inman, D. J. 2001. *Engineering vibration,* United States of America, Prentice - Hall, Inc.

Kalombo, R. B., Loubser, R. & Moodley, P. Bending stress of stockbridge damper messenger cable: Experimental data and modelling. 18th World Conference on Non-destructive Testing, 2012. 16-20.

Kelly, S. G. 1993. *Fundamentals of mechanical vibrations,* Singapore, McGraw Hill, Inc.

Kim, C.-J. 2017. Design sensitivity analysis of a Stockbridge damper to control resonant frequencies. *Journal of Mechanical Science and Technology,* 31**,** 4145-4150.

Lilien, J., Guérard, S. & Godard, B. 2013. Power Line Aeolian Vibrations. *Published by University of Liège Department of Electronics, Electricity and Computer Sciences, Liège, Belgium*.

Markiewicz, M. 1995. Optimum dynamic characteristics of stockbridge dampers for dead-end spans. *Journal of sound and vibration,* 188**,** 243-256.

Palm Iii, W. J. 2007. *Mechanical vibration,* United States of America, John Wiley and Sons, Inc.

Seto, W. W. 1964. *Mechanical vibrations,* Singapore, McGrraw Hill Book Company.

Stroud, K. A. & Booth, D. J. 2001. *Engineering mathematics,* New York, Replika Press Pvt Ltd.

Vaja, N., Barry, O. & Tanbour, E. 2018. On the modeling and analysis of a vibration absorber for overhead powerlines with multiple resonant frequencies. *Engineering Structures,* 175**,** 711-720.

Zill, D. G. & Cullen, M. R. 2005. *Defferential equationss*, Brooks/Cole Publishing Company.